



Representation of the Terrestrial Carbon Cycle in CMIP6



Bettina K. Gier^{1,2}, Manuel Schlund², Pierre Friedlingstein^{3,4}, Chris D. Jones⁵, Colin Jones⁶,
Sönke Zaehle⁷, and Veronika Eyring^{2,1}

¹University of Bremen, Institute of Environmental Physics (IUP), Bremen, Germany

²Deutsches Zentrum für Luft- und Raumfahrt (DLR), Institut für Physik der Atmosphäre, Oberpfaffenhofen, Germany

³College of Engineering, Mathematics and Physical Sciences, University of Exeter, Exeter, EX4 4QE, United Kingdom

⁴LMD/IPSL, ENS, PSL Université, École Polytechnique, Institut Polytechnique de Paris,
Sorbonne Université, CNRS, Paris, France

⁵Met Office Hadley Centre, Exeter, UK

⁶National Centre for Atmospheric Science, University of Leeds, UK

⁷Biogeochemical Signals Department, Max Planck Institute for Biogeochemistry, Jena, Germany

Correspondence: Bettina K. Gier (gier@uni-bremen.de)

Abstract. Improvements in the representation of the land carbon cycle in Earth system models participating in the Coupled Model Intercomparison Project Phase 6 (CMIP6) include interactive treatment of both the carbon and nitrogen cycles, improved photosynthesis, and soil hydrology. To assess the impact of these model developments on aspects of the global carbon cycle, the Earth System Model Evaluation Tool (ESMValTool) is expanded to compare CO₂ concentration and emission driven historical simulations from CMIP5 and CMIP6 to observational data sets. A particular focus is on the differences in models with and without an interactive terrestrial nitrogen cycle. Overestimations of photosynthesis (gross primary productivity (GPP)) in CMIP5 were largely resolved in CMIP6 for participating models with an interactive nitrogen cycle, but remaining for models without one. This points to the importance of including nutrient limitation. Simulating the leaf area index (LAI) remains challenging with a large model spread in both CMIP5 and CMIP6. In ESMs, global mean land carbon uptake (net biome productivity (NBP)) is well reproduced in the CMIP5 and CMIP6 multi-model means. However, this is the result of an underestimation of NBP in the northern hemisphere, which is compensated by an overestimation in the southern hemisphere and the tropics. Carbon stocks remain a large uncertainty in the models. While vegetation carbon content is slightly better represented in CMIP6, the inter-model range of soil carbon content remains the same between CMIP5 and CMIP6. Overall, a slight improvement in the simulation of land carbon cycle parameters is found in CMIP6 compared to CMIP5, but with many biases remaining, further improvements of models in particular for LAI and NBP is required. Models from modeling groups participating in both CMIP phases generally perform similarly or better in their CMIP6 compared to their CMIP5 models. This improvement is not as significant in the multi-model means due to more new models in CMIP6, especially those using older versions of the Community Land Model (CLM). Emission driven simulations perform just as well as concentration driven models despite the added process-realism. Due to this we recommend ESMs in future CMIP phases to perform emission driven simulations as the standard so that climate-carbon cycle feedbacks are fully active. The inclusion of nitrogen limitation led to a large improvement in photosynthesis compared to models not including this process, suggesting the need to view the nitrogen





cycle as a necessary part of all future carbon cycle models. Possible benefits when including further limiting nutrients such as phosphorus should also be considered.



1 Introduction

25 Earth System Models (ESMs) simulate the climate system by interactively coupling physical general circulation models of the atmosphere, ocean, land and cryosphere with biogeochemical and biophysical cycles (Jones, 2020). The Coupled Model Intercomparison Project (CMIP, Meehl et al., 2000) was established to facilitate a consistent comparison between different ESMs through the use of common forcings and a uniform output structure in order to better understand past, present and future climate. The newest phase, CMIP6 (Eyring et al., 2016a), provides a large ensemble of model simulations and includes
30 23 CMIP6-Endorsed Model Intercomparison Projects (MIPs) which facilitate a better analysis of specific scientific questions. Every new phase of CMIP sees additional models and improved model components, making a comparison to previous phases vital to determine if known systematic biases have been reduced and model weaknesses were identified and overcome (Eyring et al., 2019), or if increased model realism through the inclusion of additional processes introduces new biases. Increasing the process-realism of models, for example by replacing time-invariant observation-based fields with interactive prognostic
35 ones, while having a neutral impact on the present day performance of the model can be viewed as a successful step in model improvement. This is particularly important for improved climate projections, even at the possible cost of worse present-day evaluation. Bock et al. (2020) assessed atmospheric variables of the CMIP6 ensemble and compared them to CMIP3 and CMIP5 output. They find that for temperature, precipitation, water vapor and zonal wind speed many long-standing biases remain in the multi-model mean, but individual models and high-resolution versions of models show some improvements in
40 many long-standing biases for temperature and precipitation. In this study, we expand this assessment to the carbon cycle.

The carbon cycle is an important part of ESMs due to the key role of anthropogenic emissions of carbon dioxide (CO₂) in driving climate change (IPCC, 2021). The land carbon cycle dominates the uncertainty of the global carbon cycle (Canadell et al., 2021). The Intergovernmental Panel on Climate Change (IPCC) Fifth Assessment Report (AR5) was largely supported by model simulations from the CMIP5 ensemble, and CMIP6 models were an important input to AR6 (IPCC, 2021). It is important
45 to evaluate these models and document their changes compared to CMIP5. The focus of this study is on the results of the CMIP6 historical simulations, split into simulations with prescribed greenhouse gas concentrations and those with prescribed CO₂ emissions. Simulations driven by carbon emissions require an interactive carbon cycle to determine the distribution of natural and anthropogenic carbon fluxes across the land, marine and atmospheric reservoirs instead of relying on prescribed atmospheric CO₂ concentrations (Friedlingstein et al., 2014). Therefore, only emission driven simulations have fully active
50 climate-carbon cycle feedbacks vital for self-consistent future projections. Sanderson et al. (2023) thus petition for the use of emission driven simulations to be prioritized in CMIP7. This leads to further importance of the evaluation of the carbon cycle as more models will be required to implement and improve their interactive carbon cycle. An analysis of idealized 1% CO₂ increase per year (1pctCO₂) simulations for CMIP5 and CMIP6 models with respect to carbon-concentration and carbon-climate feedbacks has been carried out by Arora et al. (2020). They found that while these feedback parameters have not



55 changed significantly between CMIP5 and CMIP6, the land feedback parameters are weaker for models including a nitrogen cycle coupled to the carbon cycle. Davies-Barnard et al. (2020) documented the development and inclusion of modelling of the terrestrial nitrogen cycle in ESM land-surface schemes, and show how this affects the response to elevated CO₂ across models. They find that these models show a more accurate response in the tropics than high-latitudes compared with observed responses. Gier et al. (2020) investigated the atmospheric CO₂ concentrations for emission driven CMIP5 and CMIP6 models and found
60 that while CMIP6 models show an improvement in reproducing the observations compared to CMIP5, during the period of the satellite observations (2003-2014) the growth rate is overestimated and the seasonal cycle amplitude is underestimated in both CMIP5 and CMIP6 relative to observations. Furthermore, the model spread in simulated atmospheric CO₂ (~ 45 ppmv in CMIP5, ~ 35 ppmv in CMIP6) was found to remain many times larger than the observational uncertainty of under 1 ppmv over this period.

65 Anav et al. (2013a) investigated the land and ocean carbon cycle for CMIP5 historical model simulations. While most models reproduced the main climatic variables and their seasonal evolution correctly, weaknesses were found in their ability to reproduce more specific biogeochemical fields such as a general overestimation of photosynthesis. Consequently, these were some of the main areas tackled in updating and enhancing the land carbon models of the ESMs for CMIP6, including the addition of a coupled nitrogen cycle and nitrogen limitation which can limit the rates of carbon cycling through vegetation and
70 soil, as well as photosynthesis updates and soil hydrology improvements (e.g., Danabasoglu et al., 2020; Delire et al., 2020; Wiltshire et al., 2021). This paper assesses the impacts of these model improvements and additions, especially the impact of an additional coupled nitrogen cycle, and whether they help overcome some of the weaknesses identified in CMIP5. Expanding on the analysis from Anav et al. (2013a) for CMIP5, this study uses CMIP6 concentration and emission driven historical simulations to compare to the land carbon cycle in CMIP5 and identify possible improvements in the newer model generation.
75 Jones et al. (2023) drew on expert assessment of regional carbon budgets to evaluate the terrestrial carbon cycle in CMIP6 models and came to similar conclusions. The multi-model mean performs well in most regions for most variables (both carbon fluxes and stocks), but individual models have strengths and weaknesses. In this study we restrict ESM evaluation to datasets with global extent.

Section 2 describes the data used in this study, while Section 3 contains the analysis of different carbon cycle variables in
80 the comparison between CMIP ensembles and observations. Long-term trends and the seasonal cycle of carbon cycle variables are considered, and the analysis is concluded with a performance metrics plot evaluating the climatological seasonal cycle of the models with different observational data sets. Section 4 summarizes the results and conclusions.

2 Data and Tools

2.1 CMIP simulations

85 Model simulations from both CMIP Phase 6 (Eyring et al., 2016a), and Phase 5 (Taylor et al., 2012) are used, with Tables 1 and 2 listing model characteristics such as their atmosphere and land model components in addition to their main references.



A more comprehensive summary of the land model components of the CMIP models is given in Appendix A. Models were selected due to their availability on Earth System Grid Formation (ESGF) nodes for the considered variables.

This study focuses on historical simulations, which aim to reproduce the observed climate since the pre-industrial times. They span from 1850 to 2005 (CMIP5) and 1850 to 2014 (CMIP6). Both simulations with prescribed greenhouse gas concentrations (concentration driven) and prescribed CO₂ emissions (emission driven) are considered, but evaluated separately and compared to each other. Models participating in the emission driven simulations, marked in bold in the tables, use their interactive carbon cycle to determine the distribution of natural and anthropogenic carbon fluxes across the land, marine and atmospheric reservoirs instead of relying on prescribed atmospheric CO₂ concentrations (Friedlingstein et al., 2014).

Very few CMIP5 models had a coupled carbon-nitrogen cycle. While the BNU-ESM model included carbon-nitrogen interactions, they were turned off for the CMIP5 model simulations as the nitrogen cycle had not been fully evaluated (Ji et al., 2014). Therefore, a nitrogen cycle was included in two out of 18 CMIP5 models (CESM1-BGC, NorESM1-ME) which both use the CLM4 land model and in 15 out of 23 CMIP6 models spread over six different land models - with CLM in different versions accounting for eight CMIP6 models (v5: CESM2, CESM2-WACCM, NorESM2-LM, NorESM2-MM, v4.5: CMCC-CM2-SR5, CMCC-ESM2, v4: SAM0-UNICON, TaiESM1). The other land models in CMIP6 with a coupled nitrogen cycle are LPJ-GUESS (EC-Earth3-CC, EC-Earth3-Veg), JSBACH (MPI-ESM-1-2-HAM, MPI-ESM1-2-LR), CABLE+CASA-CNP (ACCESS-ESM1-5), JULES-ES (UKESM1-0-LL) and Visit-e (MIROC-ES2L). This shows a large bias towards the CLM land model in CMIP6 which needs to be considered while analyzing the multi-model mean (MMM).

To facilitate a direct comparison of CMIP5 and CMIP6 data in figures containing temporal means, only data up to 2005 representing the end of the CMIP5 historical simulations is considered. Unless stated otherwise, figures use mean data over the time period 1986-2005. Only one realization per model is used, as different ensemble members perform similarly to each other with respect to the carbon cycle and using an ensemble mean would lead to an under representation of the internal variability present in individual ensemble members. Multi-model means (MMMs) were computed separately for each product and experiment combination, as well as an additional distinction between models with and without interactive nitrogen models, and are computed on the monthly gridded data, for which models are regridded to a common 2°x2° grid. MMMs are neither weighted according to the interdependence of the models and model components, nor according to their performance relative to observational products.

While we split models into groups only dependent on the presence of an interactive nitrogen cycle in this study, vegetation dynamics is another important process for ESM comparison. Models interactively simulating vegetation cover may simulate trees or grasses in the wrong areas compared to models using observational land cover maps, impacting variables with a strong relation to land cover, such as LAI or GPP. While models with prescribed land cover may show better LAI in the present day, they cannot predict future changes in vegetation cover nor their impact on regional climate and carbon processes. For reference, Tables 1 and 2 note models with dynamic vegetation with a D in the comment column.



2.2 Reference Data

120 A large range of observations and reanalysis data sets have been used to assess model performance. These data sets are listed
in Table 3 along with their main reference(s), their source, the variables used and their temporal coverage. Both observational
and reanalysis data sets will be referred to as “observations” from here on, to contrast the results from the CMIP model
simulations. The longest observational records are derived from reanalyses, while satellite observations only provide data since
the late 20th century. Since most reference data sets do not come with observational uncertainty, a common approach is to
125 use several reference data sets per variable where available, as noted in Seiler et al. (2022). This approach is also taken in this
study.

For the leaf area index (LAI), we use the LAI3g product (Zhu et al., 2013) that provides global monthly gridded data
starting in the year 1981. It has been generated using an artificial neural network based on data from the Advanced Very High
Resolution Radiometer (AVHRR) and the Moderate Resolution Imaging Spectroradiometer (MODIS). Furthermore, we also
130 use the newly released GIMMS LAI4g data set (Cao et al., 2023) which is based on the same satellite data as LAI3g but
employs a newer NDVI data set base which removes the effects of the satellite orbital drift and AVHRR sensor degradation,
which plagued many other LAI data sets. Furthermore, LAI4g uses a large number of high-quality Landsat LAI samples to
increase the spatiotemporal consistency of the data set. Lastly, the Global Land Surface Satellite (GLASS; Liang et al., 2021)
is a product suite with 12 products, of which we employ both the leaf area index (LAI) and gross primary productivity (GPP)
135 products. Similarly to LAI3g and LAI4g, GLASS is based on data obtained from AVHRR and MODIS. As newer GLASS data
products only use MODIS and thus start from 2000, this paper uses a previous GLASS version (v4.0) which includes AVHRR
data and thus starts in 1981 for LAI and 1982 for GPP respectively. GLASS LAI uses general regression neural networks
trained on preprocessed reflectance data of an entire year to estimate the one-year LAI profile for each pixel. The LAI product
is one of the variables used to estimate GLASS GPP with an Eddy Covariance-Light Use Efficiency model. Both GLASS
140 products are available on a 0.05° grid with a frequency of 8 days.

Another GPP product, MTE (Jung et al., 2011), provides global monthly gridded data starting in 1982. It uses an upscaling
of data from the FLUXNET eddy covariance tower network based on the model tree ensembles (MTE) approach. Similarly,
the FLUXCOM product (Jung et al., 2019) is also based on an upscaling of FLUXNET site level observations, but additionally
incorporates a larger variety of machine learning methods, and also includes remote sensing (from MODIS) and meteorological
145 data. Here, we use a global monthly gridded version of FLUXCOM (starting in 1980) from the RS+METEO setup. Due to the
assumption of an unchanging average CO_2 level, both MTE and FLUXCOM data is known to have an unrealistic non-existent
trend (0.01 PgC yr^{-2} globally) (Anav et al., 2015). Thus trend analysis on GPP should exclude these data sets.

The main data set for the land-atmosphere carbon flux (NBP) is the JENA-CarboScope (version sEXTocNEET_v2020)
product (Rödenbeck, 2005), which provides global daily gridded data starting from the year 1957. This data set provides
150 surface-atmosphere CO_2 fluxes based on atmospheric measurements calculated from an atmospheric transport inversion. The
inversion used here (NEE-T inversion) involves a regression of interannual net ecosystem exchange (NEE) anomalies against
air temperature anomalies (T). In total, JENA-CarboScope uses data from 156 atmospheric measurement sites distributed



across the entire globe. The alternative data set for the land-atmosphere carbon flux is a further inversion product from the Copernicus Atmosphere Monitoring Service (CAMS; Chevallier et al., 2005, 2010; Chevallier, 2013). CAMS provides global gridded data on a monthly resolution starting in 1979 (other temporal resolutions are also available). The inversion product we use here (v20r2) is based on surface measurements from more than 100 sites. A third data set used for comparing the global annual mean NBP is the Global Carbon Project (GCP; Friedlingstein et al., 2022), which estimates the global carbon budget using several observations and models. It provides estimates for emissions from fossil fuel combustion and industrial processes, emissions from land-use change, atmospheric CO₂ growth rate, ocean sink, land sink, cement carbonation sink and the budget imbalance from combining all these terms. The land-atmosphere carbon flux for GCP has to be calculated by subtracting the land-use change emissions from the residual land sink. The land sink was obtained from averaging the results from seventeen Dynamic Global Vegetation Models (DGVMs) which reproduce the observed mean total land uptake of the 1990s and is given with an uncertainty of $\pm 0.5 \text{ PgC yr}^{-1}$ on average. The land use change emissions are estimated from the average of three bookkeeping models with an uncertainty of $\pm 0.7 \text{ PgC yr}^{-1}$, making it one of the only data sets with direct estimations for uncertainties.

For each of the remaining carbon cycle variables, only a single reference data set is taken into account. For the vegetation and soil carbon pools, the NDP-017b (Gibbs, 2006) and HWSD+NCSCD (Wieder, 2014; Hugelius et al., 2013) products are used, respectively. Both data sets provide global gridded annual data for the single year 2000. NDP-017b uses an updated database that extends the methodology of Olson et al. (1985), who developed a global carbon stocks map of above and below ground biomass using 20 years of field investigations, consultations and literature analysis, to more up-to-date land cover conditions of the Global Land Cover Database (GLC2000). The Harmonized World Soil Database (HWSD) uses large volumes of regional and national soil information to create an empirical data set that provides soil parameter estimates for topsoil (0–30 cm) and subsoil (30–100 cm). Similar to Varney et al. (2022) we combine the HWSD data set with the Northern Circumpolar Soil Carbon Database (NCSCD; Hugelius et al., 2013) to complement the HWSD data in the polar region. It uses data on soil order coverage to calculate soil organic carbon content and mass with 1778 pedon data. Wherever overlap between the two data sets occurs, the NCSCD data is chosen.

2.3 ESMValTool



The analysis in this paper was produced using the Earth System Model Evaluation Tool (ESMValTool) version 2 (Righi et al., 2020; Eyring et al., 2020; Lauer et al., 2020; Weigel et al., 2021; Schlund et al., 2023). ESMValTool is an open source community diagnostics and performance metrics tool which has been developed to routinely evaluate ESMs contributing to CMIP and compare them with other ESMs, predecessor versions, as well as observations. Since its first release (Eyring et al., 2016b), ESMValTool has been updated for increased performance in its core functionality to deal with the increased data volume of CMIP6, and now features full traceability and reproducibility through provenance, as well as new and updated diagnostics and metrics, which can be applied to many models and variables. Available diagnostics cover a large range of scientific topics and are described in three papers. They include large-scale diagnostics for quasi-operational and comprehensive evaluation of ESMs (Eyring et al., 2020), diagnostics for extreme events, regional model and impact evaluation and analysis



(Weigel et al., 2021), and diagnostics for emergent constraints and analysis of future projections (Lauer et al., 2020). A new suite of recipes has been developed covering the work of this study, as well as some improvements on previous diagnostics for the carbon cycle available in ESMValTool. This facilitates the evaluation of the carbon cycle in future studies, including the analysis of upcoming CMIP7 simulations that can be easily compared to CMIP5 and CMIP6 to assess improvements.

3 CMIP model performance

General climate variables, such as temperature and precipitation have a large influence on the carbon cycle. It is therefore important to assess how well these variables are simulated by the ESMs. If they are well reproduced but carbon cycle variables are not, it is likely due to a poor representation of processes specific to the carbon cycle, while a poor performance in the physical variables makes an attribution of the cause of poor performance in the carbon cycle variables more difficult. The CMIP6 ensemble has been assessed compared to observations by Flato et al. (2013) and Eyring et al. (2021) respectively. A detailed analysis was also done by Bock et al. (2020) and references therein, who compare the surface temperature, pressure, precipitation, radiation, and clouds of CMIP3, CMIP5 and CMIP6 historical simulations for annual means. The CMIP6 models show better correlations for these variables than the CMIP5 models for all parameters, with smaller improvements for variables such as temperature which were already well represented in previous CMIP phases. However, the model spread is not significantly reduced but instead largely remains the same. Here, we expand the analysis to the carbon cycle. However it should be mentioned, that many carbon cycle processes are affected by physical variables on much smaller timescales, such as timing of precipitation throughout the day, or if surface temperatures fall below the freezing point at any time of the day may impact the growth of plants more than their monthly means suggest. This study uses monthly mean data which does not resolve many of these important events and thus does not investigate the impact of physical variables further, as any analysis would still be lacking many possible impacts of sub-frequency effects. Future studies using higher frequency data will put more emphasis also on the physical drivers of carbon processes.

3.1 Leaf Area Index

The Leaf Area Index (LAI) is the ratio of one-s leaf area per unit ground area (Anav et al., 2013a) as a measure of the canopy structure. Models use LAI to calculate the photosynthetic uptake of the total canopy, also known as gross primary productivity (GPP). While LAI is an important building block for the carbon cycle, it was also one of the weaknesses of the carbon cycle in the CMIP5 ensemble and tended to be overestimated (Anav et al., 2013a, b).

Carbon uptake by land follows a pronounced seasonal cycle, with CO₂ removed from the atmosphere through plant photosynthesis and released back through plant and soil respiration. With LAI describing the canopy structure and more plants thriving in summer, it is strongly linked to the seasonal cycle of atmospheric CO₂. The seasonal cycles for LAI for CMIP5 and CMIP6 MMMs for concentration and emission driven simulations are shown in Figure 1, split into models with (Ncycle) and without interactive nitrogen cycle (non-Ncycle), as well as different regional means: Global, Northern Hemisphere (20°N - 90°N; NH), Southern Hemisphere (20°S - 90°S; SH) and Tropics (20°S - 20°N). From here on, concentration driven sim-




ulations will be denoted by c, such as CMIP5c and CMIP6c, and emission driven simulations by e (CMIP5e, CMIP6e). The
220 BNU-ESM and MRI-ESM1 CMIP5 models were removed from the MMM due to featuring an unrealistically high mean LAI,
almost doubling the LAI of the reference data and the other models in the SH and the tropics. A common mask is applied to
all data sets which includes all missing values in any data set to allow for direct comparison between the models and reference
data sets. This increases the LAI compared to unmasked regional means, as missing values are more common in desert and
mountainous regions with low LAI (Fig. 3). The chosen reference data sets LAI3g, LAI4g, and GLASS agree well across all
225 regions, which was to be expected as they are all based on the same raw satellite data from AVHRR and MODIS. Xiao et al.
(2017) found that the GLASS product outperformed other products, which included LAI3g, when compared to LAI from high-
resolution reference maps. As such, GLASS, which is also the reference data set with the largest coverage, will be considered
the main reference data set for our analysis of LAI.

There is a strong seasonal cycle in the NH, dominated by high-latitude vegetation in Eurasia and North America. The NH
230 seasonal cycle is the dominant contribution to the global mean due to the higher relative land fraction in the higher latitudes of
the global north compared to the global south. The tropics do not show a seasonal cycle due to the absence of strong seasons,
while the vegetation in the SH is dominated by forests closer to the tropics, which also lack strong seasonality. All models
overestimate LAI in all regions, but the CMIP6 models reproduce the reference data better than the CMIP5 models. According
to Anav et al. (2013b), the overestimation in the mid-latitudes is likely partly due to a wet bias and its control on soil moisture,
235 a saturation of satellite instrumentation, and missing parametrizations of disturbances. The annual mean precipitation wet bias
is minimally reduced in CMIP6 (Bock et al., 2020) and new parametrizations such as nutrient limitations through interactive
nitrogen cycle have been introduced in some models, leading to a reduced LAI in the CMIP6 MMMs compared to CMIP5.
The seasonal cycle in the NH is reproduced, but while the CMIP5 non-Ncycle models reproduce the amplitude well with a
positive offset of approximately $0.7 \text{ m}^2/\text{m}^2$, the CMIP6 non-Ncycle models are better at reproducing the peak value. Both
240 CMIP5 Ncycle models (CESM1-BGC and NorESM1-ME) use the CLM4 land model with known issues regarding LAI, such
as underestimating LAI in dry regions due to elevated CO_2 and overestimating LAI in moist regions (Lee et al., 2013), as well
as an unrealistically strong nitrogen limitation (Wieder et al., 2019), hindering plant growth. This leads to these models showing
a larger overestimation in LAI in both the Southern Hemisphere and Tropics dominated by moist rainforests. Additionally, the
seasonal cycle amplitude is strongly reduced in the NH while the mean LAI is larger than for the reference data sets. Both CMIP
245 projects show a weakness in simulating the end of the growing season, shown by the later decline of LAI in winter, which also
leads to a smaller seasonal cycle amplitude, consistent with the findings of Park and Jeong (2021). The drawdown in autumn
signifying the end of the growing season is smaller in Ncycle models compared to non-Ncycle models. The differences between
the concentration and emission driven simulations are small, with models participating in both simulations having very similar
results (individual models not shown). Larger differences occurring here and in later analysis between the concentration and
250 emission driven simulations are likely due to the different subset of models in the historical simulations, and not due to the
experiment design.

Figure 2 shows the mean and trend of LAI averaged over 1986-2005 and depicts project-experiment simulations with one
type of marker each for a better overview: Blue '<' markers are assigned to CMIP5 models, red '>' markers to CMIP6 models,



an 'x' in the corresponding color denotes the multi-model means, and the black  '★' represents the mean of the reference
255 data with error bars showing its standard deviation. Within the CMIP projects, the darker color is used for data from the
emission driven simulations, while the lighter color denotes results from the historical simulations. Filled symbols are used for
models or multi-model means with nitrogen cycle. Exact numbers for all data sets are found in the supplementary information
(Tables S1-S2). The errors given in the tables refer to the standard deviation of the mean as a measure for the interannual
variability (IAV), while the standard error of the trend is the error of the linear regression calculating the trend. For the individual
260 reference data, LAI3g and LAI4g agree well in mean and trend, while GLASS agrees with their mean but shows a significantly
higher trend in all regions, leading to the large trend error bar. Xiao et al. (2017) analyzed the trend of several LAI products for
different biome types for 1982-2011 and found GLASS to have significantly higher trends in savannahs and shrubs compared
to LAI3g, but lower trends in deciduous broadleaf forests, evergreen needleleaf forests and even a negative trend for deciduous
needleleaf forests, while grasses, cereal crops and evergreen broadleaf forests trends are similar for GLASS and LAI3g. This
265 results in larger trend differences in the SH ($0.009 \text{ m}^2/\text{m}^2 \text{ yr}^{-1}$) and Tropics ($0.010 \text{ m}^2/\text{m}^2 \text{ yr}^{-1}$) than the NH ($0.003 \text{ m}^2/\text{m}^2$
 yr^{-1}). The MMM global means show a significant overestimation compared to the reference data, with the overestimation of
the CMIP5 MMMs of $0.7 \text{ m}^2/\text{m}^2$ reduced by half for CMIP6 MMMs, as previously seen in Figure 1. This large improvement
for the CMIP6 models is not related to the difference between Ncycle and non-Ncycle models, as their LAI MMM global
means are comparable for CMIP6. Due to the large difference in trends in the reference data sets, the global mean trends of all
270 CMIP MMMs lie within the range of the reference data. The model trends range between slightly negative to strong positive.
Unlike the mean, the LAI trend does not show a strong difference between CMIP projects, nor any other grouping method we
employed. The CMIP6 models only show a slightly smaller range in trend compared to the CMIP5 models, but more CMIP5
models have a lower trend compared to the reference data sets than CMIP6 models.

The other regions reflect these global MMM comparisons as well. CMIP6 means are closer to the reference data than CMIP5
275 in all regions, albeit still overestimating LAI, and agree well with each other no matter the experiment or Ncycle status. The
only exception is the NH CMIP6c Ncycle MMM, which shows a larger mean than the other three CMIP6 groupings. This is
due to the CMCC-ESM2 and CMCC-CM2-SR5 models, which show a much higher LAI in the NH compared to the reference
data, but fit well in the other regions. These two models use the CLM4.5 land model, which Li et al. (2022) found to have a
far longer peak growing season and to overestimate LAI in boreal forests compared to MODIS reference data, consistent with
280 our results. The CLM5 models (CESM2, CESM2-WACCM, NorESM2-LM, NorESM2-MM) perform much better in mean
LAI than CLM4.5 in the NH, but are still overestimating LAI compared to the reference data. The trends in the NH for the
reference data are on the lower end of a large model range. Only the CMIP5 non-Ncycle MMMs agree with the reference data,
while the other MMMs show a larger trend than the reference data but comparable to each other. CMIP6 MMM LAI mean
and trend agree well with the reference data in the tropics and the SH, while the CMIP5 MMMs overestimate the mean by \approx
285 $0.7 \text{ m}^2/\text{m}^2$ in the SH and $\approx 0.6 \text{ m}^2/\text{m}^2$ in the tropics for non-Ncycle, as well as $\approx 1.2 \text{ m}^2/\text{m}^2$ in the SH and $\approx 1.1 \text{ m}^2/\text{m}^2$ in the
tropics for Ncycle MMMs, but show a similar trend to LAI3g, LAI4g, and CMIP6 MMMs. The larger mean LAI in the CLM4
(CMIP5 Ncycle MMMs) can be traced back to the overestimation of LAI in moist regions mentioned before. Some models



show a significant negative trend in LAI in the SH and the tropics resulting in a globally negative trend even with a positive trend in the NH.

290 Maps of the LAI reference data are found in Figure 3, without the common mask to see the different coverages. Coverage of the different reference data sets varies a lot due to different quality control criteria and algorithms, with most missing values found in desert or mountainous regions such as the Sahara and the Himalayas. Additionally, a mean of the reference data and the range of the reference data per grid cell is shown, along with the global mean of the values in the upper right corner. GLASS has a larger coverage over desert and mountainous regions, which are regions with low plant coverage and thus low
295 LAI, resulting in a lower global mean LAI of $1.36 \text{ m}^2/\text{m}^2$ compared to $1.67 \text{ m}^2/\text{m}^2$ and $1.71 \text{ m}^2/\text{m}^2$ from LAI3g and LAI4g respectively. This underlines the importance of the common mask used for figures 1 and 2 to obtain comparable results. The different data sets show the same pattern of LAI distribution, with the absolute values ranging between 1 and $6 \text{ m}^2/\text{m}^2$, while the differences are below $2 \text{ m}^2/\text{m}^2$ with the largest difference occurring in tropical rain forests and northern high latitudes, the regions with the largest absolute LAI values. For a gridcell bias comparison of the different model groupings (Fig. 4)
300 a combined reference data set was computed as the mean of the other reference data sets. Due to the different coverages, some areas are only calculated from the GLASS data, while others are an average of all three data sets. The range of values per gridcell going into the combined data set is plotted in the lower right of Figure 3. The largest difference occur in the areas with larger LAI as the tropical rainforests followed by boreal forests, with a global mean average range of $0.38 \text{ m}^2/\text{m}^2$. For the MMM bias maps shown in Figure 4 hatching is added where the MMMs agree with the reference mean within the
305 MMM standard deviation. CMIP5 Ncycle MMMs show the issue of CLM4 in overestimating LAI in wet regions, with LAI in tropical rainforests almost doubling the reference value, while drier regions show a significant negative bias. While this results in a global mean bias of 0.66 to $0.67 \text{ m}^2/\text{m}^2$ smaller than $0.89 \text{ m}^2/\text{m}^2$ for CMIP5e non-Ncycle MMMs, it is still the worst performing model grouping when considering a gridcell basis due to its extreme biases in both directions. The hatching showing the agreement can be ignored in this case, as only two models contributed to the MMM std. The CMIP5e non-Ncycle
310 MMM shows a strong overestimation across the northern latitudes besides Greenland. This can be attributed to the GFDL-ESM2G and GFDL-ESM2M models, which are known to have established coniferous trees in areas which should contain tundra or cold deciduous trees, as its vegetation spin-up only coniferous trees are allowed to grow in cold regions, but not grasses or deciduous trees which would have a lower LAI (Anav et al., 2013b). While the GFDL models show this problem in both CMIP5c and CMIP5e, due to the larger number of MMMs contributing to the concentration driven simulations, their
315 effect is reduced. In CMIP6, GFDL-ESM4 still has a large positive LAI bias throughout these areas, but it is significantly reduced compared to its CMIP5 predecessor. The second prominent overestimation is around the tropical rainforests, where models like BNU-ESM, MRI-ESM1, and in lesser extent also the GFDL models extend the LAI hotspot to larger areas around it compared to the reference mean. In CMIP5c HadGEM2-CC and HadGEM2-ES also show this overestimation. CMIP5c non-Ncycle MMM shows no special bias patterns, but instead a general overestimation in almost all areas with hatching present
320 throughout the globe. CMIP6 MMMs show a reduced mean bias of less than half the CMIP5 overestimation, with almost no pronounced patterns and a bias reduction in all areas, with the largest improvements found in the northern high latitudes. The largest bias is in southeast asia for CMIP6c Ncycle MMMS which can be tracked to the CMCC-ESM2 and CMCC-CM2-SR5




models, and makes the mean bias of the CMIP6c Ncycle MMM higher than that of CMIP6c non-Ncycle MMM. Otherwise, the bias pattern looks similar for CMIP6 Ncycle and non-Ncycle models.

325 While CMIP6 LAI has improved compared to CMIP5, especially a significantly reduced mean bias, a general overestimation of LAI remains, along with issues of correctly reproducing the length of the growing season in the northern hemisphere, and a large model spread in mean and trend LAI. Neither the introduction of an interactive nitrogen cycle nor the comparison between emission and concentration driven simulations show large differences in the overall quality of the CMIP6 simulations for LAI.

330 3.2 Gross Primary Productivity

Gross primary productivity (GPP) represents the CO₂ uptake on land due to photosynthesis. This was one of the biggest weaknesses of the CMIP5 ensemble, with most models overestimating photosynthesis as well as leaf area index (Anav et al., 2013a). The seasonal cycle of GPP (Fig. 5) shows good agreement between the GLASS and MTE reference data, while the FLUXCOM data shows a lower GPP in all regions, as well as a shorter growing season in the Northern Hemisphere. All models
335 reproduce a similar shape of the NH seasonal cycle to the GLASS and MTE data in both model generations and experiments. As found in Anav et al. (2013a) the CMIP5 non-Ncycle models overestimate GPP in all regions, while the CMIP5 Ncycle models strongly underestimate the peak of the seasonal cycle in the NH. CMIP6 models perform better than CMIP5, but while the CMIP6 non-Ncycle models still overestimate the GPP peak in summer similarly to CMIP5 for the NH, the Ncycle models show a very good agreement for both CMIP6c and CMIP6e. Nitrogen limitation is stronger in northern latitudes
340 through boreal forests and tundra (Du et al., 2020), as compared to tropical and subtropical forests, which are more limited by phosphorus. However, from the CMIP models used in this study, only ACCESS-ESM1-5 includes an interactive phosphorus cycle. It therefore makes sense that Ncycle models show a decreased GPP compared to non-Ncycle models in the NH, closer to reference data. The model spread remains large in CMIP6, albeit smaller for Ncycle models, which is denoted by horizontal hatching. Following LAI, there is no strong discernible seasonal cycle in neither the SH nor the Tropics, but the CMIP6 models
345 are closer to the mean GPP than the CMIP5 models, with lower values for Ncycle models.

The temporal mean and linear trend of the spatial sums for GPP during the time period 1986-2005 is shown in Figure 6. MTE and FLUXCOM data  shown to have an unrealistic non-existent trend (0.01 PgC yr⁻² globally) due to the assumption of an unchanging average CO₂ level (Anav et al., 2015) in these data sets. As such, the model trend should not be compared to the trend of these two reference data sets, and we have omitted these data sets from the calculation of the reference trend.
350 The mean and trend for GPP of all regions of these data sets along with all other numerical values from the plot can be found in Tables S3-S4. The trend of GLASS is closely linked to the high trend of LAI GLASS, one of the main influences on GPP. The reference data sets agree well in mean GPP with the largest difference being a lower mean for FLUXCOM in the NH. The models show a large range with MRI-ESM1 CMIP5e as an outlier, which shows an even larger mean GPP in all regions. The CMIP5 models are on the higher side of this range, with the Ncycle CMIP5 models much lower due to their underestimation
355 in the NH as seen in Figure 5. The CMIP6 Ncycle MMMs agree very well with the reference data, while the CMIP6 non-Ncycle MMMs show a larger mean GPP. The global trend of GLASS is positive, which is well matched by the non-Ncycle



CMIP6c MMM with the other MMMs showing a smaller trend. In the NH, more CMIP5 models overestimate the mean GPP than CMIP6 models. The MMMs span a large range, with the Ncycle MMMs showing a lower mean GPP than the non-Ncycle MMMs which are overestimating GPP compared to the reference data. The models are clustered around the GLASS trend, with outliers for MRI-ESM2-0 in both its CMIP6c and CMIP6e runs. The CMIP6 non-Ncycle MMM shows a higher trend than the other MMMs due to the MRI-ESM2-0 outliers. In the SH mean GPP, the CMIP6 MMMs match the reference data well with lower values for Ncycle than for non-Ncycle MMMs. The CMIP5 MMMs are slightly above these, with the non-Ncycle CMIP5e having a much larger value due to the outlier of MRI-ESM1 and FIO-ESM both with values well above 100 PgC yr^{-1} . The MMMs underestimate the trend compared to the reference data. The distribution in the tropics is very similar as the SH. The reference data trend is underestimated by the MMMs. In summary, the Ncycle MMM shows a better performance than the non-Ncycle MMM in the NH, while it shows a slight underestimation in the tropics and a similar performance in the SH. The model spread over the trend in GPP stays similar throughout the model generations, with the mean trend being largely consistent with the GLASS reference data set in all regions but underestimated everywhere but in the NH.

As for LAI, the coverage of the GLASS data is larger than for the other reference data, with missing values for FLUXCOM and MTE mainly found over the Sahara and the Himalayas (Fig. 7), GLASS shows a larger GPP in the tropical rainforests and boreal forests, explaining the larger mean GPP seen before. The reference mean data set has hardly any missing values left and the largest difference in the data sets are at places with the highest GPP, with discrepancies in the areas bordering the hotspots of the rainforests and boreal forests. Even though the GPP bias maps (Fig. 8) for Ncycle CMIP5 MMMs have a global mean bias almost two magnitudes smaller than the CMIP5 non-Ncycle MMMs, they show the same pattern of overestimation in wet regions and underestimation in dry regions found for LAI (Fig. 4), underlining the strong influence of LAI on GPP. The CMIP5 non-Ncycle MMMs also shows similar patterns to the LAI bias maps, but the overestimation in the areas around the tropical rainforests is strongly reinforced, while the previous strong overestimation of LAI in the northern high latitudes for the non-Ncycle CMIP5e MMM is reduced. The CMIP5c non-Ncycle MMM additionally shows a strong underestimation at the northeastern coast of South America. The global mean bias for CMIP5 non-Ncycle MMMs lies at $3.6 \cdot 10^{-13} \text{ PgC m}^{-2} \text{ yr}^{-1}$ for CMIP5e and is reduced by half for CMIP5c. This bias is further reduced to approximately $1.0 \cdot 10^{-13} \text{ PgC m}^{-2} \text{ yr}^{-1}$ for CMIP6 non-Ncycle MMMs, which show similar bias patterns to CMIP5 non-Ncycle MMMs but overall reduction to the bias patterns, with a larger reduction in the savannah regions of Africa. The global mean bias for the CMIP6 Ncycle MMMs is further reduced to $0.01 \cdot 10^{-13} \text{ PgC m}^{-2} \text{ yr}^{-1}$ for CMIP6e and a negative bias of $-0.4 \cdot 10^{-13} \text{ PgC m}^{-2} \text{ yr}^{-1}$ for CMIP6c. Both show a reduction in the northern hemisphere bias of the open shrublands, turning some into a negative bias, as well as southwest Africa, while the slight overestimation in North America remains, as well as the underestimation at the north eastern part of South America. This is summarized in Figure 9, which shows the zonal sums of the reference data and the MMMs. Unlike the seasonal cycle and scatterplots shown before, a common mask is not applied here, but instead values are masked out if a data set has more than 15% of a latitudes land points set to missing values. The large overestimation of non-Ncycle CMIP5e can be seen which is reduced in non-Ncycle CMIP5c, with both showing a peak slightly north of the equator which is not seen in the reference data and which is due to the overestimation of the shrublands south of the Sahara. The CMIP6 non-Ncycle MMMs show a much better approximation across all latitudes, with a slight reduction of the bias in the NH, but



still show a significant overestimation in the tropics. This is remedied in the CMIP6 Ncycle models, which show a very good agreement with the reference data across all latitudes, now with slight underestimations at high latitudes.

3.3 Land-Atmosphere Flux

395 The net carbon flux from the atmosphere into the land (net biome productivity, NBP) characterizes the balance between carbon
uptake due to photosynthesis and carbon release by respiration, as well as other processes like fires and de- and afforestation.
Positive values of NBP denote carbon uptake by land. The CMIP6 EC-Earth models (EC-Earth3-CC, EC-Earth-Veg) are
excluded from the MMM for NBP because they show a very strong land source in December in seemingly random grid cells
all over the globe. MIROC-ESM and MIROC-ESM-CHEM are also removed for a similar reason: they contain grid cells which
400 seemingly randomly show large sources and sinks popping up in random months. Due to their appearance at random months
instead of only in December like in EC-Earth, it does not influence regional means or climatologies as much, but can be seen
in mean map plots very well.

Figure 10 shows the global evolution of the land-atmosphere flux for CMIP5e, CMIP5c, CMIP6e and CMIP6c simulations in
order from top to bottom. Each panel shows the MMM of all models with simulations in the respective project and experiment
405 combinations (blue line), as well as the two MMMs of models with (dashed orange) and without (dashed green) nitrogen cycle.
The colored shading represents the standard deviation of their respective MMMs. For comparison with observations, data from
CAMS (dashed black), Jena CarboScope (solid black), and GCP (dash-dotted black) are added to each panel. There is a large
year-to-year variability, which can also be seen in the models. All project-experiment combinations agree with all reference
410 data sets, with the CMIP6 simulations showing a better agreement in the 1990s, during which the CMIP5 models generally
underestimate the land carbon sink. From 1850 to 1970 the models do not show a significant carbon source or sink, only the
CMIP6e MMM shows a small carbon source in this time period. However, the model variance as indicated by the shaded areas
is large enough to be in agreement with a neutral state. Since the 1980s the land has been acting as a carbon sink which is
increasing over time. This increase has previously been attributed mainly to the fertilization effect from rising atmospheric CO₂
415 concentrations (Canadell et al., 2021). In the CMIP5 simulations, Ncycle and non-Ncycle models do not show any significant
differences before 1980, after which the Ncycle models show a slightly lower carbon flux. Ncycle CMIP6 models show a
slightly lower land-atmosphere carbon flux over the full time period compared to non-Ncycle models.

The global seasonal cycle for NBP (Fig. 11) is dominated by the northern hemisphere, with almost no discernible cycle
in the southern hemisphere or the tropics. There is generally a good agreement between the two inversions, but the CAMS
inversions shows a larger seasonal cycle in the SH and tropics of approximately 6 PgC yr⁻¹, where CarboScope shows no clear
420 seasonal cycle. In the NH, and due to its large contribution to the total also globally, CAMS has a higher NBP at the start of
the year and to a lesser degree at the end of the year, where CarboScope shows a larger negative NBP and thus carbon sink.
The models agree with the carbon sink of CarboScope in these months, but have a weaker carbon sink (higher NBP) in NH
autumn. The CMIP5 Ncycle MMMs have a smaller seasonal cycle amplitude compared to any of the other MMMs and the
reference data, carried over from GPP. The other MMMs reproduce the seasonal cycle well, while the non-Ncycle CMIP6
425 MMM is shifted late by a month, showing possible issues with the start and end of the growing season. In the SH and tropics,



where CarboScope found no significant cycle and CAMS had a slightly larger one in the tropics, the Ncycle models follow the shape and timing of the CAMS data, while the non-Ncycle models have a seasonal cycle shifted to two months earlier. There is no significant difference between CMIP5 and CMIP6 nor between c and e experiments in the MMM.

The temporal mean and trend of spatially summed NBP is shown in Figure 12 with specific values given in Tables S5 and
430 S6. CAMS shows a larger mean NBP compared to CarboScope in all regions but the tropics, which is consistent with the NBP averages from Seiler et al. (2022) using this data set and who found its NBP to be larger than comparable data sets and model results. GCP as a global average is only available as reference data set for the global panel. The models show a far larger range for global mean NBP than the reference data, with outliers for the INM-CM CMIP6c models showing a far larger mean NBP than the other models. The Ncycle CMIP5 means have a negative mean NBP, while the other MMMs show
435 a better agreement with the reference data. The Ncycle MMMs have significantly smaller mean NBPs than the non-Ncycle MMMs. The relatively good overall agreement of the models' global mean NBP with the reference data does not hold for the different regions. Most models and all MMMs simulate a lower carbon sink in the northern hemisphere when compared to the inversions, with Ncycle models generally showing a smaller mean NBP, but no large discernible differences between the different groupings. Conversely, while the inversions estimate both the southern hemisphere as well as the tropics to be a
440 slight carbon source due to deforestation, the MMMs with the exception of the CMIP5 Ncycle show a carbon uptake by land in these regions. The large values for the non-Ncycle CMIP6c MMM are again due to the overestimation of the INM-CM4-8 and INM-CM5-0 models, but as their mean NBP in the NH is not a large outlier, we did not remove these from the MMM. The underestimation in the NH combined with the overestimation in the SH and tropics leads to the good global agreement of the total carbon sink. This is in agreement with the findings from IPCC AR6 (Eyring et al., 2021; Canadell et al., 2021). The
445 inclusion of a nitrogen cycle and therefore the inclusion of nitrogen limitations on CO₂ fertilization was expected to address this discrepancy of the distribution of the carbon sinks (Canadell et al., 2021), but the data does not support this, as the Ncycle MMMs do not show a different performance to the non-Ncycle MMMs in CMIP6. While the models show a large range of trends, the MMMs agree well with the reference data, and this continues in the other regions as well. While N-limitation is not expected to be substantial at present day, it represents a major limitation on future land-carbon uptake (Zaehle et al., 2015),
450 and thus its inclusion a major advance in being able to robustly simulate future carbon balance of the terrestrial carbon cycle.

As seen before, the reference data sets show different means, trends and slightly different seasonal cycles in the different regions. For a more detailed look, Figure 13 shows maps of the reference data. The hatched area is the area where the data sets agree on the sign or within a margin of half the bin size of the contour plot. While in large parts of the globe the data sets agree in sign, there are significant differences. In North America CAMS shows a much larger carbon sink than CarboScope
455 which instead shows some carbon sources along the west coast and throughout South America. In CAMS South America is split into a much stronger carbon source in the amazonian rainforests and a carbon sink in the southern part. The data sets also disagree in Europe, which is a carbon source according to CAMS but a sink in CarboScope. Literature found Europe to be a carbon sink for the first part of the 21st century (Ciais et al., 2013; Reuter et al., 2014) using different reference data sets
This would support the CarboScope data set but due to the different time frames considered it is not definitive. CAMS also
460 sees a carbon sink in tropical Africa where CarboScope has a slight carbon source. In South East Asia, CarboScope has a large



carbon sink, where CAMS shows a neutral carbon flux. The area of most agreement is in the NH as a large carbon sink where there is no deforestation and a bit of a forestation. The Amazon region was a large carbon sink which is becoming a source due to deforestation (Gatti et al., 2021). CAMS sees the Amazon as a strong carbon source, while CarboScope shows a smaller source, with a sink in the northwestern region. Keenan and Williams (2018) found inverse models to show South America as both a carbon source, as well as a carbon sink and is thus a hotly debated area. Kou-Giesbrecht et al. (2023) attribute the weak agreement between CarboScope and CAMS to differences in the inversion models and atmospheric CO₂ measurements used, with larger differences at latitudes with smaller land areas. Due to the difference between the observational data sets, the bias maps to a reference mean shown for the other considered variables so far have been omitted. Instead, the area weighted zonal sums are plotted in Figure 14 for comparison of the MMMs with both reference data sets. The reference data sets disagree for almost all latitudes, thus making the model comparison to the reference data in these regions not very meaningful. The area where the reference data is in most agreement is in the northern high latitudes (50–80 °N), where both of them show a strong carbon sink, about double of that shown in both CMIP5 and CMIP6 models. While the issues in CLM4 and thus the CMIP5 Ncycle models are clearly visible (similarly to LAI and GPP), the other MMMs show similar NBP in all latitudes.

3.4 Carbon Stocks


Another large uncertainty in CMIP5 was the amount of carbon stored in soil and vegetation. This leads to large uncertainties in land-use change emissions which are important for quantifying cumulative emissions as well as climate mitigation strategies (Friedlingstein et al., 2023). Varney et al. (2023b) investigated the carbon-climate feedbacks of soil and vegetation carbon and found soil carbon to be the dominant response of the land surface, highlighting the need to reduce the uncertainty in carbon storage to better quantify future changes of the climate system. Figure 15 shows a scatterplot of the global soil and vegetation carbon against the combined soil and litter carbon. The observational soil (HWSD+NCSCD) and vegetation carbon (NDP) data sets are derived from in situ measurements taken over a long period of time and are thus given without a time coordinate, while the models were averaged over 1986-2005. Note that some models (CanESM5-CanOE CMIP6c, GFDL-ESM4 CMIP6e, INM-CM4-8 CMIP6c, INM-CM5-0 CMIP6c, FIO-ESM CMIP5e, CanESM2 CMIP5c and Inmcm4 CMIP5c) did not have data on the ESGF nodes for soil or vegetation carbon and are thus missing from the carbon stocks analysis. BNU-ESM CMIP5c and CMIP5e shows a far larger vegetation carbon than the other models and is thus removed in the calculation of the mean. Additionally, CLM5 and thus CESM2, CESM2-WACCM, NorESM2-LM, and NorESM2-MM include a full vertical soil profile. For these models, the *cSoilAbove1m* variable is used for better comparison with the other models, as done in Varney et al. (2022). The large spread in the global carbon stocks still remains in CMIP6 as shown in Figure 15 with values for each data set listed in Table S7. In CMIP5 vegetation carbon was spread between 335 PgC (MPI-ESM-LR CMIP5c) and 802 PgC (GFDL-ESM2M CMIP5e) with the outlier of BNU-ESM even reaching values above 1200 PgC. The spread has only marginally been reduced in CMIP6 to a range of 333 PgC (EC-Earth3-Veg CMIP6c) to 724 PgC (CNRM-ESM2-1 CMIP6e). The reference data are at a value of 478 PgC, in the lower range of the models, with the MMMs ranging between 465 PgC (non-Ncycle CMIP6c) and 547 (Ncycle CMIP5e). The spread in soil carbon is even larger with a CMIP5 range of 513 PgC (CESM1-BGC CMIP5c) up to 3092 PgC (MPI-ESM-MR CMIP5c). The overestimation by MPI-ESM is due to its decomposition parameterization



495 depending on soil moisture and showing maxima in continental dry lands. In CMIP6 MPI-ESM1-2 the soil carbon model was
changed to YASSO which simulates more plausible soil carbon content (Mauritsen et al., 2019). The spread in soil carbon was
not significantly reduced in CMIP6 with a range of 514 PgC (GFDL-ESM4 CMIP6c) to 2913 PgC (CMCC-ESM2 CMIP6c),
with the reference value for HWSO+NCSCD at 1561 PgC. The CMIP5 Ncycle models have a soil carbon on the lower end
of the range, consistent with the CMIP6 models TaiESM1 and SAM0-UNICON which also use CLM4. The CMIP5 Ncycle
500 MMMs are on the very low end of the range with 532 PgC and 534 PgC for CMIP5 and CMIP5e respectively, while the other
MMMs are closer to the reference data and range between 1197 PgC for non-Ncycle CMIP6c and 2040 PgC for non-Ncycle
CMIP5e. While the CMIP6 Ncycle MMMs are closer to the reference data, no significant improvement due to the inclusion of
the interactive nitrogen cycle can be seen when considering the whole spread of the models. This is consistent with Wang et al.
(2022) who found that changing models from C to CN coupling often result in lowered ecosystem storage, but due to different
505 parametrizations simulate similar carbon pools. Varney et al. (2022) suggest that much of the uncertainty in carbon stocks is
due to the simulation of below-ground processes - this is backed up by the differences in soil carbon being much greater than
in GPP, and thus implicating differences in simulated residence times (Carvalhais et al., 2014; Todd-Brown et al., 2014). For
a more in-depth discussion on we would like to refer to dedicated studies, such as Varney et al. (2022) and Wei et al. (2022).
Furthermore, Varney et al. (2023a) found that while the CMIP6 future soil carbon projections have a lower model spread
510 compared to CMIP5, the structure of soil carbon models within CMIP6 ESMs has likely contributed towards this reduction.

3.5 Overall Model Performance

In this Section we assess the overall performance of CMIP5 and CMIP6 models with respect to carbon cycle variables. Figure
16 shows a performance metrics (portrait) plot similar to Gleckler et al. (2008). It is produced by calculating the normalized
relative space-time root mean square difference (RMSD) of the climatological seasonal cycle of a model variable with respect
515 to a reference observation. The normalization is done relative to the ensemble median of both CMIP5 and CMIP6 models,
with positive values (red) denoting a higher RMSD and thus worse performance while negative values (blue) denote a lower
RMSD than the ensemble median and thus a better performance. As the carbon stocks from the observations do not vary in
time, the calculation of the RMSD as done here is not meaningful and thus only NBP, GPP and LAI are shown in the plot
for all four considered regions (global, northern hemisphere, southern hemisphere, tropics). MMMs for both Ncycle and non-
520 Ncycle models were added, with the models which were excluded from MMMs due to various issues as stated in the previous
sections also removed from the MMM here. Note that the MMMs were calculated on the climatologies prior to calculation of
the RMSDs, so over- and underestimations can cancel each other out. This is the standard for the performance metrics plot
implemented in ESMValTool and kept for consistency. Variables with two reference data sets show the main reference in the
lower right triangle, while the alternate reference is shown for the upper left triangle. data sets marked in bold in Table 3 are
525 the main references. CMIP5 models are shown on the left and CMIP6 models on the right, with figures for both concentration
driven (Fig. 16) and emission driven models (Fig. 17). Models with a nitrogen cycle are marked with blue labels.

Most models have similar scores when compared to the different observations for GPP and LAI, showing that the inter-model
spread  CMIP6 is larger than the observational uncertainty in these variables. For NBP however, models can have different



scores to the considered reference data, which is due to the difference in the reference data found in the previous sections.
530 Models on average perform much better than CMIP5 models, with models that had a predecessor in CMIP5 improving on their CMIP5 performance in almost all variables, such as GFDL and IPSL in all variables and CESM and NorESM in LAI, with the exception of CanESM which shows a reduced performance for NBP in CMIP6. Large improvements can be found in all variables going from CMIP5 to CMIP6, especially in LAI with the exception of the models using the older CLM4 land component (SAM0-UNICON and TaiESM1) in CMIP6 and GPP, which were previously identified as weaknesses in CMIP5.
535 Only the MRI-ESM2-0 model shows a bad performance in both these variables. As mentioned before, dynamic vegetation in models plays a large role in their ability to simulate variables directly related to it, with models interactively simulating vegetation cover (marked with a D in Tables 1 and 2), showing a below average score for LAI and GPP RMSD.


Models which were remarked upon in the previous sections as having good or bad agreement with the observations in specific areas, such as the NBP problems in December for EC-Earth3 have RMSDs that reflect these statements, making this
540 metric a well-suited measure for overall performance. Most models have similar RMSDs in the different regions, with the global value reflecting a mean of the different regions. There does not seem to be a qualitative difference between Ncycle and non-Ncycle models as a whole, but the MMMs perform better than any individual model. The better performance of the MMMs is mathematically expected as long as the assumption that both observations and model simulations draw from the same distribution holds true (Christiansen, 2018). The global NBP, LAI, and GPP are also found in Figure 42 of chapter 3 of the IPCC
545 AR6 (Eyring et al., 2021), which showed not only carbon cycle variables but also other land, ocean and atmosphere variables averaged over 1980-1999 for comparison across models from CMIP3 to CMIP6. Their results are compared to reference data from JMA-TRANSCOM for NBP, LAI3g for LAI, and MTE and FLUXCOM for GPP. As other than NBP these reference sets are the same as the ones considered in this paper, the results are also the same. For NBP despite the different data set, the performance of the models is very similar to the one found for CAMS, our alternative data set. The ILAMB benchmark used in
550 chapter 5 of the IPCC AR6 (Canadell et al., 2021) also comes to the conclusion of model improvement from CMIP5 to CMIP6. No qualitative difference can be found between models that have both emission driven and concentration driven simulations compared to models with only concentration driven simulations, and models with both simulations have similar RMSDs in both. This indicates that carbon exchanges are well simulated in these models as the freely evolving fluxes are comparable to results with prescribed atmospheric concentrations.

555 Centered pattern correlations for these variables and regions are shown in Figure 18, with a score of 1 meaning perfect similarity of a model to the reference data, while a value of 0 signifies no relationship. The longer lines denote the MMM, while the grey circle shows the similarity of the alternate data set to the main reference data set. For GPP and LAI the reference data sets show very good similarity of above 0.9, while for NBP the differences of the references highlighted in Figure 13 is highlighted through a small correlation of up to 0.3, with a high anti-correlation in the southern hemisphere. Due to this,
560 the precise value of the correlation coefficient between models and reference data set is not a good measure, but it can be seen that the models show a large spread. For GPP, the CMIP6 performance in the tropics is vastly improved, with even higher correlation values for Ncycle models. Other than in the NH, the CMIP5 models show a large spread in correlation values, which has reduced for CMIP6. The correlation distribution for LAI is similar as GPP, with the highest correlation values found in the



tropics and globally, but the difference between Ncycle and non-Ncycle models is not as prominent. These overall performance
565 plots underline the specific conclusions from the separate sections above.

4 Summary and Conclusion

To be able to have confidence in  model projections of climate change, Earth System Models first need to show the ability to simulate observed climatologies and trends of the carbon cycle in the present day climate. In the Coupled Model Intercomparison Project Phase 5 (CMIP5, Taylor et al., 2012), several weaknesses of the simulated carbon cycle were found, such as a
570 general overestimation of photosynthesis and a wide range of values for carbon stocks, which became one of the main areas of focus for improvement for some model groups (Delire et al., 2020). In this study, we have analysed the land carbon cycle of models participating in the Coupled Model Intercomparison Project Phase 6 (CMIP6, Eyring et al., 2016a) to investigate whether these weaknesses were improved in the newer model generation, with a special focus on differences arising due to inclusion of an interactive terrestrial nitrogen cycle in some of the CMIP6 models. Concentration and emission driven simu-
575 lations from CMIP5 and CMIP6 models were compared to reference data sets, with 2 out of 18 CMIP5 models and 15 out of 23 CMIP6 models including carbon-nitrogen interactions. We assessed means, trends and seasonal cycles of the leaf area index (LAI), the gross primary productivity (GPP), and the land-atmosphere carbon flux (NBP). We furthermore looked at land carbon stocks to see if the large range of values simulated in CMIP5 was reduced in CMIP6.

In general, CMIP6 models show a better performance across all assessed land carbon cycle variables to differing degrees,
580 and no significant differences between the concentration driven and emission driven simulation were found in the considered variables, that cannot be explained by the number of different models. While there is a bias towards the CLM land component in the CMIP6 models, the different versions (4, 4.5, 5) do not perform the same and thus these versions can be seen as independent components for the multi-model mean.

The leaf area index was a weakness of the CMIP5 simulation, as its seasonal cycle was not well captured and its absolute
585 value was generally overestimated. While the peak of the climatological seasonal cycle of LAI is much better reproduced in CMIP6, the amplitude of the seasonal cycle is weaker in CMIP6 compared to observations due to a weaker drawdown in winter. Thus LAI should remain an area of focus for future model development. Mean LAI is much better reproduced in CMIP6, while the range of trends in the observations is large enough to cover most models for both CMIP5 and CMIP6. It should be noted that due to correlations between parameters, there are often tradeoffs for better reproducing one variable. In CLM5 such a tradeoff
590 had to be weighed between biases for GPP and LAI against high plant functional type (PFT) survivability rates (Lawrence et al., 2019). Therefore, looking at one variable separately instead of the whole model performance can lead to wrong conclusions about the model's ability of reproducing the carbon cycle, depending on which choices were made in the tuning. Similarly, models interactively simulating vegetation cover perform worse in the evaluation of present-day LAI compared to models using observationally derived landcover maps due to simulating trees and grasses in the wrong areas. However, only these models
595 with dynamic vegetation can account for future changes in vegetation and the impact of these changes on climate and carbon processes in future projections.



One of the largest improvements due to the inclusion of an interactive nitrogen cycle was seen in GPP, where the CMIP6 nitrogen cycle models were able to capture the seasonal cycle in the northern hemisphere well, which was previous overestimated. Beside the improvements in the NH, bias patterns in the tropics showing larger GPP overestimations bordering tropical rainforests are reduced in CMIP6 models, with some of these biases wholly removed in the multi-model mean of the CMIP6 models with interactive nitrogen cycle.

The land carbon sink is underestimated in the northern hemisphere regardless of CMIP phase or inclusion of nitrogen cycle. The models compensate for this by simulating a larger carbon sink in the tropics and the southern hemisphere for a global average close to the observed value. An improvement is seen in CMIP6 in capturing the amplitude of the seasonal cycle, which is controlled by carbon uptake through photosynthesis in the growth season and carbon release by respiration. This improvement can largely be attributed to the improved seasonal cycle of GPP.

The large range of soil and vegetation carbon was another large weakness of CMIP5, with inter-model differences of 900 PgC for vegetation carbon and 2500 PgC for soil carbon. This range has not significantly decreased in CMIP6, and it remains an area for improvement.

While we find a significant improvement of the inclusion of the nitrogen cycle for photosynthesis, the effects are reduced for the leaf area index and the land-atmosphere carbon flux. Despite similar NBP for models with and without interactive nitrogen cycle, models without interactive nitrogen overestimate carbon fertilization, leading to large differences of atmospheric carbon content for future scenario simulations (Kou-Giesbrecht and Arora, 2023). Therefore, the inclusion of further limiting nutrients like phosphorus is important, as they will likely have substantial impacts on future carbon uptake (Yang et al., 2023). Model performance overall has improved from CMIP5 to CMIP6 even with the added complexity introducing more degrees of freedom into the models, as also found in the latest IPCC report (Eyring et al., 2021; Canadell et al., 2021). This is a positive outlook for the future, as many aspects have to be considered when increasing model complexity, such as a need to adjust existing parametrisations after model structural changes from carbon-only to carbon-nitrogen coupling. Without such adjustments, lowered ecosystem carbon storage simulated by models with N processes would lead to an underestimation of carbon pools (Wang et al., 2022). The increased overall model performance confirms results from the individual model groups who found improved performance in carbon cycle variables compared to previous model configurations, with the biggest improvements seen in LAI and GPP (Ziehn et al., 2017; Danabasoglu et al., 2020). Many areas requiring improvement remain, such as simulated carbon stocks which saw no significant reduction in the simulated range between CMIP5 and CMIP6, or the inclusion of more nutrient limitations like an interactive phosphorus cycle. The improvement of the carbon cycle in the models since CMIP5 is a step in the right direction for a better understanding and a more accurate simulation of future trends. Based on our analysis, due to the small differences between historical concentration and emission driven simulations despite the increased process-realism, we recommend ESMs in future CMIP phases to be based on emission driven simulations to fully account for climate-carbon feedbacks in future projections, supporting the message from Sanderson et al. (2023). Similarly, due the significant improvements in GPP with the inclusion of an interactive nitrogen cycle and no detrimental change in the present day evaluation of any carbon cycle variable, we suggest that the nitrogen cycle should be seen as a necessary part of carbon cycle models in the future.



Code and data availability. The code to reproduce this study is part of ESMValTool (Righi et al., 2020; Eyring et al., 2020). The corresponding recipes can be found under the folder `gier23bg`. ESMValTool v2 is released under the Apache License, version 2.0. The latest release of ESMValTool v2 is publicly available on Zenodo at <https://doi.org/10.5281/zenodo.3401363> (Andela et al., 2023a). The source code of the ESMValCore package, which is installed as a dependency of ESMValTool v2, is also publicly available on Zenodo at <https://doi.org/10.5281/zenodo.3387139> (Andela et al., 2023b). ESMValTool and ESMValCore are developed on the GitHub repositories available at <https://github.com/ESMValGroup> (last access: 26 January 2024). CMIP data is available for download via ESGF nodes (<https://esgf-node.llnl.gov/search/cmip5/>, <https://esgf-node.llnl.gov/search/cmip6/>). Reference data sets have been formatted for use with ESMValTool using so-called CMORizers. DOIs for all data sets contributing to this study are listed in Tables 1-3 along with their references as available.

Appendix A: Carbon Cycle in the CMIP models

While a summary of the model components for each model can be found in Tables 1 and 2, some special characteristics of the carbon cycle in the land surface components are given below. As several ESMs use the same land model, the sections are listed by land model instead of ESM. If different versions of the same component were used in different CMIP models, the difference between the versions, as well as the models using each version are explained.

A1 CABLE + CASA-CNP

The Community Atmosphere-Biosphere Land Exchange model (CABLE, Kowalczyk et al., 2013) version 2.4 is a land surface model coupled to the biogeochemistry module Carnegie-Ames-Stanford Approach carbon cycle model with nitrogen and phosphorus cycles (CASA-CNP, Wang et al., 2010) used in ACCESS-ESM1-5 (Ziehn et al., 2020). CASA-CNP and thus ACCESS-ESM1.5 is the only model in this study to include a phosphorus cycle coupled to the land carbon-nitrogen cycle. A sensitivity study of allowable emissions to nutrient limitation found a reduction of the land carbon uptake by 35-40 % with nitrogen limitation and a further 20-30 % reduction with nitrogen and phosphorus limitation on the carbon cycle (Zhang et al., 2013), showing the importance of nutrient limitation.

A simple land-use scheme accounts for annual net change in the vegetation tile fractions of each grid-cell which consider 10 vegetated and three non-vegetated surfaces. Three live and six dead carbon pools are modelled. Leaf area index (LAI) in ACCESS-ESM1-5 is calculated from specific leaf area and the size of the leaf carbon pool, while phenology is prescribed. In the CMIP5 model ACCESS-ESM1, which is not considered in this paper due to a lack of variables on the ESGF, LAI was significantly higher than observations, mainly due to an overestimation of LAI in the northern hemisphere, despite a significant underestimation of LAI in the tropics. To better match the observations, two parameters were adjusted for ACCESS-ESM1-5: one PFT-specific parameter used in the parametrisation for the maximum carboxylation rate and thus related to the nitrogen cycle, as well as one global parameter related to the daytime leaf respiration rate. Further changes to the model since CMIP5 include the conservation of land carbon, which was not conserved in CMIP5, as well as the inclusion of wetland tiles in the biogeochemistry calculation and the removal of a spin-up condition which ensured a minimum nitrogen and phosphorus level in soil pools.



665 A2 CLASS + CTEM

The land component in the Canadian Earth System Models (CanESM) is divided into the physical part represented by the Canadian Land Surface Scheme (CLASS, Verseghy, 1991, 2000; Verseghy et al., 1993) and the biogeochemical processes as simulated by the Canadian Terrestrial Ecosystem Model (CTEM, Arora, 2003; Arora and Boer, 2003, 2005). In the CMIP5 model (CanESM2, Arora et al., 2011) version 2.7 of CLASS was used, while the CMIP6 models CanESM and CanESM-670 CanOE (Swart et al., 2019) employ CLASS v3.6. While neither version includes a nitrogen cycle, a parameter representing terrestrial photosynthesis downregulation is included to simulate the effect of nutrient constraints. This parameter is increased in CanESM5 compared to the previous version CanESM2, resulting in a higher land carbon uptake in CanESM5. Four PFTs are considered in CLASS, while CTEM increases the number to nine PFTs so that phenology can be simulated prognostically. LAI is dynamically simulated and three live and two dead carbon pools are considered. Added features since CanESM2 include 675 dynamic wetlands and their diagnostic methane emissions.

A3 CLM

The Community Land Model (CLM, UCAR, 2020) is the most commonly used land model in this study, with 11 models across CMIP5 and CMIP6 using 3 different versions of it. For the CMIP5 models, CLM3.5 (Oleson et al., 2008) was used by FIO-ESM and CLM4 (Lawrence et al., 2011) was used in CESM1-BGC and NorESM1-ME. In CMIP6 CLM4 is used 680 for SAM0-UNICON and TaiESM who mainly adapted the CESM1 configuration (Lee et al., 2020). CMCC-CM2-SR5 and CMCC-ESM2 use CLM4.5 (Koven et al., 2013), while the newest version CLM5 (Lawrence et al., 2019) is a part of CESM2, CESM2-WACCM, NorESM2-LM and NorESM2-MM.

While in CLM3.5 nitrogen limitation was merely represented by a downregulation factor, CLM4 introduced the coupled carbon-nitrogen cycle. Further improvements in CLM4 included transient land cover change modeling, changes to the PFT 685 distribution and more realistic modeling of permafrost regions. To reduce biases found in CLM4 such as low soil carbon stocks and unrealistic values for GPP and LAI in several regions such as a stark overestimation in the tropics, several parametrisations were changed in CLM4.5. Modifications were made to the canopy processes, including co-limitations on photosynthesis and photosynthetic parameters. Newly introduced features included a vertically resolved soil biogeochemistry with vertical mixing of soil carbon and nitrogen and a more realistic distribution of biological fixation over the year. The structure of the litter and 690 soil carbon and nitrogen pools was adapted to the Century model and ^{13}C and ^{14}C carbon isotopes were introduced.

Finally in CLM5 many major components of the land model were updated, with a focus on a better representation of land use and land-cover change as well as a more mechanistic treatment of key processes. Changes included a stronger soil moisture control on decomposition, the use of ^{13}C and ^{14}C isotopes for crops, and several changes to the nitrogen cycle and its impact on photosynthesis. Flexible plant C:N ratios were introduced to eliminate instantaneous down-regulation of photosynthesis, 695 leaf nitrogen was optimized in the form of the leaf use of nitrogen for assimilation (LUNA, Ali et al., 2016) model and a model handling the fixation and uptake of nitrogen (FUN, Shi et al., 2016) was included. With respect to the land use and land



cover aspect of the model, land unit weights are no longer fixed during the simulation and the transient PFT distribution was updated. CLM5 considers 22 live and 7 dead carbon pools as well as 22 PFTs.

A4 CoLM+BNU-DGVM

700 The Common Land Model (CoLM, Dai et al., 2003) which shares an initial version with CLM but was then developed separately, is the land model component for the CMIP5 model BNU-ESM in the CoLM2005 version. CoLM includes a photosynthesis-stomatal conductance model for sunlit and shaded leaves separately. While carbon-nitrogen cycle interactions were included in the model, they were turned off for the CMIP5 simulations due to not being fully evaluated at the time (Ji et al., 2014).

705 A5 HAL

The land model for the MRI models in both its CMIP5 version MRI-ESM1 and the CMIP6 version MRI-ESM2-0 is the Hydrology, Atmosphere, and Landsurface model (HAL, Hosaka, 2011). It consists of three submodels called SiByl (vegetation) with grass and canopy vegetation layers, SNOWA (snow), and SOILA (soil) with 14 soil layers in the CMIP5 experiments.



A6 ISBA-CTRIP

710 The land component for the CNRM-ESM2-1 model is presented by the Interaction Soil-Biosphere-Atmosphere (ISBA) land surface model and the total runoff integrating pathways (CTRIP) river routing model (Decharme et al., 2019; Delire et al., 2020). ISBA-CTRIP simulates plant physiology, leaf phenology, carbon allocation and turnover, wild fires and carbon cycling through litter and soil (Séférian et al., 2019). Land use processes are prescribed instead of simulated, while land cover changes are used to represent anthropogenic disturbances. While the model does not include an interactive nitrogen cycle, its effects
715 are included through an artificial downregulation of photosynthesis and a reduced specific leaf area with increasing CO₂ concentration. Six live and seven dead carbon pools are considered, along with 16 PFTs (Gibelin et al., 2008). Changes since the previous version used in CNRM-ESM-1 include improvements to the photosynthetic and autotrophic respiration schemes.

CTRIP includes carbon leaching through the soil and subsequent transport of dissolved organic carbon to the ocean. As chemical species such as dissolved inorganic carbon are not included, the air-water carbon exchange in the river routing model
720 CTRIP cannot be computed. This leads to a carbon cycle which is not fully bounded.

A7 JSBACH

JSBACH is the land component of the MPI-ESM model, with version 3.2 used for MPI-ESM1.2 (Mauritsen et al., 2019). In the previous version, parameters in the model for decomposition of dead organic matter were tuned to reproduce the historical atmospheric CO₂ concentrations, with soil and litter carbon stocks merely being the result of this tuning. In version 3.2 de-
725 composition is handled by the YASSO model (Tuomi et al., 2011) based on litter and soil data resulting in no unconstrained parameters. YASSO simulates four fast soil carbon pools and one slow pool. A total of 18 dead carbon pools are considered



due to a different application based on the woody and non-woody origins, as well as above and below ground decomposition. Additionally, three live carbon pools (natural vegetation, crops, pasture) and 13 PFTs are simulated by JSBACH, while permafrost carbon is not considered. The dynamical vegetation component interacts with the land use changes, modifying the land use data set to conform to the JSBACH setup. JSBACH3.2 includes an interactive terrestrial nitrogen cycle (Goll et al., 2017) driven by the nitrogen demand of the carbon cycle. Further adjustments in v3.2 include the change for carbon timescales in wood pools to be PFT specific.

A8 JULES

The joint UK land environment simulator (JULES, Best et al., 2011; Clark et al., 2011) is the land model for the CMIP5 models HadGEM2-CC and HadGEM2-ES with the terrestrial carbon cycle following the Top-down Representation of Interaction of Foliage and Flora Including Dynamics (TRIFFID, Cox, 2001) dynamic vegetation scheme. The CMIP6 model UKESM1-0-LL (Sellar et al., 2019) employs JULES version 5.0.

Improvements in the version used for UKESM1-0-LL include the introduction of nitrogen cycling, as well as developments to plant physiology and functional types and land use. In this model, nitrogen controls biomass and leaf area index within TRIFFID, thus only indirectly affecting photosynthetic capacity, as well as limiting the decomposition of litter into soil carbon. For better agreement with observations, global total GPP was tuned down through a reduction of the quantum efficiency of photosynthesis. Furthermore, crop and pasture areas were separated and a harvest carbon flux was introduced. UKESM1 has four soil carbon pools, nine natural PFTs - increased from five in prior versions - and four PFTs for crop and pasture.

A9 LM

The GFDL Land Model (LM, Anderson et al., 2004) is used in the GFDL Earth System Models, with the CMIP5 models GFDL-ESM2G and GFDL-ESM2M (Dunne et al., 2012, 2013) using version 2.0 and the CMIP6 model GFDL-ESM4 employing version 4.1 (Dunne et al., 2020). Neither version includes an interactive nitrogen cycle.

Improvements since CMIP5 include updated soil types in the CORPSE model (Sulman et al., 2014, 2019), hydrology, radiation, as well as the inclusion of a new fire model FINAL (Rabin et al., 2018) with daily computations instead of previously annual figures and a new model for vegetation dynamics through the Perfect Plasticity Approximation (Weng et al., 2015, PPA). LM4.1 includes six live carbon pools for leaves, fine roots, heartwood, sapwood, seeds and nonstructural carbon, 20 vertical soil levels split into separate fast and slow pools and pools for soil microbes and microbial products. Six PFTs are included representing C3 grass, C4 grass, tropical trees, temperate deciduous trees, and cold evergreen trees. Land use is accounted for through annual wood harvesting, crop planting and harvesting, pasture grazing, and newly included rangelands.

755 A10 LPJ-GUESS

The Lund-Potsdam-Jena General Ecosystem Simulator (LPJ-GUESS, Smith et al., 2014) in combination with the Hydrology Tiled ECMWF Scheme of Surface Exchanges over Land (HTESSEL, Balsamo et al., 2009) is the land model used in the



760 EC-Earth models EC-Earth3-CC and EC-Earth3-Veg (Döscher et al., 2022). The model described as "CC" additionally include ocean biogeochemistry (PISCES) and atmospheric composition for CO₂ (TM5), letting it perform CO₂ emission driven simulations.

HTESSEL solves the energy and water balance at the land surface, while vegetation types and vegetation coverage is interactively provided by the coupled LPJ-GUESS, which includes an interactive nitrogen cycle. Compared to the common area-based vegetation schemes, the interactive coupling of LPJ-GUESS to an atmospheric model should improve realism on longer timescales (Döscher et al., 2022). LPJ-GUESS includes 10 litter pools, seven vegetation carbon pools, as well as five soil carbon pools. Wildfires, disturbances and land use change are simulated on a yearly time step and distributed evenly throughout the year to conserve carbon mass. Land-use change dynamics are considered together with a crop module (Lindeskog et al., 2013) including five crop functional types. Three types of plant phenology - evergreen, seasonal-deciduous, and stress-deciduous - are considered, with only the latter two being simulated with an explicit phenological cycle. Seasonal-deciduous PFTs have a fixed growing season length of 210 days, while the growing season for stress-deciduous PFTs is determined by a threshold for the water stress.

A11 MATSIRO + SEIB-DGVM/VISIT-e

775 The Minimal Advanced Treatments of Surface Interaction and RunOff (MATSIRO, Takata et al., 2003) is the physical land model for the MIROC-ESM family—MIROC-ESM and MIROC-ESM-CHEM (with coupled atmospheric chemistry) for CMIP5 (Watanabe et al., 2011) and MIROC-ES2L for CMIP6 (Hajima et al., 2020)—which consists of a single layer canopy, three snow layers and six soil layers down to a depth of 14m. For the CMIP6 version a physically based parametrization for snow distribution and snow-derived wetlands was added. Biogeochemistry in MIROC-ESM and MIROC-ESM-CHEM is simulated by the Spatially Explicit Individual-Based Dynamic Global Vegetation Model (SEIB-DGVM, Sato et al., 2007). It includes 13 PFTs split into two for grass and eleven for trees, as well as two organic carbon pools. Light capture competition among trees is explicitly modeled instead of parametrized.

780 MIROC-ES2L for CMIP6 uses the Vegetation integrative SIMulator for Trace gases model (VISIT, Ito and Inatomi, 2012), with changes for coupling to the ESM (adding the -e suffix), such as including leaf-nitrogen concentrations and thus limitations to enable fully coupled climate-carbon-nitrogen projections, and land-use change processes to get more use out of new LUC forcing data sets, such as using five types of land cover. The model does not simulate explicit dynamic vegetation. Three Vegetation carbon pools (leaf, stem, and root) are dynamically regulated and have constant turnover rates to three litter and three soil pools. 12 vegetation types are considered. A daily timestep is used for the land ecosystem and land biogeochemistry.

A12 ORCHIDEE

790 The ORganizing Carbon and Hydrology in Dynamic EcosystEms (ORCHIDEE, Krinner et al., 2005; Boucher et al., 2020) land model is used in the IPSL models, version 1 for the CMIP5 models IPSL-CM5A-LR, IPSL-CM5A-MR, and version 2 in the CMIP6 model IPSL-CM5B-LR. The model considers 15 PFTs, as well as 8 vegetation carbon, 4 litter carbon and 3 soil carbon pools. Plant and soil carbon fluxes are computed every 15 min (the same as the atmospheric physics time step), while



slow processes like soil and litter carbon dynamics are computed daily instead. The CMIP5 model used a two-layer bucket model for its soil hydrology, while in CMIP6 an 11-layer soil hydrology scheme is employed. Photosynthesis is parametrized based on the common Farquhar and Collatz schemes for C3 and C4, respectively. Nutrient limitation in CMIP6 is introduced through downregulation using a logarithmic function of the CO₂ concentration.

795 **A13 Other: INMCM**

The carbon cycle module for INMCM (Volodin, 2007) includes a single soil carbon pool. The most important changes with respect to INMCM4 for the CMIP6 models lie in the atmospheric component of the model, as well as some upgrades to the oceanic component, but no changes to the carbon cycle (Volodin et al., 2017b).

Author contributions. BG led the writing and analysis of the paper. MS assisted with parts of the programming. VE supervised the study.

800 All authors contributed to the writing of the manuscript.

Competing interests. At least one of the (co-)authors is a member of the editorial board of Biogeosciences.

Acknowledgements. This study was funded by the European Union's Horizon 2020 research and innovation programmes "Climate-Carbon interactions in the Current Century" (4C; grant agreement No 821003) and "Earth System Models for the Future" (ESM2025; grant agreement No. 101003536). We acknowledge the World Climate Research Programme (WCRP), which, through its Working Group on Coupled
805 Modelling, coordinated and promoted CMIP6. We thank the climate modeling groups (listed in Tables 2 and 3 of this paper) for producing and making available their model output, the Earth System Grid Federation (ESGF) for archiving the data and providing access, and the multiple funding agencies who support CMIP and ESGF. The computational resources of the Deutsches Klimarechenzentrum (DKRZ, Germany) were used to compute these results and are kindly acknowledged.



References

- 810 Ali, A. A., Xu, C., Rogers, A., Fisher, R. A., Wullschleger, S. D., Massoud, E. C., Vrugt, J. A., Muss, J. D., McDowell, N. G., Fisher, J. B., Reich, P. B., and Wilson, C. J.: A global scale mechanistic model of photosynthetic capacity (LUNA V1.0), *Geoscientific Model Development*, 9, 587–606, <https://doi.org/10.5194/gmd-9-587-2016>, 2016.
- Anav, A., Friedlingstein, P., Kidston, M., Bopp, L., Ciais, P., Cox, P., Jones, C., Jung, M., Myrneni, R., and Zhu, Z.: Evaluating the Land and Ocean Components of the Global Carbon Cycle in the CMIP5 Earth System Models, *Journal of Climate*, 26, 6801–6843, <https://doi.org/10.1175/Jcli-D-12-00417.1>, 2013a.
- 815 Anav, A., Murray-Tortarolo, G., Friedlingstein, P., Sitch, S., Piao, S., and Zhu, Z.: Evaluation of Land Surface Models in Reproducing Satellite Derived Leaf Area Index over the High-Latitude Northern Hemisphere. Part II: Earth System Models, *Remote Sensing*, 5, 3637–3661, <https://doi.org/10.3390/rs5083637>, 2013b.
- Anav, A., Friedlingstein, P., Beer, C., Ciais, P., Harper, A., Jones, C., Murray-Tortarolo, G., Papale, D., Parazoo, N. C., Peylin, P., Piao, S., Sitch, S., Viovy, N., Wiltshire, A., and Zhao, M.: Spatiotemporal patterns of terrestrial gross primary production: A review, *Reviews of Geophysics*, 53, 785–818, <https://doi.org/https://doi.org/10.1002/2015RG000483>, 2015.
- 820 Andela, B., Broetz, B., de Mora, L., Drost, N., Eyring, V., Koldunov, N., Lauer, A., Mueller, B., Predoi, V., Righi, M., Schlund, M., Vegas-Regidor, J., Zimmermann, K., Adeniyi, K., Arnone, E., Bellprat, O., Berg, P., Bock, L., Caron, L.-P., Carvalhais, N., Cionni, I., Cortesi, N., Corti, S., Crezee, B., Davin, E. L., Davini, P., Deser, C., Diblen, F., Docquier, D., Dreyer, L., Ehbrecht, C., Earnshaw, P., Gier, B., Gonzalez-Reviriego, N., Goodman, P., Hagemann, S., von Hardenberg, J., Hassler, B., Hunter, A., Kadow, C., Kindermann, S., Koirala, S., Lledó, L., Lejeune, Q., Lembo, V., Little, B., Loosveldt-Tomas, S., Lorenz, R., Lovato, T., Lucarini, V., Massonnet, F., Mohr, C. W., Moreno-Chamarro, E., Amarjiit, P., Pérez-Zanón, N., Phillips, A., Russell, J., Sandstad, M., Sellar, A., Senftleben, D., Serva, F., Sillmann, J., Stacke, T., Swaminathan, R., Torralba, V., Weigel, K., Roberts, C., Kalverla, P., Alidoost, S., Verhoeven, S., Vreede, B., Smeets, S., Soares Siqueira, A., and Kazeroni, R.: ESMValTool, <https://doi.org/10.5281/zenodo.8120970>, 2023a.
- 825 Andela, B., Broetz, B., de Mora, L., Drost, N., Eyring, V., Koldunov, N., Lauer, A., Predoi, V., Righi, M., Schlund, M., Vegas-Regidor, J., Zimmermann, K., Bock, L., Diblen, F., Dreyer, L., Earnshaw, P., Hassler, B., Little, B., Loosveldt-Tomas, S., Smeets, S., Camphuijsen, J., Gier, B. K., Weigel, K., Hauser, M., Kalverla, P., Galytska, E., Cos-España, P., Pelupessy, I., Koirala, S., Stacke, T., Alidoost, S., Jury, M., Sénési, S., Crocker, T., Vreede, B., Soares Siqueira, A., Kazeroni, R., and Bauer, J.: ESMValCore, <https://doi.org/10.5281/zenodo.8112684>, 2023b.
- Anderson, J., Balaji, V., Broccoli, A., Cooke, W., Delworth, T., Dixon, K., Donner, L., Dunne, K., Freidenreich, S., Garner, S., Gudgel, R., Gordon, C., Held, I., Hemler, R., Horowitz, L., Klein, S., Knutson, T., Kushner, P., Langenhost, A., Lau, N., Liang, Z., Malyshev, S., Milly, P., Nath, M., Ploshay, J., Ramaswamy, V., Schwarzkopf, M., Shevliakova, E., Sirutis, J., Soden, B., Stern, W., Thompson, L., Wilson, R., Wittenberg, A., and Wyman, B.: The new GFDL global atmosphere and land model AM2-LM2: Evaluation with prescribed SST simulations, *Journal of Climate*, 17, 4641–4673, <https://doi.org/10.1175/JCLI-3223.1>, 2004.
- 835 Arora, V. K.: Simulating energy and carbon fluxes over winter wheat using coupled land surface and terrestrial ecosystem models, *Agricultural and Forest Meteorology*, 118, 21–47, [https://doi.org/https://doi.org/10.1016/S0168-1923\(03\)00073-X](https://doi.org/https://doi.org/10.1016/S0168-1923(03)00073-X), 2003.
- Arora, V. K. and Boer, G. J.: A Representation of Variable Root Distribution in Dynamic Vegetation Models, *Earth Interactions*, 7, 1 – 19, [https://doi.org/10.1175/1087-3562\(2003\)007<0001:AROVRD>2.0.CO;2](https://doi.org/10.1175/1087-3562(2003)007<0001:AROVRD>2.0.CO;2), 2003.
- Arora, V. K. and Boer, G. J.: A parameterization of leaf phenology for the terrestrial ecosystem component of climate models, *Global Change Biology*, 11, 39–59, <https://doi.org/https://doi.org/10.1111/j.1365-2486.2004.00890.x>, 2005.



- 845 Arora, V. K., Scinocca, J. F., Boer, G. J., Christian, J. R., Denman, K. L., Flato, G. M., Kharin, V. V., Lee, W. G., and Merryfield, W. J.: Carbon emission limits required to satisfy future representative concentration pathways of greenhouse gases, *Geophysical Research Letters*, 38, n/a–n/a, <https://doi.org/10.1029/2010gl046270>, 2011.
- Arora, V. K., Katavouta, A., Williams, R. G., Jones, C. D., Brovkin, V., Friedlingstein, P., Schwinger, J., Bopp, L., Boucher, O., Cadule, P., Chamberlain, M. A., Christian, J. R., Delire, C., Fisher, R. A., Hajima, T., Ilyina, T., Joetzjer, E., Kawamiya, M., Koven, C. D., Krasting, J. P., Law, R. M., Lawrence, D. M., Lenton, A., Lindsay, K., Pongratz, J., Raddatz, T., Séférian, R., Tachiiri, K., Tjiputra, J. F., Wiltshire, A., Wu, T., and Ziehn, T.: Carbon–concentration and carbon–climate feedbacks in CMIP6 models and their comparison to CMIP5 models, *Biogeosciences*, 17, 4173–4222, <https://doi.org/10.5194/bg-17-4173-2020>, 2020.
- 850 Balsamo, G., Beljaars, A., Scipal, K., Viterbo, P., van den Hurk, B., Hirschi, M., and Betts, A. K.: A Revised Hydrology for the ECMWF Model: Verification from Field Site to Terrestrial Water Storage and Impact in the Integrated Forecast System, *Journal of Hydrometeorology*, 10, 623 – 643, <https://doi.org/https://doi.org/10.1175/2008JHM1068.1>, 2009.
- 855 Bao, Y., Qiao, F.-L., and Song, Z.: The historical global carbon cycle simulation of FIO-ESM, p. 6834, 2012.
- Best, M. J., Pryor, M., Clark, D. B., Rooney, G. G., Essery, R. L. H., Ménard, C. B., Edwards, J. M., Hendry, M. A., Porson, A., Gedney, N., Mercado, L. M., Sitch, S., Blyth, E., Boucher, O., Cox, P. M., Grimmond, C. S. B., and Harding, R. J.: The Joint UK Land Environment Simulator (JULES), model description – Part 1: Energy and water fluxes, *Geoscientific Model Development*, 4, 677–699, <https://doi.org/10.5194/gmd-4-677-2011>, 2011.
- 860 Bock, L., Lauer, A., Schlund, M., Barreiro, M., Bellouin, N., Jones, C., Meehl, G. A., Predoi, V., Roberts, M. J., and Eyring, V.: Quantifying Progress Across Different CMIP Phases With the ESMValTool, *Journal of Geophysical Research: Atmospheres*, 125, e2019JD032321, <https://doi.org/10.1029/2019JD032321>, e2019JD032321 2019JD032321, 2020.
- Boucher, O., Servonnat, J., Albright, A. L., Aumont, O., Balkanski, Y., Bastrikov, V., Bekki, S., Bonnet, R., Bony, S., Bopp, L., Braconnot, P., Brockmann, P., Cadule, P., Caubel, A., Cheruy, F., Codron, F., Cozic, A., Cugnet, D., D’Andrea, F., Davini, P., de Lavergne, C., Denvil, S., Deshayes, J., Devilliers, M., Ducharne, A., Dufresne, J.-L., Dupont, E., Éthé, C., Fairhead, L., Falletti, L., Flavoni, S., Foujols, M.-A., Gardoll, S., Gastineau, G., Ghattas, J., Grandpeix, J.-Y., Guenet, B., Guez, Lionel, E., Guilyardi, E., Guimberteau, M., Hauglustaine, D., Hourdin, F., Idelkadi, A., Joussaume, S., Kageyama, M., Khodri, M., Krinner, G., Lebas, N., Levvasseur, G., Lévy, C., Li, L., Lott, F., Lurton, T., Luysaert, S., Madec, G., Madeleine, J.-B., Maignan, F., Marchand, M., Marti, O., Mellul, L., Meurdesoif, Y., Mignot, J., Musat, I., Ottlé, C., Peylin, P., Planton, Y., Polcher, J., Rio, C., Rochetin, N., Rousset, C., Sepulchre, P., Sima, A., Swingedouw, D., Thiéblemont, R., Traore, A. K., Vancoppenolle, M., Vial, J., Vialard, J., Viovy, N., and Vuichard, N.: Presentation and Evaluation of the IPSL-CM6A-LR Climate Model, *Journal of Advances in Modeling Earth Systems*, 12, e2019MS002010, <https://doi.org/10.1029/2019MS002010>, 2020.
- 875 Canadell, J., Monteiro, P., Costa, M., Cotrim da Cunha, L., Cox, P., Eliseev, A., Henson, S., Ishii, M., Jaccard, S., Koven, C., Lohila, A., Patra, P., Piao, S., Rogelj, J., Syampungani, S., Zaehle, S., and Zickfeld, K.: *Global Carbon and other Biogeochemical Cycles and Feedbacks*, pp. 673–816, Cambridge University Press, Cambridge, United Kingdom and New York, NY, USA, <https://doi.org/10.1017/9781009157896.007>, 2021.
- Cao, S., Li, M., Zhu, Z., Wang, Z., Zha, J., Zhao, W., Duanmu, Z., Chen, J., Zheng, Y., Chen, Y., Myneni, R. B., and Piao, S.: Spatiotemporally consistent global dataset of the GIMMS leaf area index (GIMMS LAI4g) from 1982 to 2020, *Earth System Science Data*, 15, 4877–4899, <https://doi.org/10.5194/essd-15-4877-2023>, 2023.
- 880 Carvalhais, N., Forkel, M., Khomik, M., Bellarby, J., Jung, M., Migliavacca, M., Mu, M., Saatchi, S., Santoro, M., Thurner, M., Weber, U., Ahrens, B., Beer, C., Cescatti, A., Randerson, J. T., and Reichstein, M.: Global covariation of carbon turnover times with climate in terrestrial ecosystems, *Nature*, 514, 213–217, <https://doi.org/10.1038/nature13731>, 2014.



- Cherchi, A., Fogli, P. G., Lovato, T., Peano, D., Iovino, D., Gualdi, S., Masina, S., Scoccimarro, E., Materia, S., Bellucci, A., and Navarra, A.: Global Mean Climate and Main Patterns of Variability in the CMCC-CM2 Coupled Model, *Journal of Advances in Modeling Earth Systems*, 11, 185–209, <https://doi.org/10.1029/2018MS001369>, 2019.
- 885 Chevallier, F.: On the parallelization of atmospheric inversions of CO₂ surface fluxes within a variational framework, *Geosci. Model Dev.*, 6, 783–790, 2013.
- Chevallier, F., Fisher, M., Peylin, P., Serrar, S., Bousquet, P., Bréon, F.-M., Chédin, A., and Ciais, P.: Inferring CO₂ sources and sinks from satellite observations: Method and application to TOVS data, *J. Geophys. Res.*, 110, 2005.
- 890 Chevallier, F., Ciais, P., Conway, T. J., Aalto, T., Anderson, B. E., Bousquet, P., Brunke, E. G., Ciattaglia, L., Esaki, Y., Fröhlich, M., Gomez, A., Gomez-Pelaez, A. J., Haszpra, L., Krummel, P. B., Langenfelds, R. L., Leuenberger, M., Machida, T., Maignan, F., Matsueda, H., Morguá, J. A., Mukai, H., Nakazawa, T., Peylin, P., Ramonet, M., Rivier, L., Sawa, Y., Schmidt, M., Steele, L. P., Vay, S. A., Vermeulen, A. T., Wofsy, S., and Worthy, D.: CO₂ surface fluxes at grid point scale estimated from a global 21 year reanalysis of atmospheric measurements, *J. Geophys. Res.*, 115, 2010.
- 895 Christiansen, B.: Ensemble Averaging and the Curse of Dimensionality, *Journal of Climate*, 31, 1587 – 1596, <https://doi.org/https://doi.org/10.1175/JCLI-D-17-0197.1>, 2018.
- Ciais, P., Sabine, C., Bala, G., Bopp, L., Brovkin, V., Canadell, J., Chhabra, A., DeFries, R., Galloway, J., Heimann, M., Jones, C., Le Que´re´, C., Myneni, R., Piao, S., and Thornton, P.: Carbon and Other Biogeochemical Cycles, in: *Climate Change 2013: The Physical Science Basis. Contribution of Working Group I to the Fifth Assessment Report of the Intergovernmental Panel on Climate Change*, edited by Stocker, T., Qin, D., Plattner, G.-K., Tignor, M., Allen, S., Boschung, J., Nauels, A., Xia, Y., Bex, V., and Midgley, P., book section 6, p. 465–570, Cambridge University Press, Cambridge, United Kingdom and New York, NY, USA, <https://doi.org/10.1017/CBO9781107415324.015>, 2013.
- 900 Clark, D. B., Mercado, L. M., Sitch, S., Jones, C. D., Gedney, N., Best, M. J., Pryor, M., Rooney, G. G., Essery, R. L. H., Blyth, E., Boucher, O., Harding, R. J., Huntingford, C., and Cox, P. M.: The Joint UK Land Environment Simulator (JULES), model description – Part 2: Carbon fluxes and vegetation dynamics, *Geoscientific Model Development*, 4, 701–722, <https://doi.org/10.5194/gmd-4-701-2011>, 2011.
- Collins, W. J., Bellouin, N., Doutriaux-Boucher, M., Gedney, N., Halloran, P., Hinton, T., Hughes, J., Jones, C. D., Joshi, M., Liddicoat, S., Martin, G., O’Connor, F., Rae, J., Senior, C., Sitch, S., Totterdell, I., Wiltshire, A., and Woodward, S.: Development and evaluation of an Earth-System model – HadGEM2, *Geosci. Model Dev.*, 4, 1051–1075, <https://doi.org/10.5194/gmd-4-1051-2011>, 2011.
- Cox, P. M.: Description of the TRIFFID Dynamic Global Vegetation Model, Hadley Centre, Met Office, UK, Technical Note 24, 2001.
- 910 Dai, Y., Zeng, X., Dickinson, R. E., Baker, I., Bonan, G. B., Bosilovich, M. G., Denning, A. S., Dirmeyer, P. A., Houser, P. R., Niu, G., Oleson, K. W., Schlosser, C. A., and Yang, Z.-L.: The Common Land Model, *Bulletin of the American Meteorological Society*, 84, 1013–1024, <https://doi.org/10.1175/bams-84-8-1013>, 2003.
- Danabasoglu, G., Lamarque, J.-F., Bacmeister, J., Bailey, D. A., DuVivier, A. K., Edwards, J., Emmons, L. K., Fasullo, J., Garcia, R., Gettelman, A., Hannay, C., Holland, M. M., Large, W. G., Lauritzen, P. H., Lawrence, D. M., Lenaerts, J. T. M., Lindsay, K., Lipscomb, W. H., Mills, M. J., Neale, R., Oleson, K. W., Otto-Bliesner, B., Phillips, A. S., Sacks, W., Tilmes, S., van Kampenhout, L., Versteinn, M., Bertini, A., Dennis, J., Deser, C., Fischer, C., Fox-Kemper, B., Kay, J. E., Kinnison, D., Kushner, P. J., Larson, V. E., Long, M. C., Mickelson, S., Moore, J. K., Nienhouse, E., Polvani, L., Rasch, P. J., and Strand, W. G.: The Community Earth System Model Version 2 (CESM2), *Journal of Advances in Modeling Earth Systems*, 12, e2019MS001 916, <https://doi.org/10.1029/2019ms001916>, 2020.



- Davies-Barnard, T., Meyerholt, J., Zaehle, S., Friedlingstein, P., Brovkin, V., Fan, Y., Fisher, R. A., Jones, C. D., Lee, H., Peano, D., Smith, B., Wårlind, D., and Wiltshire, A. J.: Nitrogen cycling in CMIP6 land surface models: progress and limitations, *Biogeosciences*, 17, 5129–5148, <https://doi.org/10.5194/bg-17-5129-2020>, 2020.
- Decharme, B., Delire, C., Minvielle, M., Colin, J., Vergnes, J.-P., Alias, A., Saint-Martin, D., Séférian, R., Sénési, S., and Voldoire, A.: Recent Changes in the ISBA-CTRIP Land Surface System for Use in the CNRM-CM6 Climate Model and in Global Off-Line Hydrological Applications, *Journal of Advances in Modeling Earth Systems*, 11, 1207–1252, <https://doi.org/10.1029/2018MS001545>, 2019.
- Delire, C., Séférian, R., Decharme, B., Alkama, R., Calvet, J.-C., Carrer, D., Gibelin, A.-L., Joetzjer, E., Morel, X., Rocher, M., and Tzanos, D.: The global land carbon cycle simulated with ISBA-CTRIP: improvements over the last decade, *Journal of Advances in Modeling Earth Systems*, n/a, e2019MS001886, <https://doi.org/10.1029/2019ms001886>, 2020.
- Döscher, R., Acosta, M., Alessandri, A., Anthoni, P., Arsouze, T., Bergman, T., Bernardello, R., Boussetta, S., Caron, L.-P., Carver, G., Castrillo, M., Catalano, F., Cvijanovic, I., Davini, P., Dekker, E., Doblas-Reyes, F. J., Docquier, D., Echevarria, P., Fladrich, U., Fuentes-Franco, R., Gröger, M., v. Hardenberg, J., Hieronymus, J., Karami, M. P., Keskinen, J.-P., Koenigk, T., Makkonen, R., Massonnet, F., Ménégos, M., Miller, P. A., Moreno-Chamarro, E., Nieradzic, L., van Noije, T., Nolan, P., O'Donnell, D., Ollinaho, P., van den Oord, G., Ortega, P., Prims, O. T., Ramos, A., Reerink, T., Rousset, C., Ruprich-Robert, Y., Le Sager, P., Schmith, T., Schrödner, R., Serva, F., Sicardi, V., Sloth Madsen, M., Smith, B., Tian, T., Tourigny, E., Uotila, P., Vancoppenolle, M., Wang, S., Wårlind, D., Willén, U., Wyser, K., Yang, S., Yepes-Arbós, X., and Zhang, Q.: The EC-Earth3 Earth system model for the Coupled Model Intercomparison Project 6, *Geoscientific Model Development*, 15, 2973–3020, <https://doi.org/10.5194/gmd-15-2973-2022>, 2022.
- Du, E., Terrer, C., Pellegrini, A. F., Ahlström, A., van Lissa, C. J., Zhao, X., Xia, N., Wu, X., and Jackson, R. B.: Global patterns of terrestrial nitrogen and phosphorus limitation, *Nature Geoscience*, 13, 221–226, 2020.
- Dufresne, J. L., Foujols, M. A., Denvil, S., Caubel, A., Marti, O., Aumont, O., Balkanski, Y., Bekki, S., Bellenger, H., Benshila, R., Bony, S., Bopp, L., Braconnot, P., Brockmann, P., Cadule, P., Cheruy, F., Codron, F., Cozic, A., Cugnet, D., de Noblet, N., Duvel, J. P., Ethé, C., Fairhead, L., Fichefet, T., Flavoni, S., Friedlingstein, P., Grandpeix, J. Y., Guez, L., Guilyardi, E., Hauglustaine, D., Hourdin, F., Idelkadi, A., Ghattas, J., Joussaume, S., Kageyama, M., Krinner, G., Labetoulle, S., Lahellec, A., Lefebvre, M. P., Lefevre, F., Levy, C., Li, Z. X., Lloyd, J., Lott, F., Madec, G., Mancip, M., Marchand, M., Masson, S., Meurdesoif, Y., Mignot, J., Musat, I., Parouty, S., Polcher, J., Rio, C., Schulz, M., Swingedouw, D., Szopa, S., Talandier, C., Terray, P., Viovy, N., and Vuichard, N.: Climate change projections using the IPSL-CM5 Earth System Model: from CMIP3 to CMIP5, *Climate Dynamics*, 40, 2123–2165, <https://doi.org/10.1007/s00382-012-1636-1>, 2013.
- Dunne, J. P., John, J. G., Adcroft, A. J., Griffies, S. M., Hallberg, R. W., Shevliakova, E., Stouffer, R. J., Cooke, W., Dunne, K. A., Harrison, M. J., Krasting, J. P., Malyshev, S. L., Milly, P. C. D., Phillipps, P. J., Sentman, L. T., Samuels, B. L., Spelman, M. J., Winton, M., Wittenberg, A. T., and Zadeh, N.: GFDL's ESM2 Global Coupled Climate-Carbon Earth System Models. Part I: Physical Formulation and Baseline Simulation Characteristics, *Journal of Climate*, 25, 6646–6665, <https://doi.org/10.1175/Jcli-D-11-00560.1>, 2012.
- Dunne, J. P., John, J. G., Shevliakova, E., Stouffer, R. J., Krasting, J. P., Malyshev, S. L., Milly, P. C. D., Sentman, L. T., Adcroft, A. J., Cooke, W., Dunne, K. A., Griffies, S. M., Hallberg, R. W., Harrison, M. J., Levy, H., Wittenberg, A. T., Phillips, P. J., and Zadeh, N.: GFDL's ESM2 Global Coupled Climate-Carbon Earth System Models. Part II: Carbon System Formulation and Baseline Simulation Characteristics, *Journal of Climate*, 26, 2247–2267, <https://doi.org/10.1175/Jcli-D-12-00150.1>, 2013.
- Dunne, J. P., Horowitz, L. W., Adcroft, A. J., Ginoux, P., Held, I. M., John, J. G., Krasting, J. P., Malyshev, S., Naik, V., Paulot, F., Shevliakova, E., Stock, C. A., Zadeh, N., Balaji, V., Blanton, C., Dunne, K. A., Dupuis, C., Durachta, J., Dussin, R., Gauthier, P. P. G., Griffies, S. M.,



- 960 Guo, H., Hallberg, R. W., Harrison, M., He, J., Hurlin, W., McHugh, C., Menzel, R., Milly, P. C. D., Nikonov, S., Paynter, D. J., Ploshay, J., Radhakrishnan, A., Rand, K., Reichl, B. G., Robinson, T., Schwarzkopf, D. M., Sentman, L. T., Underwood, S., Vahlenkamp, H., Winton, M., Wittenberg, A. T., Wyman, B., Zeng, Y., and Zhao, M.: The GFDL Earth System Model Version 4.1 (GFDL-ESM 4.1): Overall Coupled Model Description and Simulation Characteristics, *Journal of Advances in Modeling Earth Systems*, 12, e2019MS002015, <https://doi.org/10.1029/2019ms002015>, 2020.
- Eyring, V., Bony, S., Meehl, G. A., Senior, C. A., Stevens, B., Stouffer, R. J., and Taylor, K. E.: Overview of the Coupled Model Intercomparison Project Phase 6 (CMIP6) experimental design and organization, *Geoscientific Model Development*, 9, 1937–1958, <https://doi.org/10.5194/gmd-9-1937-2016>, 2016a.
- 965 Eyring, V., Righi, M., Lauer, A., Evaldsson, M., Wenzel, S., Jones, C., Anav, A., Andrews, O., Cionni, I., Davin, E. L., Deser, C., Ehbrecht, C., Friedlingstein, P., Gleckler, P., Gottschaldt, K. D., Hagemann, S., Juckes, M., Kindermann, S., Krasting, J., Kunert, D., Levine, R., Loew, A., Makela, J., Martin, G., Mason, E., Phillips, A. S., Read, S., Rio, C., Roehrig, R., Senftleben, D., Sterl, A., van Ulft, L. H., Walton, J., Wang, S. Y., and Williams, K. D.: ESMValTool (v1.0) - a community diagnostic and performance metrics tool for routine evaluation of Earth system models in CMIP, *Geoscientific Model Development*, 9, 1747–1802, <https://doi.org/10.5194/gmd-9-1747-2016>, 2016b.
- 970 Eyring, V., Cox, P. M., Flato, G. M., Gleckler, P. J., Abramowitz, G., Caldwell, P., Collins, W. D., Gier, B. K., Hall, A. D., Hoffman, F. M., Hurtt, G. C., Jahn, A., Jones, C. D., Klein, S. A., Krasting, J. P., Kwiatkowski, L., Lorenz, R., Maloney, E., Meehl, G. A., Pendergrass, A. G., Pincus, R., Ruane, A. C., Russell, J. L., Sanderson, B. M., Santer, B. D., Sherwood, S. C., Simpson, I. R., Stouffer, R. J., and Williamson, M. S.: Taking climate model evaluation to the next level, *Nature Climate Change*, 9, 102–110, <https://doi.org/10.1038/s41558-018-0355-y>, 2019.
- 975 Eyring, V., Bock, L., Lauer, A., Righi, M., Schlund, M., Andela, B., Arnone, E., Bellprat, O., Brötz, B., Caron, L. P., Carvalhais, N., Cionni, I., Cortesi, N., Crezee, B., Davin, E. L., Davini, P., Debeire, K., de Mora, L., Deser, C., Docquier, D., Earnshaw, P., Ehbrecht, C., Gier, B. K., Gonzalez-Reviriego, N., Goodman, P., Hagemann, S., Hardiman, S., Hassler, B., Hunter, A., Kadow, C., Kindermann, S., Koirala, S., Koldunov, N., Lejeune, Q., Lembo, V., Lovato, T., Lucarini, V., Massonnet, F., Müller, B., Pandde, A., Pérez-Zanón, N., Phillips, A., Predoi, V., Russell, J., Sellar, A., Serva, F., Stacke, T., Swaminathan, R., Torralba, V., Vegas-Regidor, J., von Hardenberg, J., Weigel, K., and Zimmermann, K.: Earth System Model Evaluation Tool (ESMValTool) v2.0 – an extended set of large-scale diagnostics for quasi-operational and comprehensive evaluation of Earth system models in CMIP, *Geosci. Model Dev.*, 13, 3383–3438, <https://doi.org/10.5194/gmd-13-3383-2020>, 2020.
- 980 Eyring, V., Gillett, N., Achuta Rao, K., Barimalala, R., Barreiro Parrillo, M., Bellouin, N., Cassou, C., Durack, P., Kosaka, Y., McGregor, S., Min, S., Morgenstern, O., and Sun, Y.: *Human Influence on the Climate System*, pp. 423—552, Cambridge University Press, Cambridge, United Kingdom and New York, NY, USA, <https://doi.org/10.1017/9781009157896.005>, 2021.
- Flato, G. M., Marotzke, J., Abiodun, B., Braconnot, P., Chou, S. C., Collins, W. D., Cox, P., Driouech, F., Emori, S., Eyring, V., Forest, C., Gleckler, P., Guilyardi, E., Jakob, C., Kattsov, V., Reason, C., and Rummukainen, M.: *Evaluation of Climate Models*, pp. 741–866, Cambridge University Press, https://www.ipcc.ch/site/assets/uploads/2018/02/WG1AR5_Chapter09_FINAL.pdf, 2013.
- 990 Friedlingstein, P., Meinshausen, M., Arora, V. K., Jones, C. D., Anav, A., Liddicoat, S. K., and Knutti, R.: Uncertainties in CMIP5 Climate Projections due to Carbon Cycle Feedbacks, *Journal of Climate*, 27, 511–526, <https://doi.org/10.1175/Jcli-D-12-00579.1>, 2014.
- Friedlingstein, P., Jones, M. W., O’Sullivan, M., Andrew, R. M., Bakker, D. C. E., Hauck, J., Le Quéré, C., Peters, G. P., Peters, W., Pongratz, J., Sitch, S., Canadell, J. G., Ciais, P., Jackson, R. B., Alin, S. R., Anthoni, P., Bates, N. R., Becker, M., Bellouin, N., Bopp, L., Chau, T. T., Chevallier, F., Chini, L. P., Cronin, M., Currie, K. I., Decharme, B., Djeutchouang, L. M., Dou, X., Evans, W., Feely, R. A., Feng,



- 995 L., Gasser, T., Gilfillan, D., Gkritzalis, T., Grassi, G., Gregor, L., Gruber, N., Gürses, O., Harris, I., Houghton, R. A., Hurtt, G. C., Iida, Y., Ilyina, T., Luijkx, I. T., Jain, A., Jones, S. D., Kato, E., Kennedy, D., Klein Goldewijk, K., Knauer, J., Korsbakken, J. I., Körtzinger, A., Landschützer, P., Lauvset, S. K., Lefèvre, N., Lienert, S., Liu, J., Marland, G., McGuire, P. C., Melton, J. R., Munro, D. R., Nabel, J. E. M. S., Nakaoka, S.-I., Niwa, Y., Ono, T., Pierrot, D., Poulter, B., Rehder, G., Resplandy, L., Robertson, E., Rödenbeck, C., Rosan, T. M., Schwinger, J., Schwingshackl, C., Séférian, R., Sutton, A. J., Sweeney, C., Tanhua, T., Tans, P. P., Tian, H., Tilbrook, B., Tubiello, F., van der Werf, G. R., Vuichard, N., Wada, C., Wanninkhof, R., Watson, A. J., Willis, D., Wiltshire, A. J., Yuan, W., Yue, C., Yue, X., Zaehle, S., and Zeng, J.: Global Carbon Budget 2021, *Earth System Science Data*, 14, 1917–2005, <https://doi.org/10.5194/essd-14-1917-2022>, 2022.
- 1000 Friedlingstein, P., O’Sullivan, M., Jones, M. W., Andrew, R. M., Bakker, D. C. E., Hauck, J., Landschützer, P., Le Quééré, C., Luijkx, I. T., Peters, G. P., Peters, W., Pongratz, J., Schwingshackl, C., Sitch, S., Canadell, J. G., Ciais, P., Jackson, R. B., Alin, S. R., Anthoni, P., Barbero, L., Bates, N. R., Becker, M., Bellouin, N., Decharme, B., Bopp, L., Brasika, I. B. M., Cadule, P., Chamberlain, M. A., Chandra, N., Chau, T.-T.-T., Chevallier, F., Chini, L. P., Cronin, M., Dou, X., Enyo, K., Evans, W., Falk, S., Feely, R. A., Feng, L., Ford, D. J., Gasser, T., Ghattas, J., Gkritzalis, T., Grassi, G., Gregor, L., Gruber, N., Gürses, O., Harris, I., Hefner, M., Heinke, J., Houghton, R. A., Hurtt, G. C., Iida, Y., Ilyina, T., Jacobson, A. R., Jain, A., Jarníková, T., Jersild, A., Jiang, F., Jin, Z., Joos, F., Kato, E., Keeling, R. F., Kennedy, D., Klein Goldewijk, K., Knauer, J., Korsbakken, J. I., Körtzinger, A., Lan, X., Lefèvre, N., Li, H., Liu, J., Liu, Z., Ma, L., Marland, G., Mayot, N., McGuire, P. C., McKinley, G. A., Meyer, G., Morgan, E. J., Munro, D. R., Nakaoka, S.-I., Niwa, Y., O’Brien, K. M., Olsen, A., Omar, A. M., Ono, T., Paulsen, M., Pierrot, D., Pockock, K., Poulter, B., Powis, C. M., Rehder, G., Resplandy, L., Robertson, E., Rödenbeck, C., Rosan, T. M., Schwinger, J., Séférian, R., Smallman, T. L., Smith, S. M., Sospedra-Alfonso, R., Sun, Q., Sutton, A. J., Sweeney, C., Takao, S., Tans, P. P., Tian, H., Tilbrook, B., Tsujino, H., Tubiello, F., van der Werf, G. R., van Ooijen, E., Wanninkhof, R., Watanabe, M., Wimart-Rousseau, C., Yang, D., Yang, X., Yuan, W., Yue, X., Zaehle, S., Zeng, J., and Zheng, B.: Global Carbon Budget 2023, *Earth System Science Data*, 15, 5301–5369, <https://doi.org/10.5194/essd-15-5301-2023>, 2023.
- 1010 Gatti, L. V., Basso, L. S., Miller, J. B., Gloor, M., Gatti Domingues, L., Cassol, H. L. G., Tejada, G., Aragão, L. E. O. C., Nobre, C., Peters, W., Marani, L., Arai, E., Sanches, A. H., Corrêa, S. M., Anderson, L., Von Randow, C., Correia, C. S. C., Crispim, S. P., and Neves, R. A. L.: Amazonia as a carbon source linked to deforestation and climate change, *Nature*, 595, 388–393, <https://doi.org/10.1038/s41586-021-03629-6>, 2021.
- 1020 Gibbs, H. K.: Olson’s major world ecosystem complexes ranked by carbon in live vegetation: An updated database using the GLC2000 land cover product, title of the publication associated with this dataset: Carbon Dioxide Information Analysis Center (CDIAC) Datasets, 2006.
- Gibelin, A.-L., Calvet, J.-C., and Viovy, N.: Modelling energy and CO₂ fluxes with an interactive vegetation land surface model-Evaluation at high and middle latitudes, *Agricultural and Forest Meteorology*, 148, 1611–1628, <https://doi.org/https://doi.org/10.1016/j.agrformet.2008.05.013>, 2008.
- 1025 Gier, B. K., Buchwitz, M., Reuter, M., Cox, P. M., Friedlingstein, P., and Eyring, V.: Spatially resolved evaluation of Earth system models with satellite column-averaged CO₂, *Biogeosciences*, 17, 6115–6144, <https://doi.org/10.5194/bg-17-6115-2020>, 2020.
- Giorgetta, M. A., Jungclaus, J., Reick, C. H., Legutke, S., Bader, J., Bottinger, M., Brovkin, V., Crueger, T., Esch, M., Fieg, K., Glushak, K., Gayler, V., Haak, H., Hollweg, H. D., Ilyina, T., Kinne, S., Kornbluh, L., Matei, D., Mauritsen, T., Mikolajewicz, U., Mueller, W., Notz, D., Pithan, F., Raddatz, T., Rast, S., Redler, R., Roeckner, E., Schmidt, H., Schnur, R., Segsneider, J., Six, K. D., Stockhouse, M., Timmreck, C., Wegner, J., Widmann, H., Wieners, K. H., Claussen, M., Marotzke, J., and Stevens, B.: Climate and carbon cycle changes from 1850 to 2100 in MPI-ESM simulations for the Coupled Model Intercomparison Project phase 5, *Journal of Advances in Modeling Earth Systems*, 5, 572–597, <https://doi.org/10.1002/jame.20038>, 2013.



- Gleckler, P. J., Taylor, K. E., and Doutriaux, C.: Performance metrics for climate models, *Journal of Geophysical Research: Atmospheres*, 113, <https://doi.org/10.1029/2007jd008972>, 2008.
- 1035 Global Carbon Project: Supplemental data of Global Carbon Project 2021, <https://doi.org/10.18160/GCP-2021>, 2021.
- Goll, D. S., Winkler, A. J., Raddatz, T., Dong, N., Prentice, I. C., Ciais, P., and Brovkin, V.: Carbon–nitrogen interactions in idealized simulations with JSBACH (version 3.10), *Geoscientific Model Development*, 10, 2009–2030, <https://doi.org/10.5194/gmd-10-2009-2017>, 2017.
- Hajima, T., Watanabe, M., Yamamoto, A., Tatebe, H., Noguchi, M. A., Abe, M., Ohgaito, R., Ito, A., Yamazaki, D., Okajima, H., Ito, A., Takata, K., Ogochi, K., Watanabe, S., and Kawamiya, M.: Development of the MIROC-ES2L Earth system model and the evaluation of biogeochemical processes and feedbacks, *Geosci. Model Dev.*, 13, 2197–2244, <https://doi.org/10.5194/gmd-13-2197-2020>, 2020.
- 1040 Hosaka, M.: A new MRI land surface model HAL, in: *AGU Fall Meeting Abstracts*, vol. 2011, pp. GC43B–0901, 2011.
- Hugelius, G., Tarnocai, C., Broll, G., Canadell, J. G., Kuhry, P., and Swanson, D. K.: The Northern Circumpolar Soil Carbon Database: spatially distributed datasets of soil coverage and soil carbon storage in the northern permafrost regions, *Earth System Science Data*, 5, 3–13, <https://doi.org/10.5194/essd-5-3-2013>, 2013.
- 1045 Hurrell, J. W., Holland, M. M., Gent, P. R., Ghan, S., Kay, J. E., Kushner, P. J., Lamarque, J.-F., Large, W. G., Lawrence, D., Lindsay, K., Lipscomb, W. H., Long, M. C., Mahowald, N., Marsh, D. R., Neale, R. B., Rasch, P., Vavrus, S., Vertenstein, M., Bader, D., Collins, W. D., Hack, J. J., Kiehl, J., and Marshall, S.: The Community Earth System Model: A Framework for Collaborative Research, *Bulletin of the American Meteorological Society*, 94, 1339–1360, <https://doi.org/10.1175/bams-d-12-00121.1>, 2013.
- 1050 IPCC: *Climate Change 2021: The Physical Science Basis. Contribution of Working Group I to the Sixth Assessment Report of the Intergovernmental Panel on Climate Change*, vol. In Press, Cambridge University Press, Cambridge, United Kingdom and New York, NY, USA, <https://doi.org/10.1017/9781009157896>, 2021.
- Ito, A. and Inatomi, M.: Water-Use Efficiency of the Terrestrial Biosphere: A Model Analysis Focusing on Interactions between the Global Carbon and Water Cycles, *Journal of Hydrometeorology*, 13, 681 – 694, <https://doi.org/10.1175/JHM-D-10-05034.1>, 2012.
- 1055 Ji, D., Wang, L., Feng, J., Wu, Q., Cheng, H., Zhang, Q., Yang, J., Dong, W., Dai, Y., Gong, D., Zhang, R. H., Wang, X., Liu, J., Moore, J. C., Chen, D., and Zhou, M.: Description and basic evaluation of Beijing Normal University Earth System Model (BNU-ESM) version 1, *Geoscientific Model Development*, 7, 2039–2064, <https://doi.org/10.5194/gmd-7-2039-2014>, 2014.
- Jones, C. D.: So What Is in an Earth System Model?, *Journal of Advances in Modeling Earth Systems*, 12, e2019MS001967, <https://doi.org/10.1029/2019ms001967>, 2020.
- 1060 Jones, C. D., Ziehn, T., Anand, J., Bastos, A., Burke, E., Canadell, J. G., Cardoso, M., Ernst, Y., Jain, A. K., Jeong, S., Keller, E. D., Kondo, M., Lauerwald, R., Lin, T.-S., Murray-Tortarolo, G., Nabuurs, G.-J., O’Sullivan, M., Poulter, B., Qin, X., von Randow, C., Sanches, M., Schepaschenko, D., Shvidenko, A., Smallman, T. L., Tian, H., Villalobos, Y., Wang, X., and Yun, J.: RECCAP2 Future Component: Consistency and Potential for Regional Assessment to Constrain Global Projections, *AGU Advances*, 4, e2023AV001024, <https://doi.org/https://doi.org/10.1029/2023AV001024>, e2023AV001024 2023AV001024, 2023.
- 1065 Jung, M., Reichstein, M., Margolis, H. A., Cescatti, A., Richardson, A. D., Arain, M. A., Arneth, A., Bernhofer, C., Bonal, D., Chen, J., Gianelle, D., Gobron, N., Kiely, G., Kutsch, W., Lasslop, G., Law, B. E., Lindroth, A., Merbold, L., Montagnani, L., Moors, E. J., Papale, D., Sottocornola, M., Vaccari, F., and Williams, C.: Global patterns of land-atmosphere fluxes of carbon dioxide, latent heat, and sensible heat derived from eddy covariance, satellite, and meteorological observations, *Journal of Geophysical Research: Biogeosciences*, 116, <https://doi.org/10.1029/2010jg001566>, 2011.



- 1070 Jung, M., Koirala, S., Weber, U., Ichii, K., Gans, F., Camps-Valls, G., Papale, D., Schwalm, C., Tramontana, G., and Reichstein, M.: The FLUXCOM ensemble of global land-atmosphere energy fluxes, *Scientific Data*, 6, 74, <https://doi.org/10.1038/s41597-019-0076-8>, 2019.
- Keenan, T. and Williams, C.: The Terrestrial Carbon Sink, *Annual Review of Environment and Resources*, 43, 219–243, <https://doi.org/10.1146/annurev-environ-102017-030204>, 2018.
- Kou-Giesbrecht, S. and Arora, V. K.: Compensatory Effects Between CO₂, Nitrogen Deposition, and Nitrogen Fertilization in Terrestrial Biosphere Models Without Nitrogen Compromise Projections of the Future Terrestrial Carbon Sink, *Geophysical Research Letters*, 50, e2022GL102618, <https://doi.org/https://doi.org/10.1029/2022GL102618>, e2022GL102618 2022GL102618, 2023.
- Kou-Giesbrecht, S., Arora, V. K., Seiler, C., Arneth, A., Falk, S., Jain, A. K., Joos, F., Kennedy, D., Knauer, J., Sitch, S., O’Sullivan, M., Pan, N., Sun, Q., Tian, H., Vuichard, N., and Zaehle, S.: Evaluating nitrogen cycling in terrestrial biosphere models: a disconnect between the carbon and nitrogen cycles, *Earth System Dynamics*, 14, 767–795, <https://doi.org/10.5194/esd-14-767-2023>, 2023.
- 1080 Koven, C. D., Riley, W. J., Subin, Z. M., Tang, J. Y., Torn, M. S., Collins, W. D., Bonan, G. B., Lawrence, D. M., and Swenson, S. C.: The effect of vertically resolved soil biogeochemistry and alternate soil C and N models on C dynamics of CLM4, *Biogeosciences*, 10, 7109–7131, <https://doi.org/10.5194/bg-10-7109-2013>, 2013.
- Kowalczyk, E., Stevens, L., Law, R., Dix, M., Wang, Y., Harman, I., Haynes, K., Srbinovsky, J., Pak, B., and Ziehn, T.: The land surface model component of ACCESS: Description and impact on the simulated surface climatology, *Australian Meteorological and Oceanographic Journal*, 63, 65–82, 2013.
- 1085 Krinner, G., Viovy, N., de Noblet-Ducoudré, N., Ogée, J., Polcher, J., Friedlingstein, P., Ciais, P., Sitch, S., and Prentice, I. C.: A dynamic global vegetation model for studies of the coupled atmosphere-biosphere system, *Global Biogeochemical Cycles*, 19, <https://doi.org/https://doi.org/10.1029/2003GB002199>, 2005.
- Lauer, A., Eyring, V., Bellprat, O., Bock, L., Gier, B. K., Hunter, A., Lorenz, R., Pérez-Zanón, N., Righi, M., Schlund, M., Senftleben, D., Weigel, K., and Zechlau, S.: Earth System Model Evaluation Tool (ESMValTool) v2.0 – diagnostics for emergent constraints and future projections from Earth system models in CMIP, *Geosci. Model Dev. Discuss.*, 2020, 1–47, <https://doi.org/10.5194/gmd-2020-60>, 2020.
- 1090 Law, R. M., Ziehn, T., Matear, R. J., Lenton, A., Chamberlain, M. A., Stevens, L. E., Wang, Y. P., Srbinovsky, J., Bi, D., Yan, H., and Vohralik, P. F.: The carbon cycle in the Australian Community Climate and Earth System Simulator (ACCESS-ESM1) – Part 1: Model description and pre-industrial simulation, *Geosci. Model Dev.*, 10, 2567–2590, <https://doi.org/10.5194/gmd-10-2567-2017>, 2017.
- 1095 Lawrence, D. M., Oleson, K. W., Flanner, M. G., Thornton, P. E., Swenson, S. C., Lawrence, P. J., Zeng, X., Yang, Z.-L., Levis, S., Sakaguchi, K., Bonan, G. B., and Slater, A. G.: Parameterization improvements and functional and structural advances in Version 4 of the Community Land Model, *Journal of Advances in Modeling Earth Systems*, 3, <https://doi.org/10.1029/2011ms000045>, 2011.
- Lawrence, D. M., Fisher, R. A., Koven, C. D., Oleson, K. W., Swenson, S. C., Bonan, G., Collier, N., Ghimire, B., van Kampenhout, L., Kennedy, D., Kluzek, E., Lawrence, P. J., Li, F., Li, H., Lombardozzi, D., Riley, W. J., Sacks, W. J., Shi, M., Vertenstein, M., Wieder, W. R., Xu, C., Ali, A. A., Badger, A. M., Bisht, G., van den Broeke, M., Brunke, M. A., Burns, S. P., Buzan, J., Clark, M., Craig, A., Dahlin, K., Drewniak, B., Fisher, J. B., Flanner, M., Fox, A. M., Gentine, P., Hoffman, F., Keppel-Aleks, G., Knox, R., Kumar, S., Lenaerts, J., Leung, L. R., Lipscomb, W. H., Lu, Y., Pandey, A., Pelletier, J. D., Perket, J., Randerson, J. T., Ricciuto, D. M., Sanderson, B. M., Slater, A., Subin, Z. M., Tang, J., Thomas, R. Q., Val Martin, M., and Zeng, X.: The Community Land Model Version 5: Description of New Features, Benchmarking, and Impact of Forcing Uncertainty, *Journal of Advances in Modeling Earth Systems*, 11, 4245–4287, <https://doi.org/10.1029/2018ms001583>, 2019.
- 1105 Lee, E., Felzer, B. S., and Kothavala, Z.: Effects of nitrogen limitation on hydrological processes in CLM4-CN, *Journal of Advances in Modeling Earth Systems*, 5, 741–754, <https://doi.org/https://doi.org/10.1002/jame.20046>, 2013.



- Lee, W. L., Wang, Y. C., Shiu, C. J., Tsai, I., Tu, C. Y., Lan, Y. Y., Chen, J. P., Pan, H. L., and Hsu, H. H.: Taiwan Earth System Model Version 1: description and evaluation of mean state, *Geosci. Model Dev.*, 13, 3887–3904, <https://doi.org/10.5194/gmd-13-3887-2020>, 2020.
- 1110 Li, X., Melaas, E., Carrillo, C. M., Ault, T., Richardson, A. D., Lawrence, P., Friedl, M. A., Seyednasrollah, B., Lawrence, D. M., and Young, A. M.: A Comparison of Land Surface Phenology in the Northern Hemisphere Derived from Satellite Remote Sensing and the Community Land Model, *Journal of Hydrometeorology*, 23, 859 – 873, <https://doi.org/https://doi.org/10.1175/JHM-D-21-0169.1>, 2022.
- Liang, S., Cheng, J., Jia, K., Jiang, B., Liu, Q., Xiao, Z., Yao, Y., Yuan, W., Zhang, X., Zhao, X., and Zhou, J.: The Global Land Surface Satellite (GLASS) Product Suite, *Bulletin of the American Meteorological Society*, 102, E323 – E337, <https://doi.org/https://doi.org/10.1175/BAMS-D-18-0341.1>, 2021.
- 1115 Lindeskog, M., Arneeth, A., Bondeau, A., Waha, K., Seaquist, J., Olin, S., and Smith, B.: Implications of accounting for land use in simulations of ecosystem carbon cycling in Africa, *Earth System Dynamics*, 4, 385–407, <https://doi.org/10.5194/esd-4-385-2013>, 2013.
- Lovato, T., Peano, D., Butenschon, M., Matera, S., Iovino, D., Scoccimarro, E., Fogli, P. G., Cherchi, A., Bellucci, A., Gualdi, S., Masina, S., and Navarra, A.: CMIP6 Simulations With the CMCC Earth System Model (CMCC-ESM2), *Journal of Advances in Modeling Earth Systems*, 14, e2021MS002814, <https://doi.org/ARTN e2021MS002814> 10.1029/2021MS002814, 2022.
- 1120 Mauritsen, T., Bader, J., Becker, T., Behrens, J., Bittner, M., Brokopf, R., Brovkin, V., Claussen, M., Crueger, T., Esch, M., Fast, I., Fiedler, S., Fläschner, D., Gayler, V., Giorgetta, M., Goll, D. S., Haak, H., Hagemann, S., Hedemann, C., Hohengger, C., Ilyina, T., Jahns, T., Jimenez-de-la Cuesta, D., Jungclaus, J., Kleinen, T., Kloster, S., Kracher, D., Kinne, S., Kleberg, D., Lasslop, G., Kornbluh, L., Marotzke, J., Matei, D., Meraner, K., Mikolajewicz, U., Modali, K., Möbis, B., Müller, W. A., Nabel, J. E. M. S., Nam, C. C. W., Notz, D., Nyawira, S.-S., Paulsen, H., Peters, K., Pincus, R., Pohlmann, H., Pongratz, J., Popp, M., Raddatz, T. J., Rast, S., Redler, R., Reick, C. H., Rohrschneider, T., Schemann, V., Schmidt, H., Schnur, R., Schulzweida, U., Six, K. D., Stein, L., Stemmler, I., Stevens, B., von Storch, J.-S., Tian, F., Voigt, A., Vrese, P., Wieners, K.-H., Wilkenskeld, S., Winkler, A., and Roeckner, E.: Developments in the MPI-M Earth System Model version 1.2 (MPI-ESM1.2) and Its Response to Increasing CO₂, *Journal of Advances in Modeling Earth Systems*, 11, 998–1038, <https://doi.org/10.1029/2018ms001400>, 2019.
- 1130 Meehl, G. A., Boer, G. J., Covey, C., Latif, M., and Stouffer, R. J.: The Coupled Model Intercomparison Project (CMIP), *Bulletin of the American Meteorological Society*, 81, 313–318, www.jstor.org/stable/26215108, 2000.
- Neubauer, D., Ferrachat, S., Siegenthaler-Le Drian, C., Stier, P., Partridge, D. G., Tegen, I., Bey, I., Stanelle, T., Kokkola, H., and Lohmann, U.: The global aerosol–climate model ECHAM6.3–HAM2.3 – Part 2: Cloud evaluation, aerosol radiative forcing, and climate sensitivity, *Geosci. Model Dev.*, 12, 3609–3639, <https://doi.org/10.5194/gmd-12-3609-2019>, 2019.
- 1135 Oleson, K. W., Niu, G.-Y., Yang, Z.-L., Lawrence, D. M., Thornton, P. E., Lawrence, P. J., Stöckli, R., Dickinson, R. E., Bonan, G. B., Levis, S., Dai, A., and Qian, T.: Improvements to the Community Land Model and their impact on the hydrological cycle, *Journal of Geophysical Research: Biogeosciences*, 113, n/a–n/a, <https://doi.org/10.1029/2007jg000563>, 2008.
- Olson, J. S., Watts, J. A., and Allison, L. J.: Major world ecosystem complexes ranked by carbon in live vegetation: a database, <http://www.osti.gov/biblio/6944260>, 1985.
- 1140 Park, H. and Jeong, S.: Leaf area index in Earth system models: how the key variable of vegetation seasonality works in climate projections, *Environmental Research Letters*, 16, 034027, <https://doi.org/10.1088/1748-9326/abe2cf>, 2021.
- Park, S., Shin, J., Kim, S., Oh, E., and Kim, Y.: Global Climate Simulated by the Seoul National University Atmosphere Model Version 0 with a Unified Convection Scheme (SAM0-UNICON), *Journal of Climate*, 32, 2917–2949, <https://doi.org/10.1175/jcli-d-18-0796.1>, 2019.



- 1145 Qiao, F. L., Song, Z. Y., Bao, Y., Song, Y. J., Shu, Q., Huang, C. J., and Zhao, W.: Development and evaluation of an Earth System Model with surface gravity waves, *Journal of Geophysical Research-Oceans*, 118, 4514–4524, <https://doi.org/10.1002/jgrc.20327>, 2013.
- Rabin, S. S., Ward, D. S., Malyshev, S. L., Magi, B. I., Shevliakova, E., and Pacala, S. W.: A fire model with distinct crop, pasture, and non-agricultural burning: use of new data and a model-fitting algorithm for FINAL.1, *Geoscientific Model Development*, 11, 815–842, <https://doi.org/10.5194/gmd-11-815-2018>, 2018.
- 1150 Reuter, M., Buchwitz, M., Hilker, M., Heymann, J., Schneising, O., Pillai, D., Bovensmann, H., Burrows, J. P., Bösch, H., Parker, R., Butz, A., Hasekamp, O., O'Dell, C. W., Yoshida, Y., Gerbig, C., Nehrkorn, T., Deutscher, N. M., Warneke, T., Notholt, J., Hase, F., Kivi, R., Sussmann, R., Machida, T., Matsueda, H., and Sawa, Y.: Satellite-inferred European carbon sink larger than expected, *Atmospheric Chemistry and Physics*, 14, 13 739–13 753, <https://doi.org/10.5194/acp-14-13739-2014>, 2014.
- Righi, M., Andela, B., Eyring, V., Lauer, A., Predoi, V., Schlund, M., Vegas-Regidor, J., Bock, L., Brötz, B., de Mora, L., Diblen, F., Dreyer, L., Drost, N., Earnshaw, P., Hassler, B., Koldunov, N., Little, B., Loosveldt Tomas, S., and Zimmermann, K.: Earth System Model Evaluation Tool (ESMValTool) v2.0 – technical overview, *Geosci. Model Dev.*, 13, 1179–1199, <https://doi.org/10.5194/gmd-13-1179-2020>, 2020.
- 1155 Rödenbeck, C.: Estimating CO₂ sources and sinks from atmospheric mixing ratio measurements using a global inversion of atmospheric transport Technical Report 6, Max Planck Institute for Biogeochemistry, Jena, http://www.bgc-jena.mpg.de/CarboScope/s/tech_report6.pdf, 2005.
- Sanderson, B. M., Booth, B. B. B., Dunne, J., Eyring, V., Fisher, R. A., Friedlingstein, P., Gidden, M. J., Hajima, T., Jones, C. D., Jones, C., King, A., Koven, C. D., Lawrence, D. M., Lowe, J., Mengis, N., Peters, G. P., Rogelj, J., Smith, C., Snyder, A. C., Simpson, I. R., Swann, A. L. S., Tebaldi, C., Ilyina, T., Schleussner, C.-F., Seferian, R., Samset, B. H., van Vuuren, D., and Zaehle, S.: The need for carbon emissions-driven climate projections in CMIP7, *EGUsphere*, 2023, 1–51, <https://doi.org/10.5194/egusphere-2023-2127>, 2023.
- 1165 Sato, H., Itoh, A., and Kohyama, T.: SEIB–DGVM: A new Dynamic Global Vegetation Model using a spatially explicit individual-based approach, *Ecological Modelling*, 200, 279–307, <https://doi.org/https://doi.org/10.1016/j.ecolmodel.2006.09.006>, 2007.
- Schlund, M., Hassler, B., Lauer, A., Andela, B., Jöckel, P., Kazeroni, R., Loosveldt Tomas, S., Medeiros, B., Predoi, V., Sénési, S., Servonnat, J., Stacke, T., Vegas-Regidor, J., Zimmermann, K., and Eyring, V.: Evaluation of native Earth system model output with ESMValTool v2.6.0, *Geoscientific Model Development*, 16, 315–333, <https://doi.org/10.5194/gmd-16-315-2023>, 2023.
- 1170 Seiler, C., Melton, J. R., Arora, V. K., Sitch, S., Friedlingstein, P., Anthoni, P., Goll, D., Jain, A. K., Joetzjer, E., Lienert, S., Lombardozzi, D., Luyssaert, S., Nabel, J. E. M. S., Tian, H., Vuichard, N., Walker, A. P., Yuan, W., and Zaehle, S.: Are Terrestrial Biosphere Models Fit for Simulating the Global Land Carbon Sink?, *Journal of Advances in Modeling Earth Systems*, 14, e2021MS002 946, <https://doi.org/https://doi.org/10.1029/2021MS002946>, e2021MS002946 2021MS002946, 2022.
- Seland, Ø., Bentsen, M., Olivié, D., Toniazzo, T., Gjermundsen, A., Graff, L. S., Debernard, J. B., Gupta, A. K., He, Y.-C., Kirkevåg, A., Schwinger, J., Tjiputra, J., Aas, K. S., Bethke, I., Fan, Y., Griesfeller, J., Grini, A., Guo, C., Ilicak, M., Karset, I. H. H., Landgren, O., Liakka, J., Moseid, K. O., Nummelin, A., Spensberger, C., Tang, H., Zhang, Z., Heinze, C., Iversen, T., and Schulz, M.: Overview of the Norwegian Earth System Model (NorESM2) and key climate response of CMIP6 DECK, historical, and scenario simulations, *Geoscientific Model Development*, 13, 6165–6200, <https://doi.org/10.5194/gmd-13-6165-2020>, 2020.
- 1175 Sellar, A. A., Jones, C. G., Mulcahy, J. P., Tang, Y., Yool, A., Wiltshire, A., O'Connor, F. M., Stringer, M., Hill, R., Palmieri, J., Woodward, S., de Mora, L., Kuhlbrodt, T., Rumbold, S. T., Kelley, D. I., Ellis, R., Johnson, C. E., Walton, J., Abraham, N. L., Andrews, M. B., Andrews, T., Archibald, A. T., Berthou, S., Burke, E., Blockley, E., Carslaw, K., Dalvi, M., Edwards, J., Folberth, G. A., Gedney, N., Griffiths, P. T., Harper, A. B., Hendry, M. A., Hewitt, A. J., Johnson, B., Jones, A., Jones, C. D., Keeble, J., Liddicoat, S., Morgenstern,
- 1180



- O., Parker, R. J., Predoi, V., Robertson, E., Siahaan, A., Smith, R. S., Swaminathan, R., Woodhouse, M. T., Zeng, G., and Zerroukat, M.: UKESM1: Description and Evaluation of the U.K. Earth System Model, *Journal of Advances in Modeling Earth Systems*, 11, 4513–4558, <https://doi.org/10.1029/2019MS001739>, 2019.
- 1185
- Shi, M., Fisher, J. B., Brzostek, E. R., and Phillips, R. P.: Carbon cost of plant nitrogen acquisition: global carbon cycle impact from an improved plant nitrogen cycle in the Community Land Model, *Global change biology*, 22, 1299–1314, <https://doi.org/10.1111/gcb.13131>, 2016.
- Smith, B., Wårlind, D., Arneth, A., Hickler, T., Leadley, P., Siltberg, J., and Zaehle, S.: Implications of incorporating N cycling and N limitations on primary production in an individual-based dynamic vegetation model, *Biogeosciences*, 11, 2027–2054, <https://doi.org/10.5194/bg-11-2027-2014>, 2014.
- 1190
- Sulman, B. N., Phillips, R. P., Oishi, A. C., Shevliakova, E., and Pacala, S. W.: Microbe-driven turnover offsets mineral-mediated storage of soil carbon under elevated CO₂, *Nature Climate Change*, 4, 1099–1102, <https://doi.org/10.1038/nclimate2436>, 2014.
- Sulman, B. N., Shevliakova, E., Brzostek, E. R., Kivlin, S. N., Malyshev, S., Menge, D. N., and Zhang, X.: Diverse Mycorrhizal Associations Enhance Terrestrial C Storage in a Global Model, *Global Biogeochemical Cycles*, 33, 501–523, <https://doi.org/https://doi.org/10.1029/2018GB005973>, 2019.
- 1195
- Swart, N. C., Cole, J. N. S., Kharin, V. V., Lazare, M., Scinocca, J. F., Gillett, N. P., Anstey, J., Arora, V., Christian, J. R., Hanna, S., Jiao, Y., Lee, W. G., Majaess, F., Saenko, O. A., Seiler, C., Seinen, C., Shao, A., Sigmond, M., Solheim, L., von Salzen, K., Yang, D., and Winter, B.: The Canadian Earth System Model version 5 (CanESM5.0.3), *Geosci. Model Dev.*, 12, 4823–4873, <https://doi.org/10.5194/gmd-12-4823-2019>, 2019.
- 1200
- Séférian, R., Nabat, P., Michou, M., Saint-Martin, D., Voldoire, A., Colin, J., Decharme, B., Delire, C., Berthet, S., Chevallier, M., Sénési, S., Franchisteguy, L., Vial, J., Mallet, M., Joetzjer, E., Geoffroy, O., Guérémy, J.-F., Moine, M.-P., Msadek, R., Ribes, A., Rocher, M., Roehrig, R., Salas-y Mélia, D., Sanchez, E., Terray, L., Valcke, S., Waldman, R., Aumont, O., Bopp, L., Deshayes, J., Éthé, C., and Madec, G.: Evaluation of CNRM Earth System Model, CNRM-ESM2-1: Role of Earth System Processes in Present-Day and Future Climate, *Journal of Advances in Modeling Earth Systems*, 11, 4182–4227, <https://doi.org/10.1029/2019MS001791>, 2019.
- 1205
- Takata, K., Emori, S., and Watanabe, T.: Development of the minimal advanced treatments of surface interaction and runoff, *Global and Planetary Change*, 38, 209–222, [https://doi.org/https://doi.org/10.1016/S0921-8181\(03\)00030-4](https://doi.org/https://doi.org/10.1016/S0921-8181(03)00030-4), project for Intercomparison of Land-surface Parameterization Schemes, Phase 2(e), 2003.
- Taylor, K. E., Stouffer, R. J., and Meehl, G. A.: An Overview of CMIP5 and the Experiment Design, *Bulletin of the American Meteorological Society*, 93, 485–498, <https://doi.org/10.1175/bams-d-11-00094.1>, 2012.
- 1210
- Team, T. H. D., Martin, G., Bellouin, N., Collins, W. J., Culverwell, I. D., Halloran, P. R., Hardiman, S. C., Hinton, T. J., Jones, C. D., McDonald, R. E., McLaren, A. J., O'Connor, F. M., Roberts, M. J., Rodriguez, J. M., Woodward, S., Best, M. J., Brooks, M. E., Brown, A. R., Butchart, N., Dearden, C., Derbyshire, S. H., Dharssi, I., Doutriaux-Boucher, M., Edwards, J. M., Falloon, P. D., Gedney, N., Gray, L. J., Hewitt, H. T., Hobson, M., Huddleston, M. R., Hughes, J., Ineson, S., Ingram, W. J., James, P. M., Johns, T. C., Johnson, C. E., Jones, A., Jones, C. P., Joshi, M. M., Keen, A. B., Liddicoat, S., Lock, A. P., Maidens, A. V., Manners, J. C., Milton, S. F., Rae, J. G. L., Ridley, J. K., Sellar, A., Senior, C. A., Totterdell, I. J., Verhoef, A., Vidale, P. L., and Wiltshire, A.: The HadGEM2 family of Met Office Unified Model climate configurations, *Geosci. Model Dev.*, 4, 723–757, <https://doi.org/10.5194/gmd-4-723-2011>, 2011.
- 1215
- Tegen, I., Neubauer, D., Ferrachat, S., Siegenthaler-Le Drian, C., Bey, I., Schutgens, N., Stier, P., Watson-Parris, D., Stanelle, T., Schmidt, H., Rast, S., Kokkola, H., Schultz, M., Schroeder, S., Daskalakis, N., Barthel, S., Heinold, B., and Lohmann, U.: The global aerosol–climate



- 1220 model ECHAM6.3–HAM2.3 – Part 1: Aerosol evaluation, *Geosci. Model Dev.*, 12, 1643–1677, <https://doi.org/10.5194/gmd-12-1643-2019>, 2019.
- Tjiputra, J. F., Roelandt, C., Bentsen, M., Lawrence, D. M., Lorentzen, T., Schwinger, J., Seland, O., and Heinze, C.: Evaluation of the carbon cycle components in the Norwegian Earth System Model (NorESM), *Geoscientific Model Development*, 6, 301–325, <https://doi.org/10.5194/gmd-6-301-2013>, 2013.
- 1225 Todd-Brown, K. E. O., Randerson, J. T., Hopkins, F., Arora, V., Hajima, T., Jones, C., Shevliakova, E., Tjiputra, J., Volodin, E., Wu, T., Zhang, Q., and Allison, S. D.: Changes in soil organic carbon storage predicted by Earth system models during the 21st century, *Biogeosciences*, 11, 2341–2356, <https://doi.org/10.5194/bg-11-2341-2014>, 2014.
- Tuomi, M., Laiho, R., Repo, A., and Liski, J.: Wood decomposition model for boreal forests, *Ecological Modelling*, 222, 709–718, <https://doi.org/https://doi.org/10.1016/j.ecolmodel.2010.10.025>, 2011.
- 1230 UCAR: CLM technical note, https://escomp.github.io/ctsm-docs/versions/release-clm5.0/html/tech_note/, last access: 2022-09, 2020.
- Varney, R. M., Chadburn, S. E., Burke, E. J., and Cox, P. M.: Evaluation of soil carbon simulation in CMIP6 Earth system models, *Biogeosciences*, 19, 4671–4704, <https://doi.org/10.5194/bg-19-4671-2022>, 2022.
- Varney, R. M., Chadburn, S. E., Burke, E. J., Jones, S., Wiltshire, A. J., and Cox, P. M.: Simulated responses of soil carbon to climate change in CMIP6 Earth system models: the role of false priming, *Biogeosciences*, 20, 3767–3790, <https://doi.org/10.5194/bg-20-3767-2023>, 2023a.
- 1235 Varney, R. M., Friedlingstein, P., Chadburn, S. E., Burke, E. J., and Cox, P. M.: Soil carbon-concentration and carbon-climate feedbacks in CMIP6 Earth system models, *EGUsphere*, 2023, 1–21, <https://doi.org/10.5194/egusphere-2023-2666>, 2023b.
- Verseghy, D. L.: Class—A Canadian land surface scheme for GCMS. I. Soil model, *International Journal of Climatology*, 11, 111–133, <https://doi.org/https://doi.org/10.1002/joc.3370110202>, 1991.
- 1240 Verseghy, D. L.: The Canadian land surface scheme (CLASS): Its history and future, *Atmosphere-Ocean*, 38, 1–13, <https://doi.org/10.1080/07055900.2000.9649637>, 2000.
- Verseghy, D. L., McFarlane, N. A., and Lazare, M.: Class—A Canadian land surface scheme for GCMS, II. Vegetation model and coupled runs, *International Journal of Climatology*, 13, 347–370, <https://doi.org/https://doi.org/10.1002/joc.3370130402>, 1993.
- Volodin, E. M.: Atmosphere-ocean general circulation model with the carbon cycle, *Izvestiya, Atmospheric and Oceanic Physics*, 43, 266–280, <https://doi.org/10.1134/s0001433807030024>, 2007.
- 1245 Volodin, E. M., Dianskii, N. A., and Gusev, A. V.: Simulating present-day climate with the INMCM4.0 coupled model of the atmospheric and oceanic general circulations, *Izvestiya, Atmospheric and Oceanic Physics*, 46, 414–431, <https://doi.org/10.1134/S000143381004002X>, 2010.
- Volodin, E. M., Mortikov, E. V., Kostykin, S. V., Galin, V. Y., Lykosov, V. N., Gritsun, A. S., Diansky, N. A., Gusev, A. V., and Yakovlev, N. G.: Simulation of modern climate with the new version of the INM RAS climate model, *Izvestiya, Atmospheric and Oceanic Physics*, 53, 142–155, <https://doi.org/10.1134/S0001433817020128>, 2017a.
- 1250 Volodin, E. M., Mortikov, E. V., Kostykin, S. V., Galin, V. Y., Lykosov, V. N., Gritsun, A. S., Diansky, N. A., Gusev, A. V., and Iakovlev, N. G.: Simulation of the present-day climate with the climate model INMCM5, *Climate Dynamics*, 49, 3715–3734, <https://doi.org/10.1007/s00382-017-3539-7>, 2017b.
- 1255 Volodin, E. M., Mortikov, E. V., Kostykin, S. V., Galin, V. Y., Lykosov, V. N., Gritsun, A. S., Diansky, N. A., Gusev, A. V., Iakovlev, N. G., Shestakova, A. A., and Emelina, S. V.: Simulation of the modern climate using the INM-CM48 climate model, *Russian Journal of Numerical Analysis and Mathematical Modelling*, 33, 367–374, <https://doi.org/10.1515/rnam-2018-0032>, 2018.



- 1260 Wang, S., Luo, Y., and Niu, S.: Reparameterization Required After Model Structure Changes From Carbon Only to Carbon-Nitrogen Coupling, *Journal of Advances in Modeling Earth Systems*, 14, e2021MS002798, <https://doi.org/https://doi.org/10.1029/2021MS002798>, e2021MS002798 2021MS002798, 2022.
- Wang, Y. P., Law, R. M., and Pak, B.: A global model of carbon, nitrogen and phosphorus cycles for the terrestrial biosphere, *Biogeosciences*, 7, 2261–2282, <https://doi.org/10.5194/bg-7-2261-2010>, 2010.
- Watanabe, S., Hajima, T., Sudo, K., Nagashima, T., Takemura, T., Okajima, H., Nozawa, T., Kawase, H., Abe, M., Yokohata, T., Ise, T., Sato, H., Kato, E., Takata, K., Emori, S., and Kawamiya, M.: MIROC-ESM 2010: model description and basic results of CMIP5-20c3m experiments, *Geoscientific Model Development*, 4, 845–872, <https://doi.org/10.5194/gmd-4-845-2011>, 2011.
- 1265 Wei, N., Xia, J., Zhou, J., Jiang, L., Cui, E., Ping, J., and Luo, Y.: Evolution of Uncertainty in Terrestrial Carbon Storage in Earth System Models from CMIP5 to CMIP6, *Journal of Climate*, 35, 5483 – 5499, <https://doi.org/https://doi.org/10.1175/JCLI-D-21-0763.1>, 2022.
- Weigel, K., Bock, L., Gier, B. K., Lauer, A., Righi, M., Schlund, M., Adeniyi, K., Andela, B., Arnone, E., Berg, P., Caron, L.-P., Cionni, I., Corti, S., Drost, N., Hunter, A., Lledó, L., Mohr, C. W., Paçal, A., Pérez-Zanón, N., Predoi, V., Sandstad, M., Sillmann, J., Sterl, A., 1270 Vegas-Regidor, J., von Hardenberg, J., and Eyring, V.: Earth System Model Evaluation Tool (ESMValTool) v2.0 – diagnostics for extreme events, regional and impact evaluation, and analysis of Earth system models in CMIP, *Geoscientific Model Development*, 14, 3159–3184, <https://doi.org/10.5194/gmd-14-3159-2021>, 2021.
- Weng, E. S., Malyshev, S., Lichstein, J. W., Farrior, C. E., Dybzinski, R., Zhang, T., Shevliakova, E., and Pacala, S. W.: Scaling from individual trees to forests in an Earth system modeling framework using a mathematically tractable model of height-structured competition, 1275 *Biogeosciences*, 12, 2655–2694, <https://doi.org/10.5194/bg-12-2655-2015>, 2015.
- Wieder, W.: RegridDED Harmonized World Soil Database v1.2, 2014.
- Wieder, W. R., Lawrence, D. M., Fisher, R. A., Bonan, G. B., Cheng, S. J., Goodale, C. L., Grandy, A. S., Koven, C. D., Lombardozzi, D. L., Oleson, K. W., and Thomas, R. Q.: Beyond Static Benchmarking: Using Experimental Manipulations to Evaluate Land Model Assumptions, *Global Biogeochemical Cycles*, 33, 1289–1309, <https://doi.org/10.1029/2018gb006141>, 2019.
- 1280 Wiltshire, A. J., Burke, E. J., Chadburn, S. E., Jones, C. D., Cox, P. M., Davies-Barnard, T., Friedlingstein, P., Harper, A. B., Liddicoat, S., Sitch, S., and Zaehle, S.: JULES-CN: a coupled terrestrial carbon–nitrogen scheme (JULES vn5.1), *Geoscientific Model Development*, 14, 2161–2186, <https://doi.org/10.5194/gmd-14-2161-2021>, 2021.
- Xiao, Z., Liang, S., and Jiang, B.: Evaluation of four long time-series global leaf area index products, *Agricultural and Forest Meteorology*, 246, 218–230, <https://doi.org/https://doi.org/10.1016/j.agrformet.2017.06.016>, 2017.
- 1285 Yang, X., Thornton, P., Ricciuto, D., Wang, Y., and Hoffman, F.: Global evaluation of terrestrial biogeochemistry in the Energy Exascale Earth System Model (E3SM) and the role of the phosphorus cycle in the historical terrestrial carbon balance, *Biogeosciences*, 20, 2813–2836, <https://doi.org/10.5194/bg-20-2813-2023>, 2023.
- Yuan, W., Liu, S., Zhou, G., Zhou, G., Tieszen, L. L., Baldocchi, D., Bernhofer, C., Gholz, H., Goldstein, A. H., Goulden, M. L., Hollinger, D. Y., Hu, Y., Law, B. E., Stoy, P. C., Vesala, T., and Wofsy, S. C.: Deriving a light use efficiency model from eddy co- 1290 variance flux data for predicting daily gross primary production across biomes, *Agricultural and Forest Meteorology*, 143, 189–207, <https://doi.org/https://doi.org/10.1016/j.agrformet.2006.12.001>, 2007.
- Yukimoto, S., Yoshimura, H., Hosaka, M., Sakami, T., Tsujino, H., Hirabara, M., Tanaka, T. Y., Deushi, M., Obata, A., Nakano, H., Adachi, Y., Shindo, E., Yabu, S., Ose, T., and Kitoh, A.: Meteorological Research Institute-Earth System Model Version 1 (MRI-ESM1), Technical Reports, 64, 88, <https://doi.org/10.11483/mritechrepo.64>, 2011.



- 1295 Yukimoto, S., Kawai, H., Koshiro, T., Oshima, N., Yoshida, K., Urakawa, S., Tsujino, H., Deushi, M., Tanaka, T., Hosaka, M., Yabu, S., Yoshimura, H., Shindo, E., Mizuta, R., Obata, A., Adachi, Y., and Ishii, M.: The Meteorological Research Institute Earth System Model Version 2.0, MRI-ESM2.0: Description and Basic Evaluation of the Physical Component, *Journal of the Meteorological Society of Japan*, Ser. II, 97, 931–965, <https://doi.org/10.2151/jmsj.2019-051>, 2019.
- Zaehle, S., Jones, C. D., Houlton, B., Lamarque, J.-F., and Robertson, E.: Nitrogen Availability Reduces CMIP5 Projections of Twenty-First-Century Land Carbon Uptake, *Journal of Climate*, 28, 2494 – 2511, <https://doi.org/10.1175/JCLI-D-13-00776.1>, 2015.
- 1300 Zhang, Q., Pitman, A. J., Wang, Y. P., Dai, Y. J., and Lawrence, P. J.: The impact of nitrogen and phosphorous limitation on the estimated terrestrial carbon balance and warming of land use change over the last 156 yr, *Earth System Dynamics*, 4, 333–345, <https://doi.org/10.5194/esd-4-333-2013>, 2013.
- Zhu, Z., Bi, J., Pan, Y., Ganguly, S., Anav, A., Xu, L., Samanta, A., Piao, S., Nemani, R., and Myneni, R.: Global Data Sets of Vegetation Leaf Area Index (LAI)3g and Fraction of Photosynthetically Active Radiation (FPAR)3g Derived from Global Inventory Modeling and Mapping Studies (GIMMS) Normalized Difference Vegetation Index (NDVI3g) for the Period 1981 to 2011, *Remote Sensing*, 5, 927–948, <https://doi.org/10.3390/rs5020927>, 2013.
- 1305 Ziehn, T., Lenton, A., Law, R. M., Matear, R. J., and Chamberlain, M. A.: The carbon cycle in the Australian Community Climate and Earth System Simulator (ACCESS-ESM1) – Part 2: Historical simulations, *Geosci. Model Dev.*, 10, 2591–2614, <https://doi.org/10.5194/gmd-10-2591-2017>, 2017.
- 1310 Ziehn, T., Chamberlain, M. A., Law, R. M., Lenton, A., Bodman, R. W., Dix, M., Stevens, L., Wang, Y.-P., and Srbnovsky, J.: The Australian Earth System Model: ACCESS-ESM1.5, *Journal of Southern Hemisphere Earth Systems Science*, 70, 193, <https://doi.org/10.1071/es19035>, 2020.



Table 1: CMIP6 models analysed in this study. Under Comments, D stands for models including dynamic vegetation and N for models including Nitrogen cycles. Models for which emission driven simulations are also analysed are marked in bold script.

Model	Institute	Atmosphere model	Land model	Comment	Main reference
ACCESS-ESM1-5	Commonwealth Scientific and Industrial Research Organisation, Australia	UM7.3	CABLE2.4, CASA-CNP	N	Law et al. (2017); Ziehn et al. (2017, 2020)
CanESM5	Canadian Center for Climate Modeling and Analysis, Canada	CanAM5	CLASS3.6, CTEM1.2	D	Swart et al. (2019)
CanESM5-CanOE	Canadian Center for Climate Modeling and Analysis, Canada	CanAM5	CLASS3.6, CTEM1.2	D	Swart et al. (2019)
CESM2	National Center for Atmospheric Research, USA	CAM6	CLM5	N, D	Danabasoglu et al. (2020)
CESM2-WACCM	National Center for Atmospheric Research, USA	WACCM6	CLM5	N, D	Danabasoglu et al. (2020)
CMCC-CM2-SR5	The Euro-Mediterranean Centre on Climate Change, Italy	CAM5	CLM4.5	N	Cherchi et al. (2019)
CMCC-ESM2	The Euro-Mediterranean Centre on Climate Change, Italy	CAM5	CLM4.5-BGC	N	Lovato et al. (2022)



CNRM-ESM2-1	CNRM-CERFACS, France	ARPEGE-Climate v6.3 + SURFEX v8.0	ISBA + CTRIP			Séférian et al. (2019)
EC-Earth3-CC	EC-Earth Consortium, Europe	IFS 36r4 + HTES- SEL + TM5	LPJ-GUESS	N, D		Döscher et al. (2022)
EC-Earth3-Veg	EC-Earth Consortium, Europe	IFS 36r4 + HTES- SEL	LPJ-GUESS	N, D		Döscher et al. (2022)
GFDL-ESM4	Geophysical Fluid Dynamics Laboratory, United States	AM4.1	LM4.1	D		Dunne et al. (2020)
INM-CM4-8	Institute for Numerical Mathematics, Russian Academy of Science, Russia	Inbuilt	Inbuilt			Volodin et al. (2018)
INM-CM5-0	Institute for Numerical Mathematics, Russian Academy of Science, Russia	Inbuilt	Inbuilt			Volodin et al. (2017a, b)
IPSL-CM6A-LR	L'Institut Pierre-Simon Laplace, France	LMDZ6A	ORCHIDEEv2			Boucher et al. (2020)
MIROC-ES2L	MIROC, Japan	MIROC-AGCM + SPRINTARS	VISIT-e & MAT- SIRO6	N		Hajima et al. (2020)
MPI-ESM-1-2-HAM	HAMMOZ- Consortium, Europe	ECHAM6.3- HAM2.3	JSBACH3.2			Neubauer et al. (2019); Tegen et al. (2019)
MPI-ESM1-2-LR	HAMMOZ- Consortium, Europe	ECHAM6.3	JSBACH3.2	N, D		Mauritsen et al. (2019)



MRI-ESM2-0	Meteorological Research Institute, Japan	MRI-AGCM3.5 + MASINGAR mk-2r4c + MRI-CCM2.1	HAL			Yukimoto et al. (2019)
NorESM2-LM	NorESM Climate Modeling Consortium, Norway	Modified CAM6	CLM5	N, D		Seland et al. (2020)
NorESM2-MM	NorESM Climate Modeling Consortium, Norway	Modified CAM6	CLM5	N, D		Seland et al. (2020)
UKESM1-0-LL	Met Office Hadley Centre, United Kingdom	Unified Model + UKCA	JULES-ES-1.0	N, D		Sellar et al. (2019)
SAM0-UNICON	Seoul National University, Republic of Korea	CAM5 + UNICON	CLM4	N		Park et al. (2019)
TaiESM1	Research Centre for Environmental Changes, Academia Sinica, Taiwan	Modified CAM5.3	Modified CLM4	N		Lee et al. (2020)



Table 2: CMIP5 models used in this study, notations as in Table 1.

Model	Institute	Atmosphere model	Land model	Comment	Main reference
BNU-ESM	College of Global Change and System Science, China	CAM3.5	CoLM + BNU-DGVM	D	Ji et al. (2014)
CanESM2	Canadian Center for Climate Modeling and Analysis, BC, Canada	CanAM4	CLASS2.7 + CTEM1		Arora et al. (2011)
CESM1-BGC	National Center for Atmospheric Research, United States	CAM4	CLM4	N	Hurrell et al. (2013)
GFDL-ESM2G	Geophysical Fluid Dynamics Laboratory, USA	AM2	LM3.0	D	Dunne et al. (2012, 2013)
GFDL-ESM2M	Geophysical Fluid Dynamics Laboratory, USA	AM2	LM3.0	D	Dunne et al. (2012, 2013)
HadGEM2-CC	Met Office Hadley Centre, United Kingdom	Unified v6.6	Model JULES + TRIF-FID	D	Collins et al. (2011); Team et al. (2011)
HadGEM2-ES	Met Office Hadley Centre, United Kingdom	Unified v6.6	Model JULES + TRIF-FID	D	Collins et al. (2011); Team et al. (2011)
Inmcm4	Institute for Numerical Mathematics, Russia	Inbuilt	Inbuilt		Volodin et al. (2010)
FIO-ESM	The First Institute of Oceanography, SOA, China	CAM3.0	CLM3.5 + CASA		Bao et al. (2012); Qiao et al. (2013)



IPSL-CM5A-LR	L'Institut Simon France	Pierre- Laplace,	LMDZ5	ORCHIDEE		Dufresne (2013)	et al.
IPSL-CM5B-LR	L'Institut Simon France	Pierre- Laplace,	LMDZ5	ORCHIDEE		Dufresne (2013)	et al.
MIROC-ESM	Japan Agency for Marine-Earth Science and Technology, Japan;	Agency for Sci- ence and Technology, Atmosphere and Ocean Research Institute, Japan	MIROC-AGCM + SPRINTARS	MATSIRO SEIB-DGVM	+ D	Watanabe (2011)	et al.
MIROC-ESM-CHEM	Japan Agency for Marine-Earth Science and Technology, Japan;	Agency for Sci- ence and Technology, Atmosphere and Ocean Research Institute, Japan	MIROC-AGCM + SPRINTARS	MATSIRO SEIB-DGVM	+ D	Watanabe (2011)	et al.
MPI-ESM-LR	Max Planck Institute for Meteorology, Ger- many		ECHAM6	JSBACH BETHY	+ D	Giorgetta (2013)	et al.
MPI-ESM-MR	Max Planck Institute for Meteorology, Ger- many		ECHAM6	JSBACH BETHY	+ D	Giorgetta (2013)	et al.
MRI-ESM1	Meteorological Re- search Institute, Japan		MRI-AGCM3.3	HAL		Yukimoto (2011)	et al.
NorESM1-ME	Norwegian Climate Center, Norway		CAM4-Oslo	CLM4	N	Tjiputra et al. (2013)	



Table 3. Reference data sets used in this study. data sets in bold are the main reference data set and those in italics the alternate reference for Figures 16-18.

Data set	Source	Variable	Start Year	Reference
JENA-CarboScope (sEXTocNEET_v2020)	Inversion	Land-Atmosphere Flux (NBP)	1957	Rödenbeck (2005)
<i>CAMS (v20r2)</i>	Inversion	Land-Atmosphere Flux (NBP)	1979	Chevallier et al. (2005, 2010); Chevallier (2013)
GCP	Dynamic global vegetation and bookkeeping model averages	Land-Atmosphere Flux (NBP)	1959	Friedlingstein et al. (2022); Global Carbon Project (2021)
FLUXCOM ANN-v1	Mix	Gross Primary Productivity (GPP)	1980	Jung et al. (2019)
MTE	Upscaled in situ	Gross Primary Productivity (GPP)	1982	Jung et al. (2011)
<i>GLASS</i>	Satellite	Gross Primary Productivity (GPP), Leaf Area Index (LAI)	1982 (GPP), 1981 (LAI)	Yuan et al. (2007); Liang et al. (2021)
LAI3g	Satellite	Leaf Area Index (LAI)	1981	Zhu et al. (2013)
LAI4g	Satellite	Leaf Area Index (LAI)	1982	Cao et al. (2023)
NDP-017b	Mix	Carbon Mass in Vegetation (cVeg)	-	Gibbs (2006)
HWSD+NCSCD	Empirical	Carbon Mass in Soil Pool (cSoil)	-	Wieder (2014); Hugelius et al. (2013)

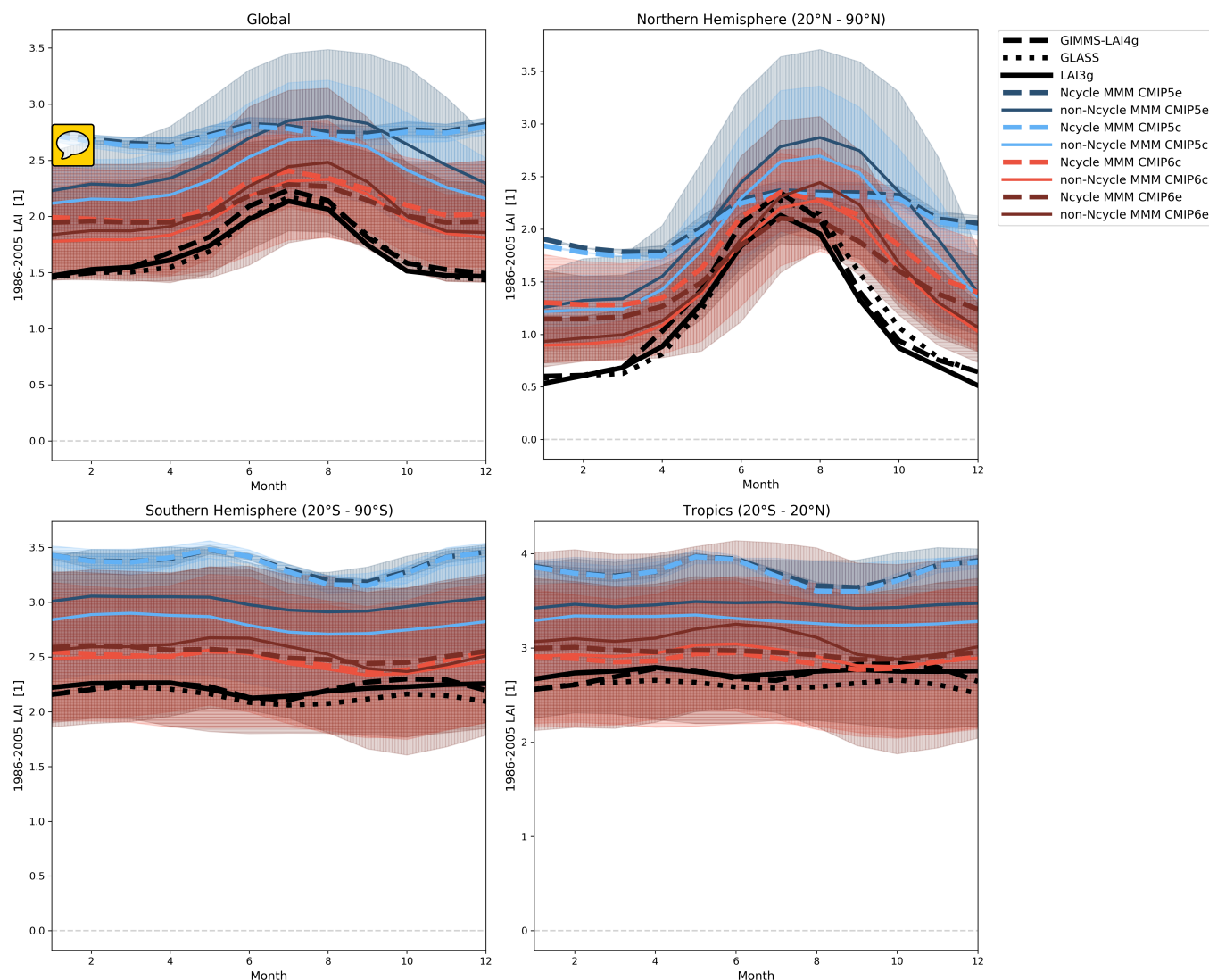


Figure 1. Seasonal Cycle of leaf area index (LAI) for a climatological mean of 1986-2005 for different regional averages: Global, Northern Hemisphere (20°N - 90°N), Southern Hemisphere (20°S - 90°S) and Tropics (20°S - 20°N). The reference data sets (LAI3g, solid line; LAI4g, dashed line; GLASS, dotted line) are shown in black, while the MMMs for the different project-experiment combinations are denoted by blue for CMIP5, red for CMIP6, with darker colors for the emission driven simulations (dark blue CMIP5e, dark red CMIP6e) and lighter colors for concentration driven simulations (light blue CMIP5c, light red CMIP6c). MMMs derived from models with coupled nitrogen cycle (Ncycle) are dashed, while solid lines represent MMMs of models without coupled nitrogen cycle (non-Ncycle). The shading represents the standard deviation of the MMMs, with vertical hatching for models without and horizontal hatching for models with coupled nitrogen cycle. For comparison with the reference data which contain many missing values, a common mask was applied to all data sets, removing values where any data set is missing a value.

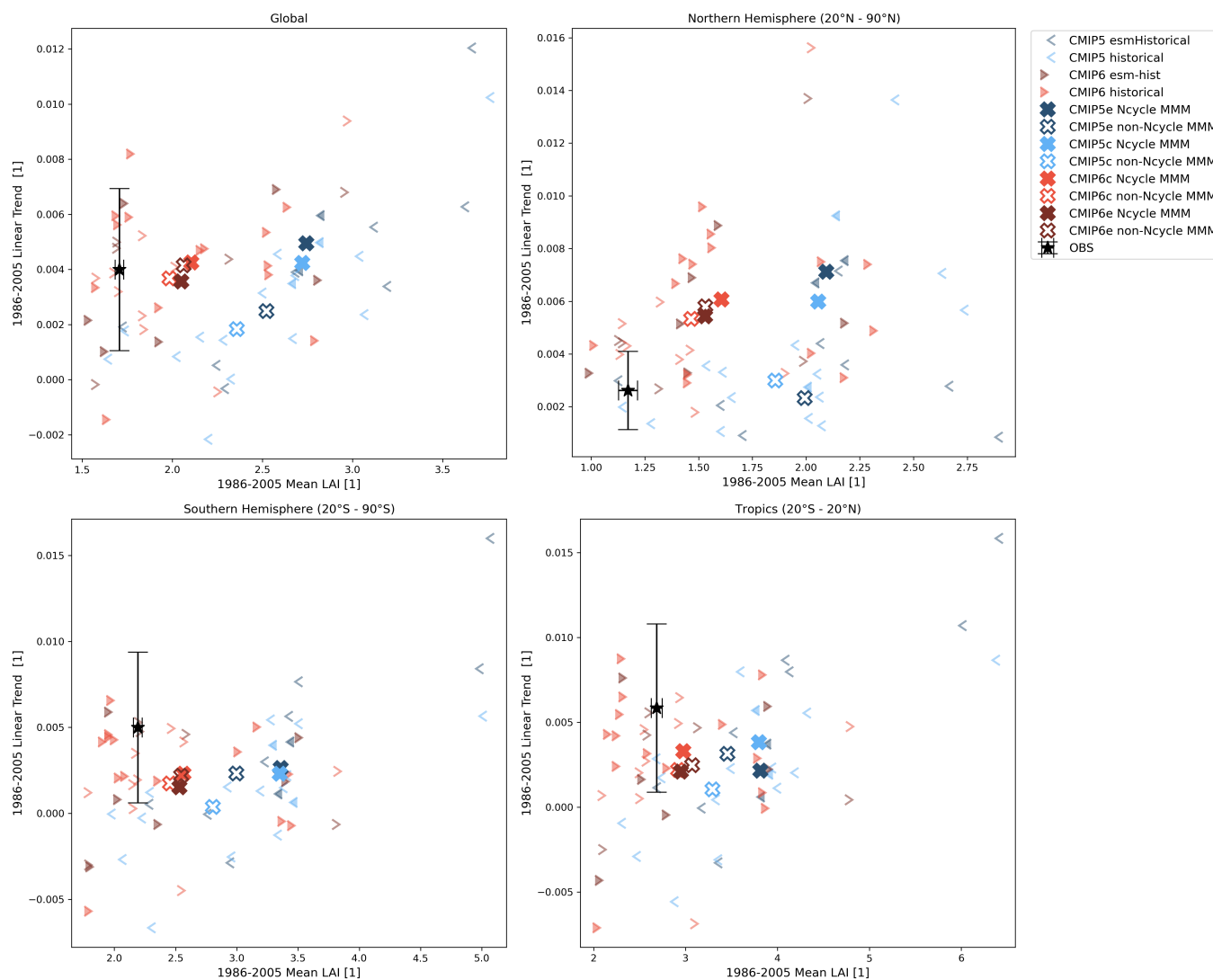


Figure 2. Mean and Trend of LAI computed over 1986-2005 for different regions: Global, Northern Hemisphere (20°N - 90°N), Southern Hemisphere (20°S - 90°S) and Tropics (20°S - 20°N). The mean of the reference data sets (LAI3g, LAI4g and GLASS) is denoted by a black star, with errorbars for the standard deviation. Models for project-experiment combinations are shown with a single symbol each, blue smaller than (<) sign for CMIP5 and red greater than (>) sign for CMIP6, with darker colors for emission driven and lighter colors for concentration driven simulations, as well as Ncycle models being denoted with a filled symbol. MMMs are depicted with cross symbols, filled for Ncycle MMMs and using the color assigned to their project-experiment combination.

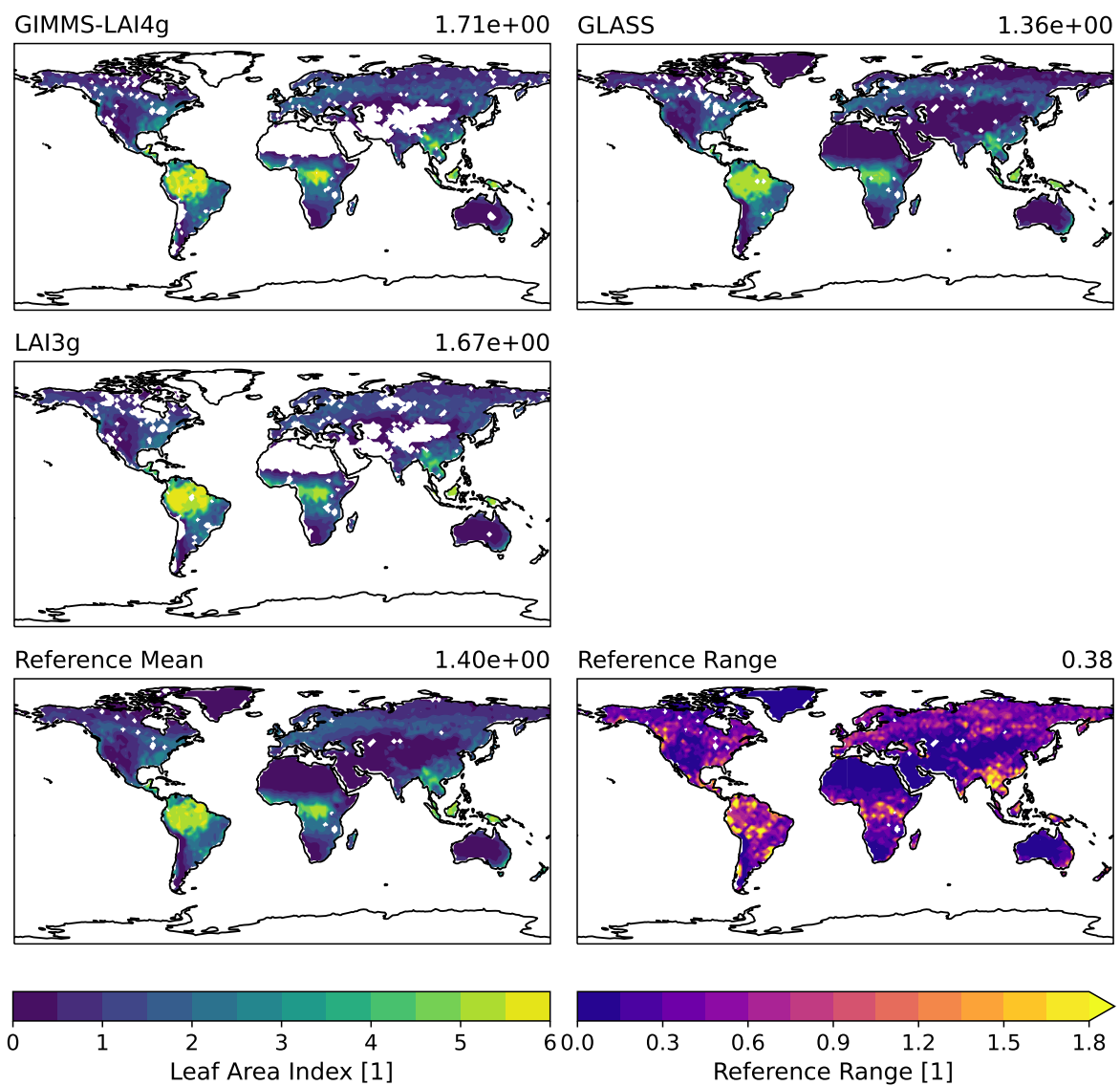


Figure 3. Global maps of LAI averaged over 1986-2005 for all reference data sets, as well as the mean and range between lowest and highest values per grid cell of the reference data sets.

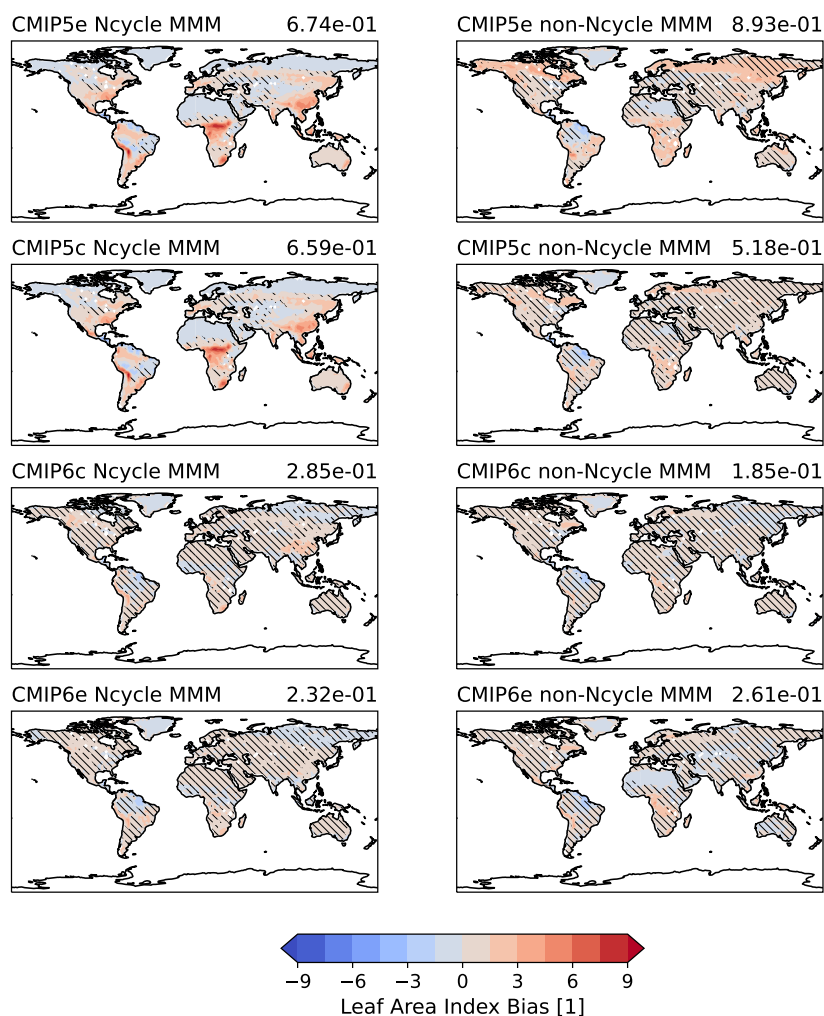


Figure 4. Global maps of LAI bias for 1986-2005 with respect to the reference data set mean shown in Figure 3. The panels show the MMMs of the models with (left) and without (right) coupled nitrogen cycle for the different project-experiment combinations. The hatching represents the areas where the MMM of the models and reference mean agree within the MMM std.

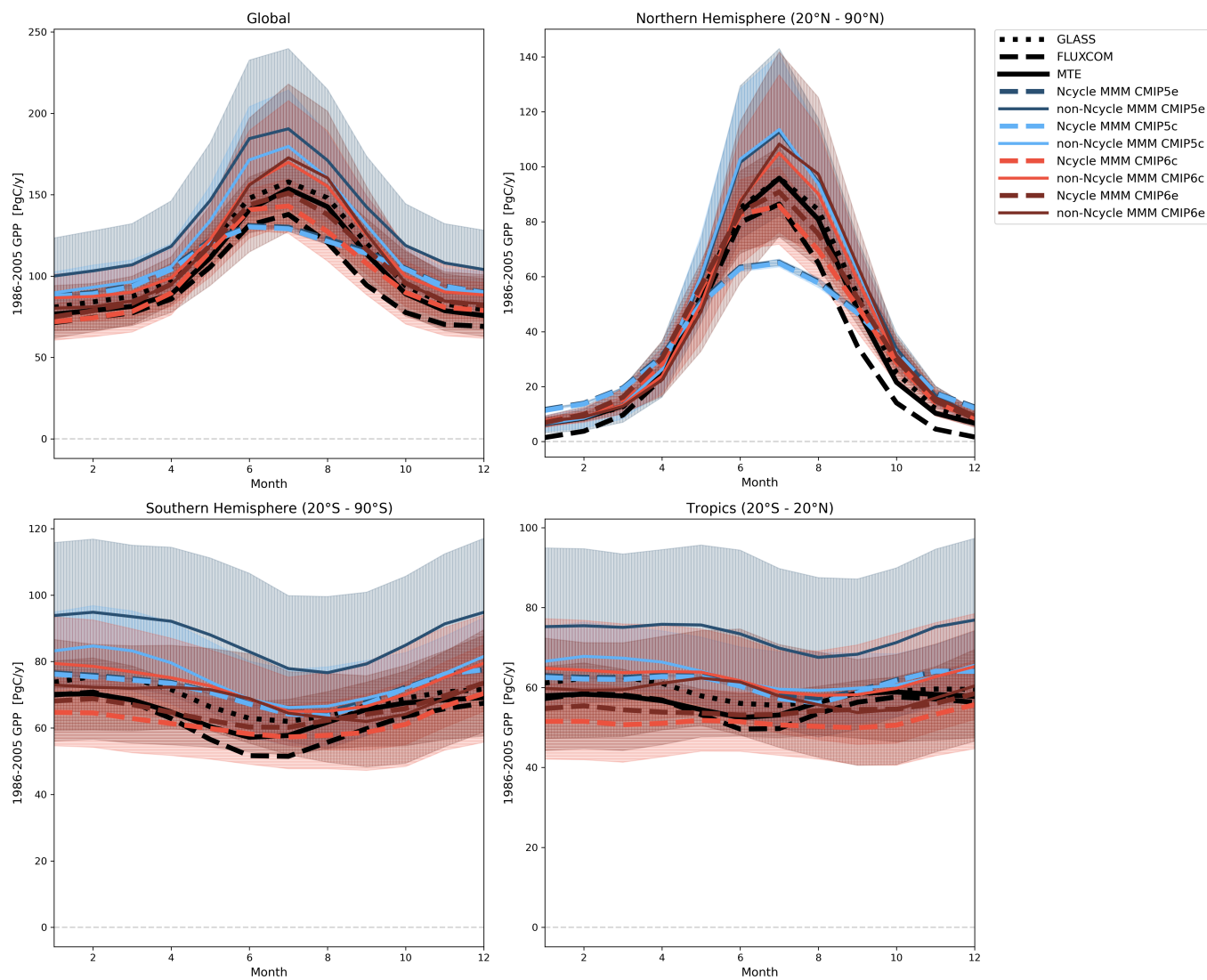


Figure 5. As Figure 1 but for gross primary production using GLASS, FLUXCOM and MTE reference data. Additionally, the regional GPP is calculated as the area weighted sum instead of the mean of the gridcells used for LAI.

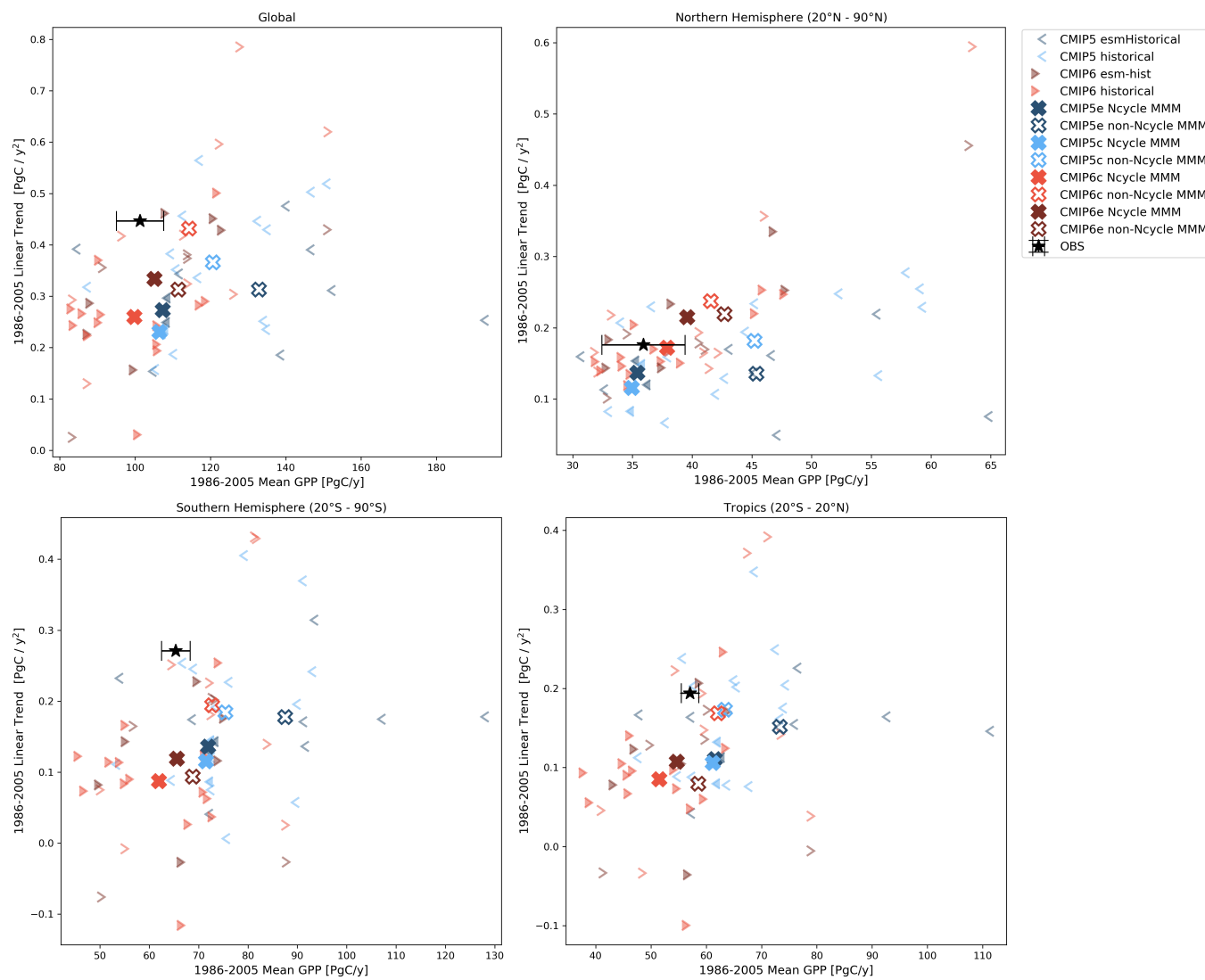


Figure 6. As Figure 2 but for gross primary production using GLASS, FLUXCOM and MTE reference data.

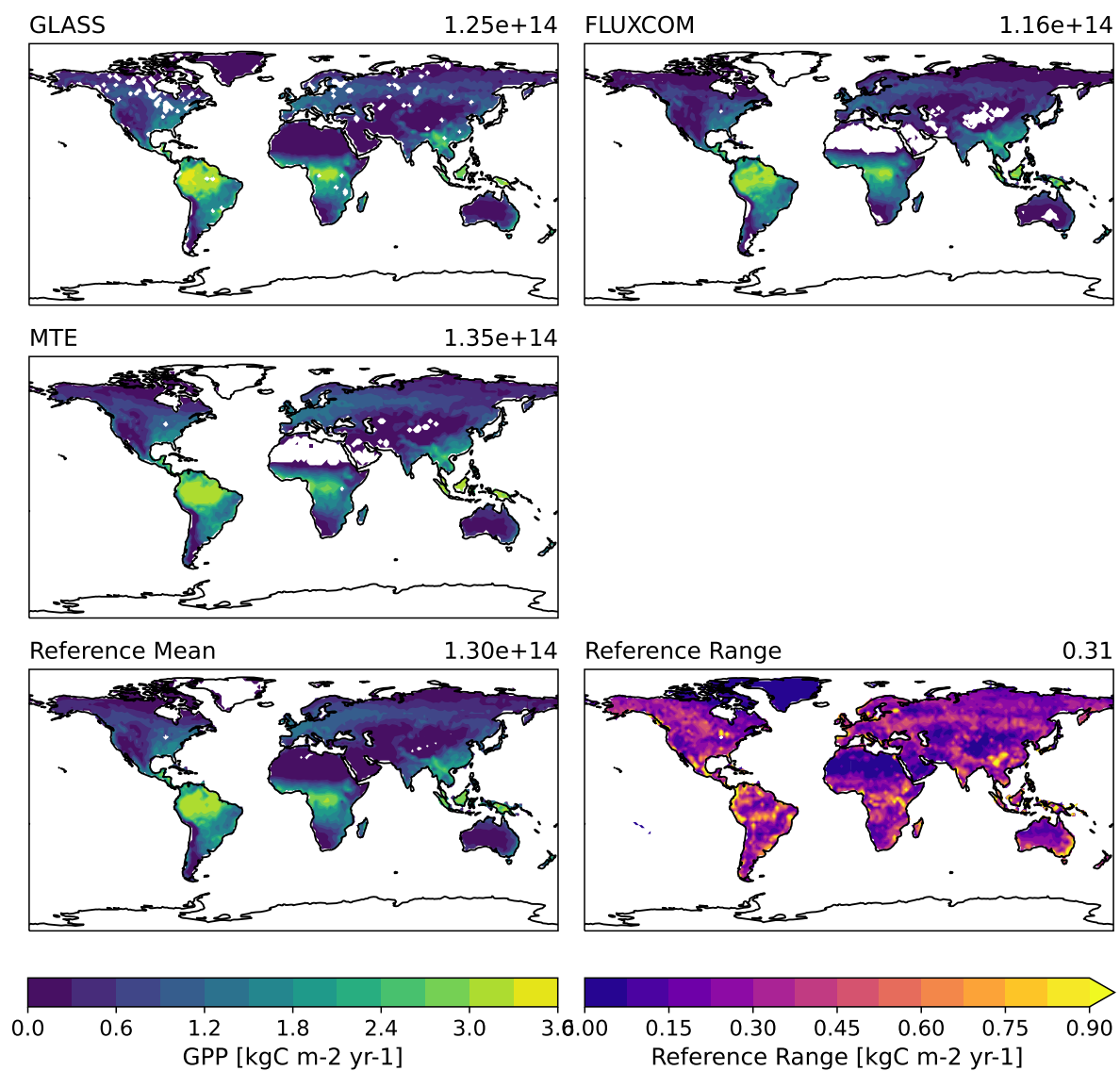


Figure 7. Global maps of GPP averaged over 1986-2005 for all reference data sets (GLASS, FLUXCOM and MTE), as well as the mean and range between lowest and highest values per grid cell of the reference data sets. The number in the top right denotes the global GPP flux.

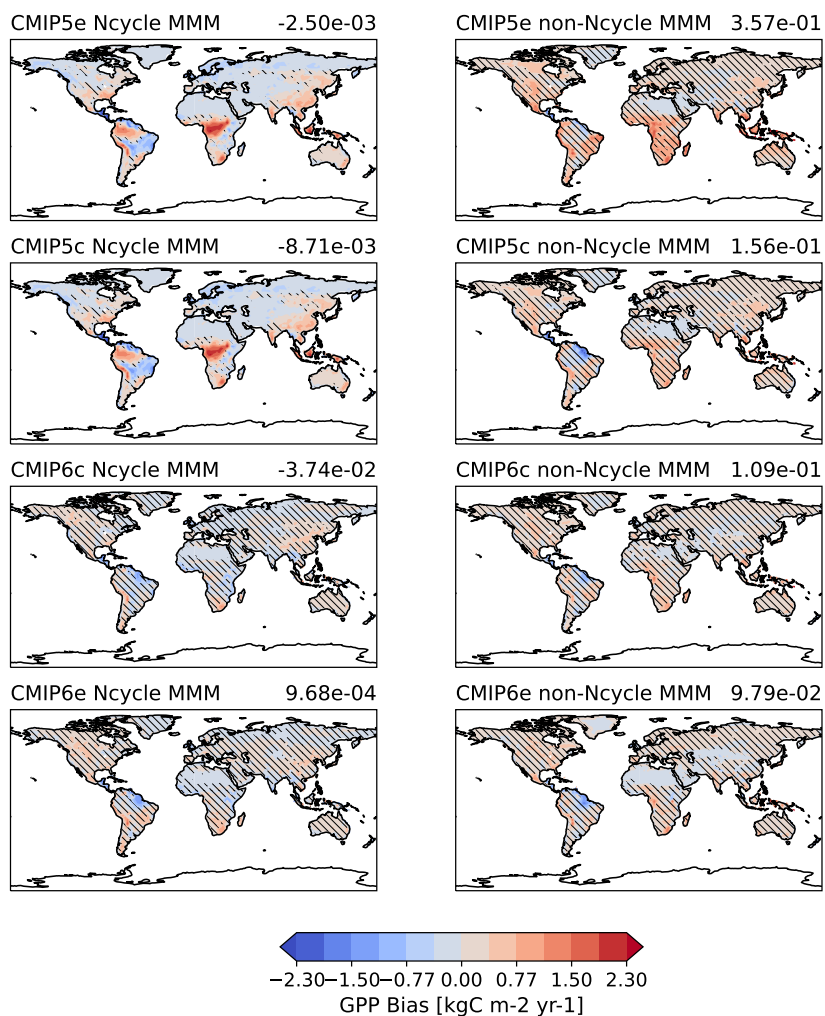


Figure 8. Global maps of GPP bias for 1986-2005 with respect to the reference data set mean shown in Figure 7. The panels show the MMMs of the models with (left) and without (right) coupled nitrogen cycle for the different project-experiment combinations. The hatching represents the areas where the MMM of the models and reference mean agree within the MMM std, while the number in the top right denotes the global mean bias.

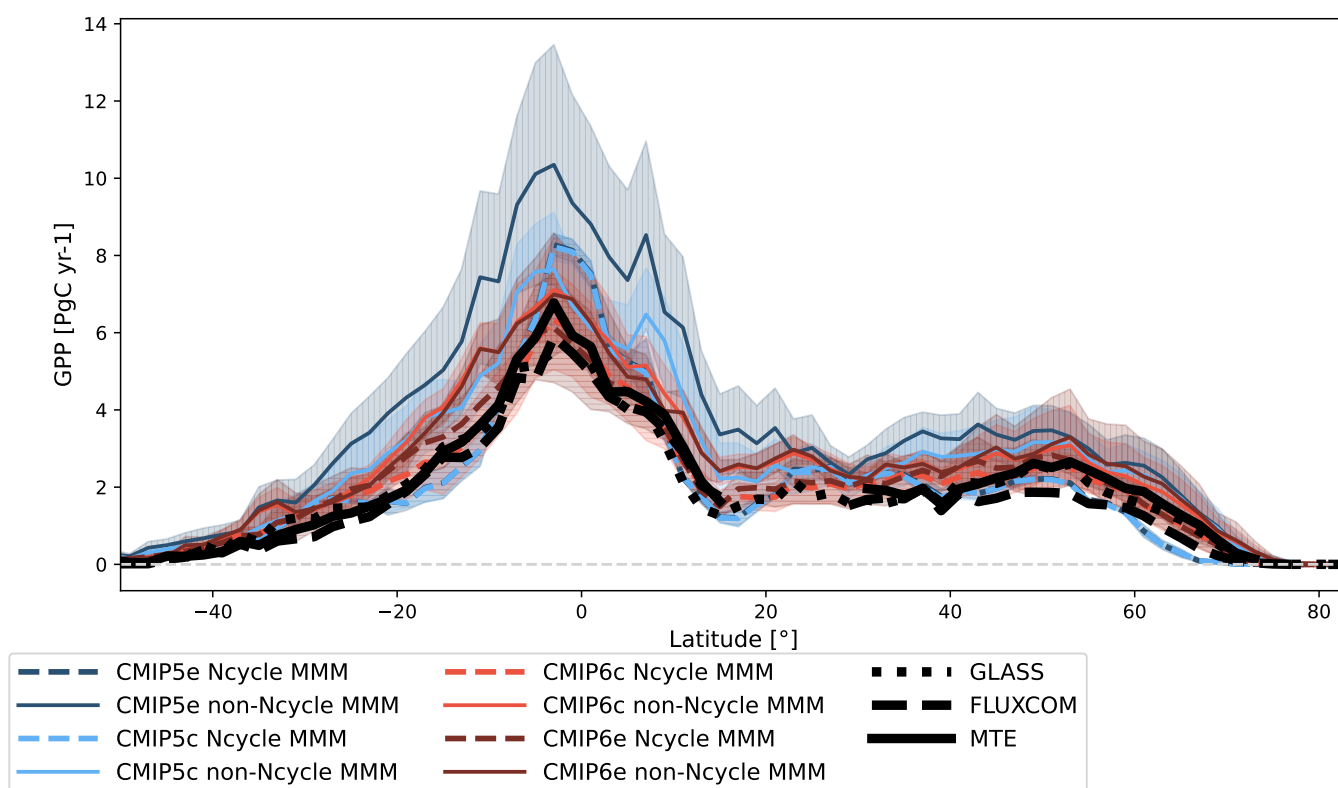


Figure 9. Area weighted zonal sums of gross primary production and the reference data sets GLASS, FLUXCOM and MTE. No common masking is applied, but latitudes were set to missing if more than 15% of the land grid cells contained missing data. The hatching depicts the MMM standard deviation, with a horizontal hatching for models with and vertical hatching for models without interactive nitrogen cycle.

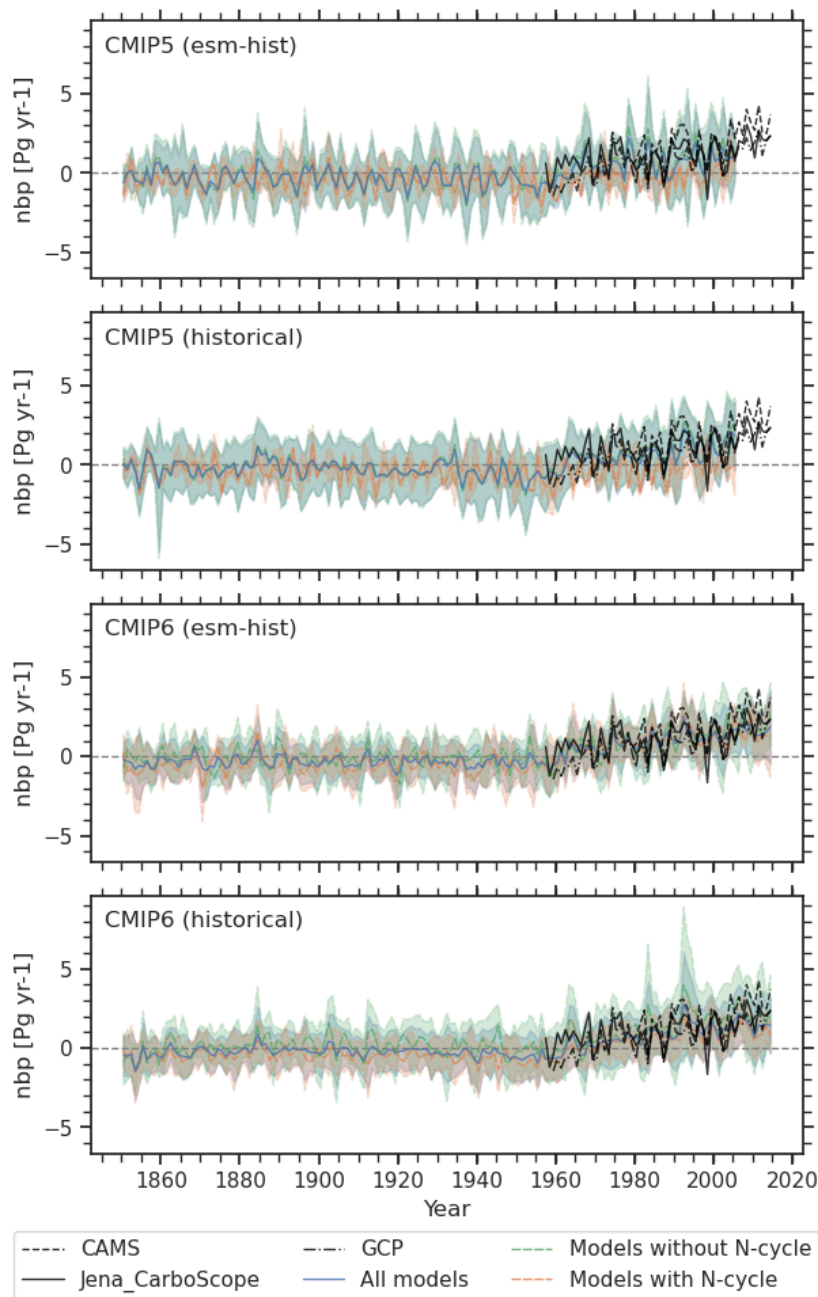


Figure 10. Global Land-Atmosphere carbon flux time series for CMIP5 (top two panels) and CMIP6 (bottom two panels) concentration (panels 2 & 4) and emission driven (panels 1 & 3) historical simulations. Model results are separated into MMMs of models with (orange dashed line) and without interactive nitrogen cycle (green dashed line), with the MMM of all models shown in blue and the reference data sets CarboScope (solid), CAMS (dashed), and GCP (dash-dotted) shown in black. The standard deviation of the MMM is given by the shaded areas.

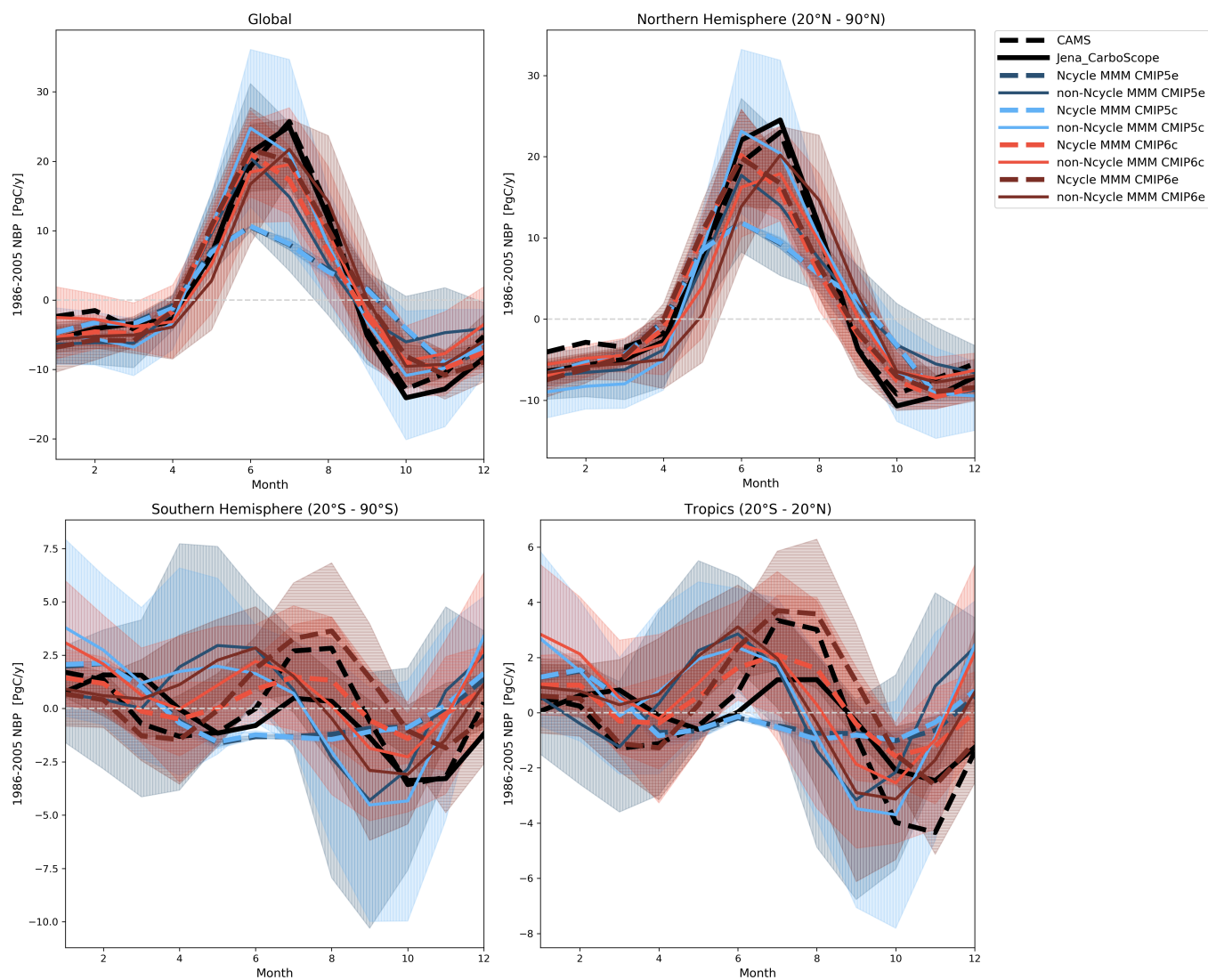


Figure 11. As Figure 1 but for land-atmosphere carbon flux and the reference data sets CAMS and CarboScope.

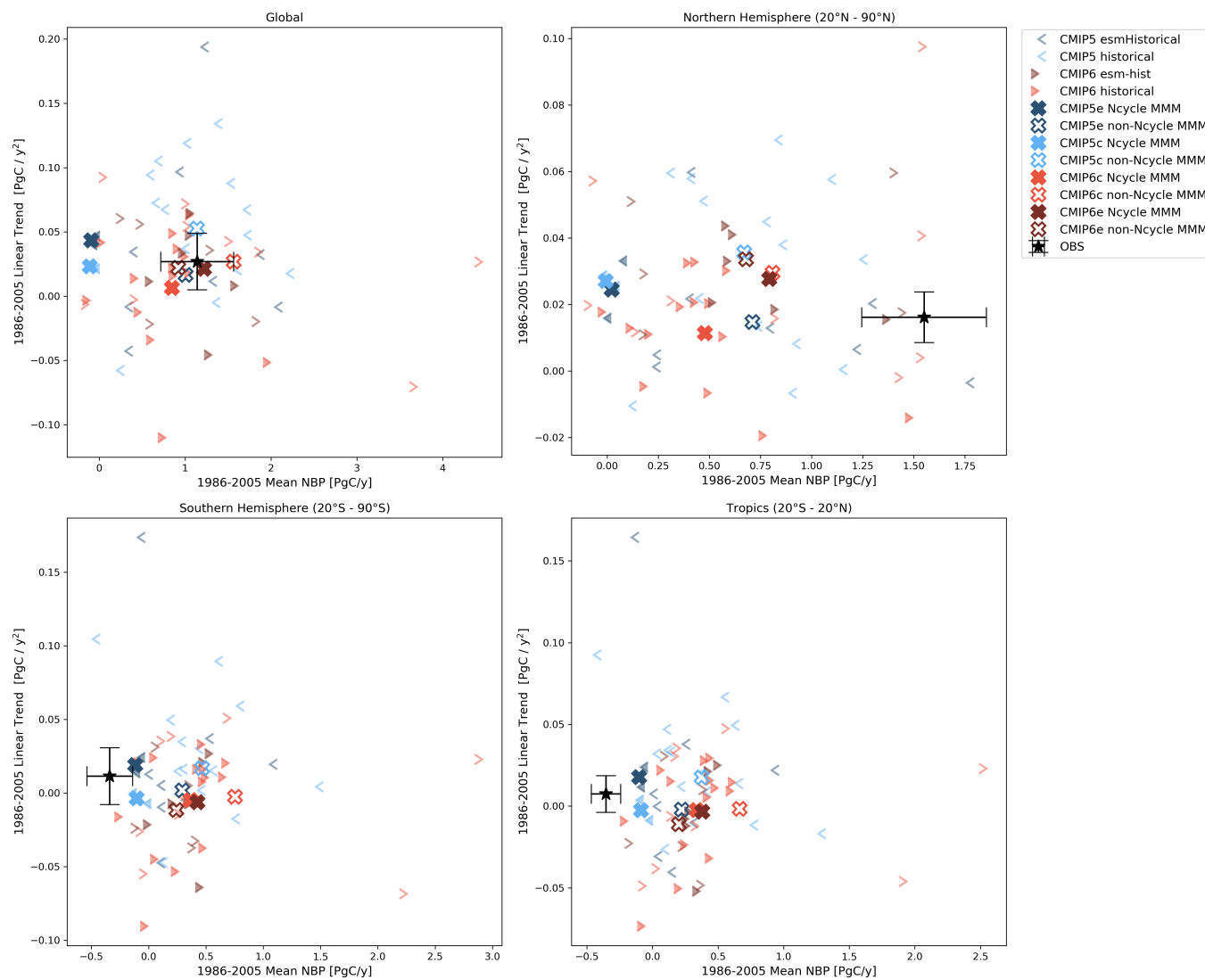


Figure 12. As Figure 2 but for land-atmosphere carbon flux and the reference data sets CAMS and CarboScope. The GCP data is a globally averaged timeseries and thus only appears in the global plot.

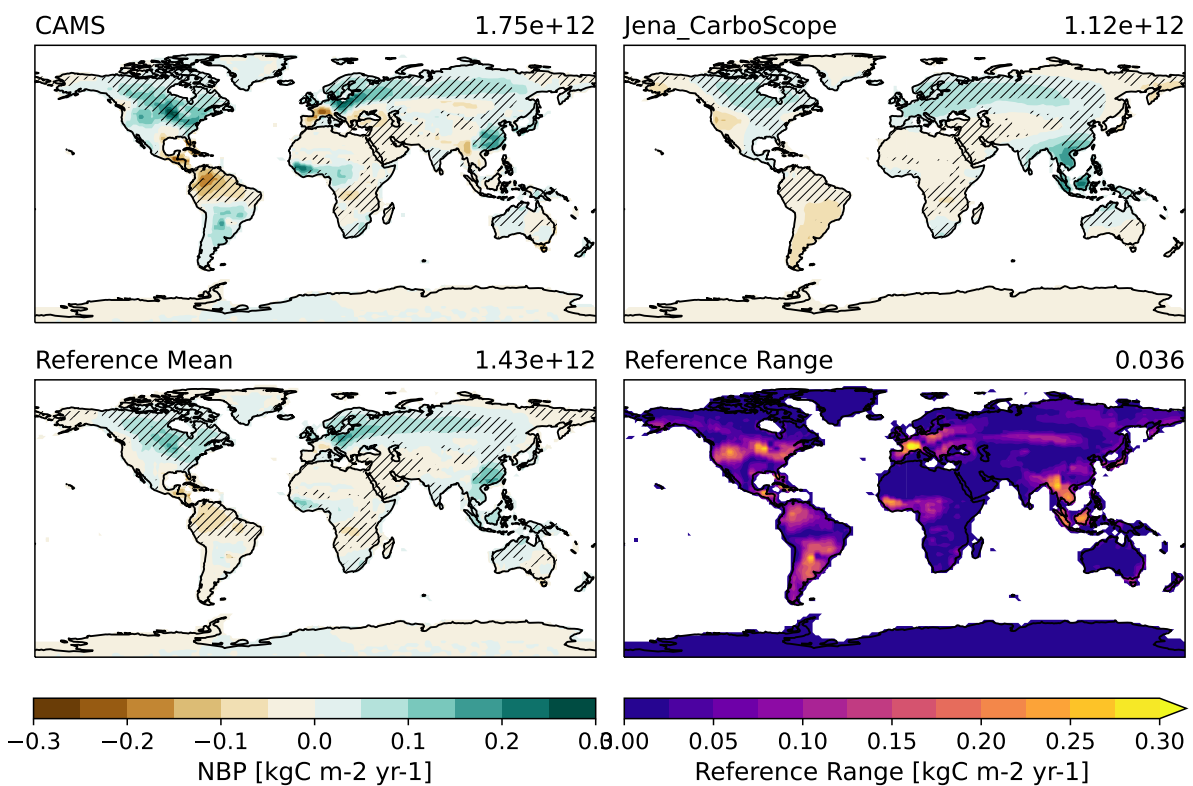


Figure 13. Similar to 7 but for land-atmosphere carbon flux. Additionally, the forward slash hatching symbolizes areas where the reference data sets agree on the sign or where the difference is smaller than the size of one bin of the contour plot.

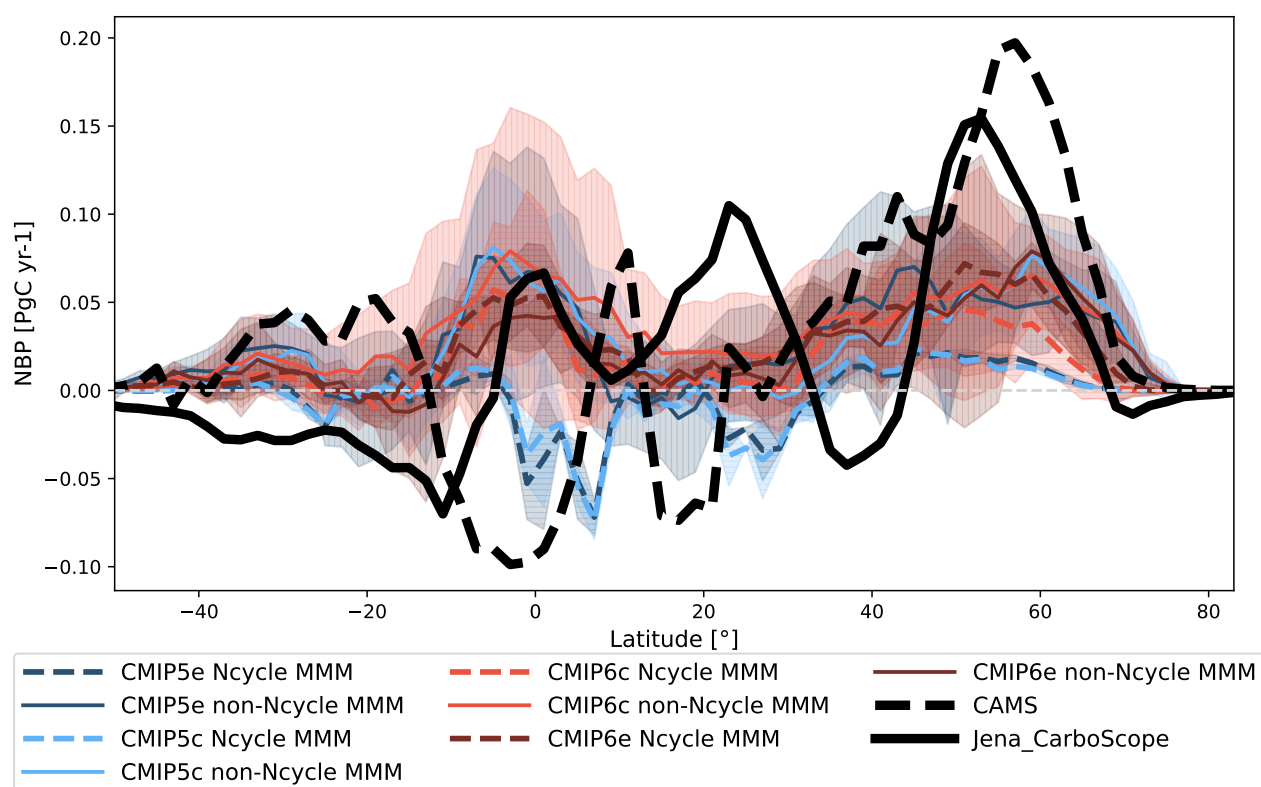


Figure 14. As Figure 9 but for land-atmosphere carbon flux with CAMS and CarboScope reference data.

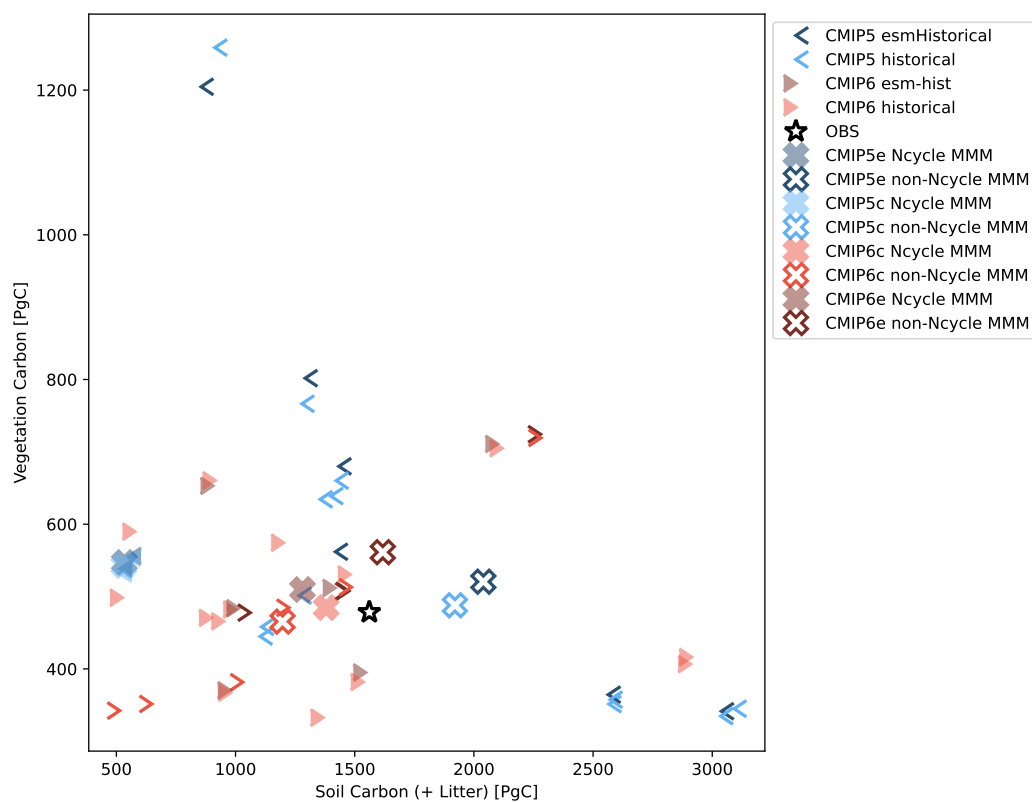


Figure 15. Scatter plot of global mean vegetation and soil carbon over 1986-2005, with observations from NDP (vegetation carbon) and HWSD+NCSCD (soil carbon). As in Figure 2, filled symbols denote models with nitrogen cycle.

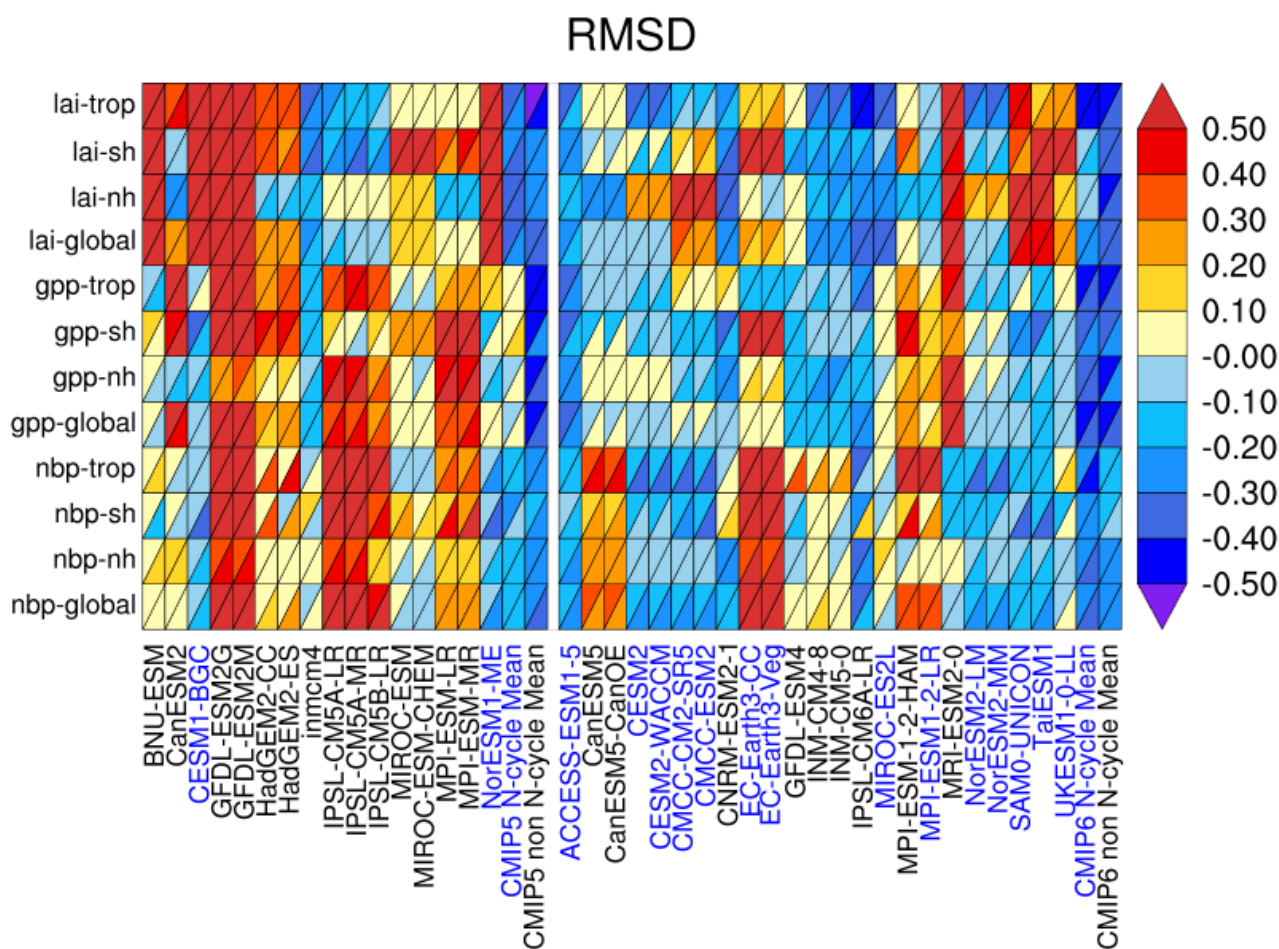


Figure 16. Relative space-time root-mean-square deviation (RMSD) performance metrics for CMIP5 (left) and CMIP6 (right) concentration driven simulations for variables relevant to the carbon cycle compared to reference data sets. Blue shading indicates a performance better than the median RMSD of all models in the plot, while the redder the color, the worse the performance. The RMSD is normalized relative to the median of all models. The considered time periods depend on the start of the observational data (see Table 3) and end in 2005 to accommodate the end of the CMIP5 data. When using two observational references, a diagonal split is introduced, with the default reference data set being shown on the lower right, while the alternate data set is used for the top left triangle. The default and alternate reference data sets are marked in Table 3 and are as follows: LAI: LAI4g (main), GLASS (alt); GPP: FLUXCOM (main), GLASS(alt); NBP: CarboScope (main), CAMS (alt).

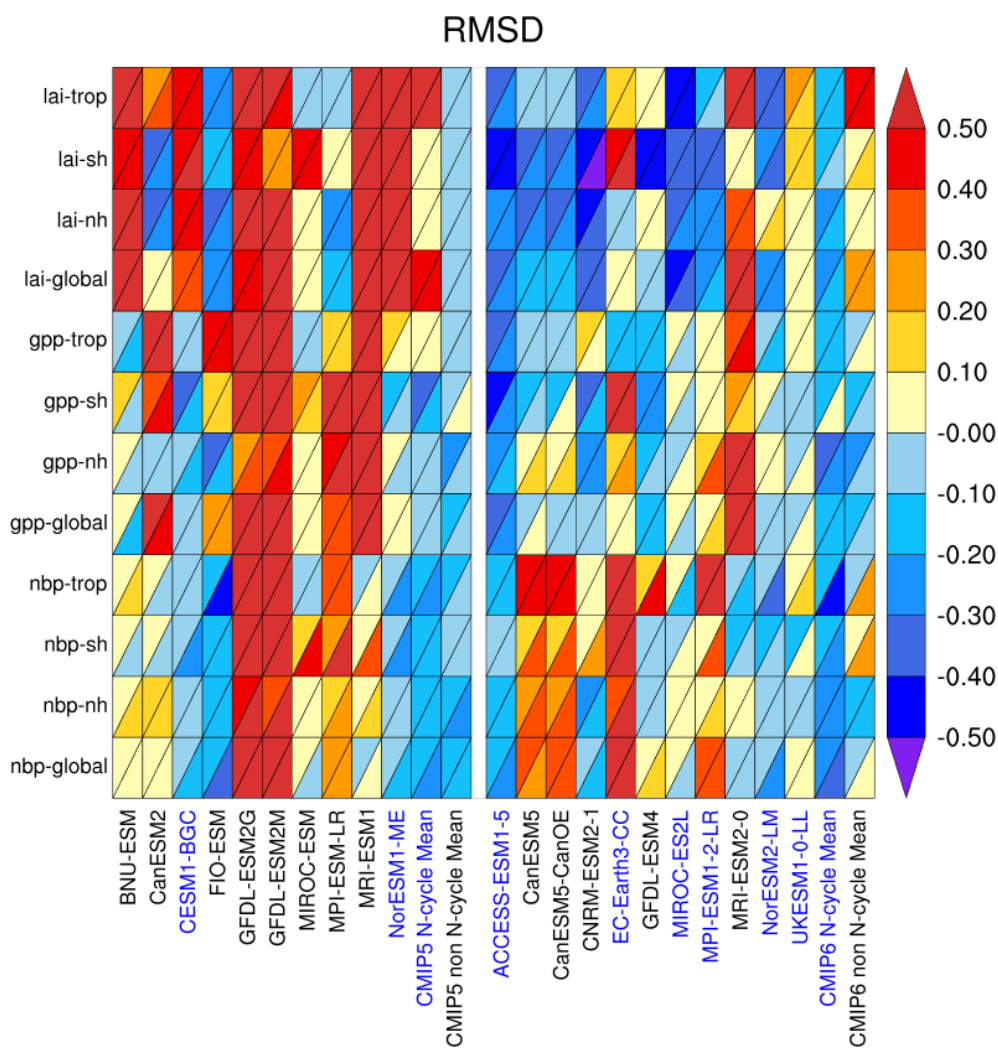


Figure 17. As Figure 16 but for emission driven simulations.

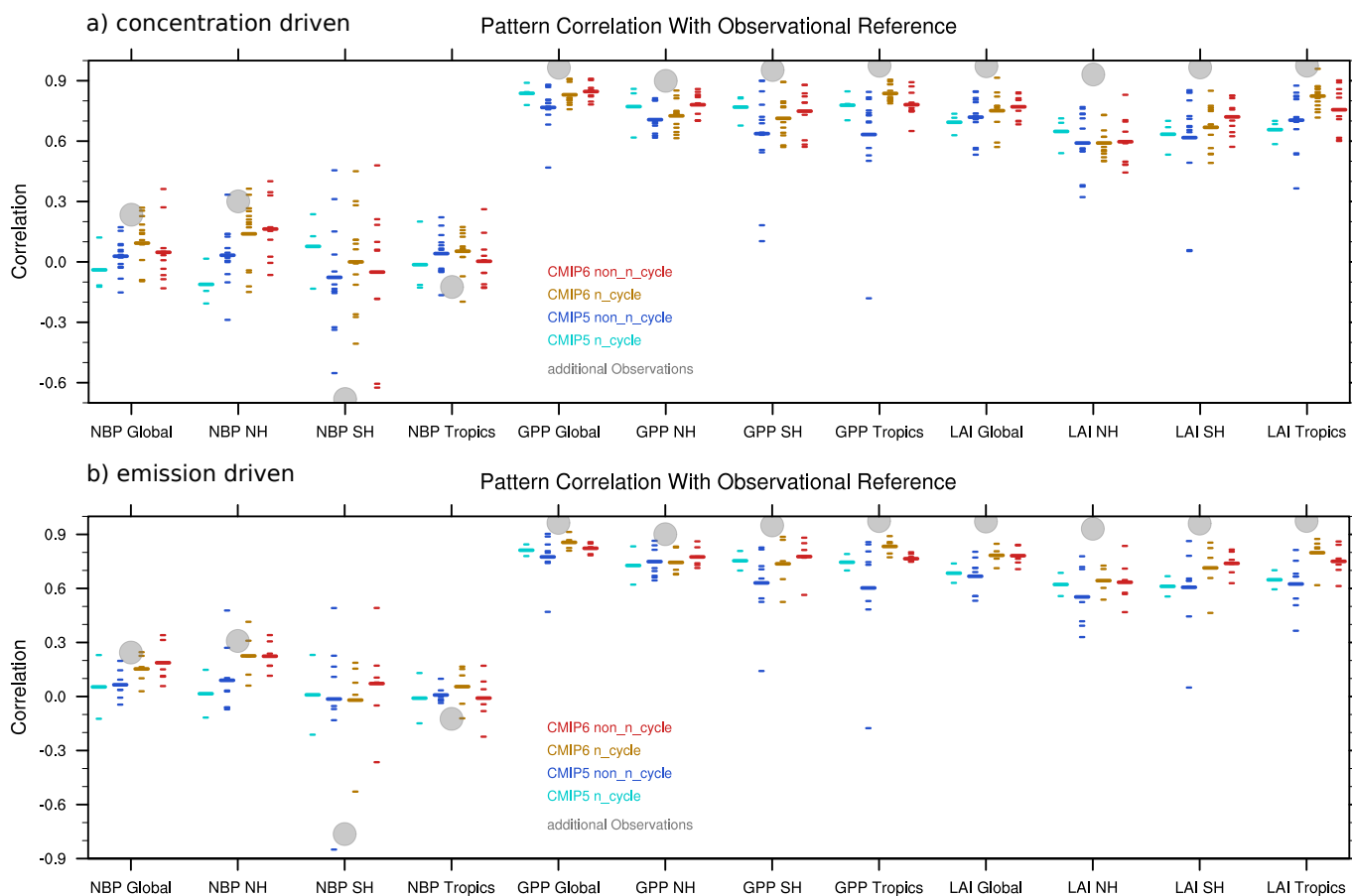


Figure 18. Centered pattern correlations between models and reference data sets for annual mean climatology for concentration driven (a) and emission driven (b) CMIP5 and CMIP6 models, split into Ncycle and non-Ncycle models. Main and alternate observations are the same as in Figure 16.